AN ABSTRACT OF THE DISSERTATION OF

Zachary Eric Kayler for the degree of Doctor of Philosophy in Forest Science presented on December 10, 2008
Title: The Methodology, Implementation and Analysis of the Isotopic Composition of Soil Respired CO_2 in Forest Ecological Research

Abstract approved:

Barbara J. Bond

Soils are the largest terrestrial pool of carbon, therefore it is critical to understand what controls soil carbon efflux to the atmosphere in light of current climate uncertainty. The primary efflux of carbon from soil is soil respiration which is typically categorized into autotrophic and heterotrophic respiration. These two components have different responses to changes in the environment, thus necessitating a means to quantify the contributions of each. Natural abundance ^{13}C can identify autotrophic and heterotrophic sources of respiration, but there is a paucity of research concerning the soil isotope methodology and the subsequent analysis. This dissertation documents my contributions to the advancement of understanding carbon metabolism in forest ecosystems of the Pacific Northwest through the use of the natural abundance carbon isotopic signature of soil respiration.

The results of this research represent significant progress in the use of ^{13}C in forest ecology. I show in a laboratory setting that a change in the isotopic signature of soil gas can take at least 48 hours to reach equilibrium. A change in the isotopic source of respiration is one mechanism behind non steady-state conditions while another mechanism is dynamic gas transport. I explored the impact of a negative pressure potential across the soil surface by inducing advection and found the isotopic signature of respiration to be 1‰ less than the theoretical steady-state value. I performed a source partitioning experiment in which I identified a highly depleted source of carbon contributing to respiration. I also considered the impacts of the potential errors associated

with collecting and measuring isotopic samples on mixing-models currently used to identify the isotopic signature of respiration. I found that the effect of CO_2 and $\delta^{13}C$ measurement error on large CO_2 concentration regime to be substantially different than small concentration regimes, necessitating a unique mixing-model and regression-model combination for estimating the isotopic signal of respiration. Finally, I built upon the progress made in the previous experiments and analyze almost two years of soil respiration and its isotopic signature to determine potential environmental and biological drivers. I found that: transpiration was highly correlated with both respiration and the carbon isotopic signature; soil moisture primarily influenced tree processes related to respiration; and I found evidence of soil respiration under isotopic non steady-state conditions.

The Methodology, Implementation and Analysis of the Isotopic Composition of Soil Respired CO_2 in Forest Ecological Research

by
Zachary Eric Kayler

A DISSERTATION
Submitted to
Oregon State University

in partial fulfillment of
the requirements for the
degree of

Doctor of Philosophy

Presented December 10, 2008
Commencement June 2009

Doctor of Philosophy dissertation of Zachary Eric Kayler presented on December 10, 2008.

APPROVED:

Major Professor, representing Forest Science

Head of the Department of Forest Ecosystems and Society

Dean of the Graduate School

I understand that my dissertation will become part of the permanent collection of Oregon State University libraries. My signature below authorizes release of my dissertation to any reader upon request.

Zachary Eric Kayler, Author

ACKNOWLEDGEMENTS

Every doctoral experience is unique, and we each experience the peaks of success and the troughs of disappointment and at times, despair. The loss of Professor Elizabeth Sulzman was the lowest point of my experience. I lost a partner in the field, an ally in the laboratory, and a mentor I admired. I will carry her memory and the experiences we shared with me for the rest of my life.

I thank all of my friends and lab mates that helped me get through these hard times as well as celebrate each crucial step that brought us closer to our goals. I share a special bond with the first cohort of the Ecosystem Informatics IGERT group: Stephen Mitchell, Geoff Hosack, Liz Burrows, and Alan Tepley among others. I want to thank my friends in Crop and Soil Science who accepted me as their own despite my origins in the Forest Science department: Elizabeth Brewer, Marco Keiluweit, and Laurel Kluber. I simply would not have survived without Holly Barnard, Chris Graham, and Claire Phillips.

I thank my committee, especially Renee Brooks, a great friend of Elizabeth Sulzman, who joined my committee at a difficult time. I also want to thank Professor Barb Bond and each committee member for their patience and true generosity in reviewing my research and refereeing my program with little to nothing in return.

I thank all of my funders: Ecosystem Informatics IGERT administered by Professor Julia Jones and Katherine Hoffman, OSU Pipeline Fellowship, and the Airshed Project of Barb Bond. I also want to acknowledge all of the support staff in Forest Science and Crop and Soil Science who helped me navigate the OSU bureaucracy: Cheryll Alex, Jeannette Harper, Jayne Smith, and Tracy Mitzel.

I thank Professors John Battles and Markus Kleber who inspire me to be excited about science and discovery despite great odds and poor funding. I am extremely indebted to my family: to my sisters who were first to put me in my place, to my mother who encouraged my imagination, and my father for teaching me the meaning of hard work. I need to thank Mary Zaske for all of her babysitting. Finally, let it be known that the very idea of me attaining a degree no less a Ph.D. is a result of my incredible wife, Sara, my partner in life and mother of my wonderful child, Sophia.

CONTRIBUTION OF AUTHORS

Chapter 2: Dr. Barbara Bond, Dr. Elizabeth Sulzman and Dr. Alan Mix provided assistance with data interpretation and editing of the manuscript. Dr. John Marshall and Bill Rugh provided technical assistance.

Chapter 3: Dr. Barbara Bond, Dr. Elizabeth Sulzman, Dr. Alan Mix, Dr. Don Phillips, Dr. Renee Brooks, and Dr. Mark Harmon provided assistance with data interpretation and editing of the manuscript. Dr. Lisa Ganio assisted with the simulation development, interpretation of the results, and writing of the manuscript. Mark Hauck and Dr. Tom Pypker provided ecosystem respiration data.

Chapter 4: Dr. Barbara Bond, Dr. Elizabeth Sulzman and Dr. Alan Mix provided assistance with data interpretation and editing of the manuscript.

Chapter 5: Dr. Barbara Bond, Dr. Elizabeth Sulzman and Dr. Alan Mix provided assistance with data interpretation and editing of the manuscript as well as assistance in data collection. Holly Barnard provided transpiration data.

TABLE OF CONTENTS

TABLE OF CONTENTS (continued)

LIST OF FIGURES

LIST OF FIGURES (continued)

Figure Page

LIST OF FIGURES (continued)

Figure Page

LIST OF TABLES

Chapter 1 Introduction

Significant progress towards understanding the processes by which ecosystems return carbon (C) to the atmosphere, and the turnover time of C in ecosystems, is of fundamental importance to informing global action to stabilize atmospheric CO_2 levels; it is also crucial for explaining what role terrestrial ecosystems play in interannual and decadal changes in CO_2 (Trumbore 2006). The largest terrestrial pool of carbon is soil (Amundson 2001) and soil respiration is the second largest carbon flux globally, approximately an order of magnitude greater than the combined flux of fossil fuel and deforestation (Schimel et al. 1995). Despite its global significance, we have only a limited understanding of processes controlling soil respiration within and across ecosystems (Raich and Potter 1995). Estimates of future change in atmospheric CO_2 depend strongly on the feedbacks of ecosystems to climate change, in particular the balance of C uptake and loss from ecosystems in a warmer world. In high latitude ecosystems, there is already debate as to whether increased heterotrophic respiration is changing local net ecosystem exchange (Goulden et al., 1998).

We have entered a period of great uncertainty with regards to the global climate and it is crucial that we develop a thorough understanding of the physical and biological controls of the evolution and egress of soil CO_2. Analyses of the isotopic composition and rate of CO_2 evolution from soil has increasingly been used in studies of C dynamics in the soil-plant-atmosphere system (Högberg et al. 2005; Högberg et al. 2006).Variations in carbon isotope composition ($\delta^{13}C$, or better, the $^{12}C/^{13}C$ ratio expressed with reference to a standard) allow researchers to trace carbon dioxide from its sources to atmospheric and terrestrial sinks. In many cases, $\delta^{13}C$ analyses allow the identification of components of soil CO_2 efflux as well as the relative contribution of soil carbon pools to overall ecosystem CO_2 fluxes (Ehleringer et al., 2000; Bowling et al. 2008; Tu and Dawson. 2005). However, while the processes of C isotope fractionation within plants are reasonably well known (Högberg et al., 2005), considerable uncertainty exists regarding the processes determining the isotopic composition of CO_2 efflux from soils.

A large degree of uncertainty remains in the methodology, implementation and analysis of ^{13}C in forest ecosystems. The work presented in this dissertation was designed to bring confidence to these three broad areas of soil isotope ecology:

Methodology: The second chapter is a simple laboratory study comparing a static chamber at equilibrium method of estimating the isotopic signature of soil respiration ($\delta^{13}C_{R\text{-}s}$) and one using the soil $^{13}CO_2$ concentration profile (soil probe). There are few, if any, laboratory studies that consider how ($\delta^{13}C_{R\text{-}s}$) is measured or that consider the assumptions behind these methods. The fundamental difference between the methods I chose is the location from which $^{13}CO_2$ is sampled: soil CO_2 is collected from the surface using a static chamber at equilibrium whereas the soil probe samples soil CO_2 at depth in the soil. The two methods are similar in that they assume soil CO_2 efflux is at steady-state; a condition when the isotopic signature of the CO_2 emitting from the soil surface is equal to the isotopic source of respired CO_2 (Amundson et al. 1998). To test the static chamber at equilibrium and soil probe methods, we constructed a column filled with sand and plumbed a single CO_2 source of known isotopic value and concentration. We hypothesized that for CO_2 diffusing at steady-state both methods will estimate the source gas isotopic composition.

Analysis: In chapter three, using a simulation approach I determined the most accurate and precise mixing model and regression approach for estimating $\delta^{13}C_{R\text{-}s}$, where carbon dioxide concentration ranges ($[CO_2]_{range}$) tend to be large. The objective of this chapter was to evaluate how factorial combinations of two mixing models and two regression approaches (Keeling-OLS, Miller-Tans-OLS, Keeling-GMR, Miller-Tans- GMR) compare in small $[CO_2]_{range}$ vs. large $[CO_2]_{range}$ regimes, with different combinations of pertinent variables ($[CO_2]_{range}$, $[CO_2]_{error}$, $\delta^{13}C_{error}$ and n) that are realistic for experimental applications in each of the two regimes. My approach was to conduct a series of simulations using artificial datasets. From these simulations I report 1) how the bias and uncertainty of estimates of $\delta^{13}C_R$ in large concentration and small concentration regimes differ, 2) which simulation input variables influence $\delta^{13}C_R$ bias and uncertainty, and 3) which mixing and regression model produces the least bias and uncertainty when applied to samples from large $[CO_2]_{range}$ systems.

Implementation: The fourth and fifth chapters are accounts of two field studies. In chapter four, I measure ($\delta^{13}C_{R\text{-}s}$) using two established methods, one aboveground and the other a belowground method. There is a clear need to assess whether or not the assumptions concerning the measurement and analysis of $\delta^{13}C_{R\text{-}s}$ are appropriate given the variability in carbon sources and soil properties in forest ecosystems. I designed a series of field experiments to investigate the impact of soil gas transport on estimates of $\delta^{13}C_{R\text{-}s}$. To accomplish this I sampled soil gas belowground using a soil probe and aboveground using a mini-tower to estimate $\delta^{13}C_{R\text{-}s}$. I hypothesized that there will not be a difference between the two estimates when the soil probe estimate is corrected for kinetic fractionation due to diffusion. I also implemented isotopic data from the soil profile in a steady state model of $^{13}CO_2$ based on transport solely by diffusion and a model that accounts for both advection and diffusion. I also considered that advection may be difficult to detect and so to further explore the potential influence of advection on aboveground estimates of $\delta^{13}C_{R\text{-}s}$, I induced a negative pressure gradient on the soil surface. Finally, I put the estimates of $\delta^{13}C_{R\text{-}s}$ in an ecological context by comparing the estimated source of respiration with the isotopic signature of carbon in soluble extracts from leaves and phloem as well as the isotopic signature of bulk soil organic matter. Then, using an isotope mixing model, I determined the contribution of new and old carbon sources to $\delta^{13}C_{R\text{-}s}$ for a Douglas-fir stand in the Pacific Northwest.

In chapter five, I measured soil respiration and $\delta^{13}C_{R\text{-}s}$ over the late growing season of 2004 and the entire 2006 growing season along with soil moisture, soil temperature, VPD and transpiration across a steep catchment. I hypothesized that recently-fixed photosynthates are an important driver of soil respiration during the growing season. I found that soil respiration was dominated by tree belowground inputs over the growing season. Both soil respiration and $\delta^{13}C_{R\text{-}s}$ were highly correlated with transpiration rates 0 to 4 days prior. Levels of vapor pressured

deficit, however, were only weakly correlated with both measures of CO_2 efflux. Temperature explained 53% of the respiration variability and by including soil moisture we were able to explain 56% of the overall variation in respiration. Furthermore, based on the analysis of $\delta^{13}C_{R\text{-}s}$ soil moisture was negatively correlated with $\delta^{13}C_{Rs}$ at our site indicating that soil moisture influences on soil respiration are related to the oxidation of recently-fixed photosynthates from plants rather than carbon from SOM.

In the final chapter, I summarize the conclusions of my dissertation research. I frame my findings within the overall goal of understanding the sources of soil respired carbon to the global carbon budget and why stable isotope analysis is an important part of this goal. I also discuss possible research directions that stem from the findings presented here.

References

Amundson, R., L. Stern, T. Baisden and Y. Wang.1998. The isotopic composition of soil and soil-respired CO_2. Geoderma 82(1-3): 83-114.

Amundson, R.2001. The carbon budget in soils. Annual Review of Earth and Planetary Sciences 29: 535-562.

Bowling, D.R., D.E. Pataki, J.T. Randerson .2008. Carbon isotopes in terrestrial ecosystem pools and CO_2 fluxes. New Phytologist 178(1): 24-40.

Ehleringer, J. R., N. Buchmann and L. B. Flanagan.2000. Carbon isotope ratios in belowground carbon cycle processes. Ecological Applications 10(2): 412-422.

Goulden, M. L., S. C. Wofsy, J. W. Harden, S. E. Trumbore, P. M. Crill, S. T. Gower, T. Fries, B. C. Daube, S. M. Fan, D. J. Sutton, A. Bazzaz and J. W. Munger.1998. Sensitivity of boreal forest carbon balance to soil thaw. Science 279(5348): 214-217.

Högberg , P., A. Ekblad, A. Nordgren, A. H. Plamboeck, A. Ohlsson, Bhupinderpal-Singh and M. Hoegber.2005. Factors determining the ^{13}C abundance of soil-respired CO2 in Boreal Forests. Stable Isotopes and Biosphere-Atmosphere Interactions. L. B. Flanagan, J. R. Ehleringer and D. E. Pataki. San Francisco, USA, Elsevier: 47-68.

Högberg , P. and D. J. Read.2006. Towards a more plant physiological perspective on soil ecology. Trends in Ecology & Evolution 21(10): 548-554.

Raich, J. W. and C. S. Potter.1995. Global Patterns of Carbon-Dioxide Emissions from Soils. Global Biogeochemical Cycles 9(1): 23-36.

Schimel, D. S.1995. Terrestrial Ecosystems and the Carbon-Cycle. Global Change Biology 1(1): 77-91.

Trumbore, S. 2006. Carbon respired by terrestrial ecosystems - recent progress and challenges. Global Change Biology 12:141-153.

Tu, K. and T. Dawson. 2005. Partitioning Ecosystem Respiration Using Stable Carbon Isotope Analyses of CO_2. Stable Isotopes and Biosphere-Atmoshpere Interactions. J. R. Ehleringer, D.E. Pataki, L.B. Flanagan. San Francisco, Ca, USA, Elsevier.

Chapter 2 A laboratory comparison of two methods used to estimate the isotopic composition of soil $\delta^{13}CO_2$ efflux at steady-state

Zachary Kayler, Elizabeth W. Sulzman, John D. Marshall, Alan Mix, William Rugh and Barbara J. Bond

Rapid Communications in Mass Spectrometry

John Wiley & Sons Inc
350 Main Street
Malden MA 02148
USA

Volume 22 pp. 2533-2538.

Abstract

The stable isotopic composition of soil $^{13}CO_2$ flux is an important tool for monitoring soil biological and physical processes. While several methods exist to measure the isotopic composition of soil flux, we do not know how effective each method is at achieving this goal. To provide clear evidence of the accuracy of current measurement techniques we created a column filled with quartz sand through which a gas of known isotopic composition (-34.2‰) and concentration (3000 PPM) diffused for 7 hours. We used a static chamber at equilibrium and a soil probe technique to test whether they could identify the isotopic signature of the known gas source. The static chamber is designed to identify the source gas isotopic composition when in equilibrium with the soil gas, and the soil probe method relies on a mixing model of samples withdrawn from 3 gas wells at different depths to identify the gas source. We sampled from ports installed along the side of the sand column to describe the isotopic and concentration gradient as well as serve as a control for the soil probe. The soil probe produced similar isotopic and concentration values, as well as Keeling intercepts, as the control ports. The static chamber at equilibrium did not identify the source gas, but when applied in a two end-member mixing model, the chamber did produce a similar Keeling intercept as derived from the control ports. Neither of the methods was able to identify the source gas isotopic signature via the Keeling plot method most likely because CO_2 profiles did not reach isotopic steady-state. Our results showed that the static chamber at equilibrium should be used only with a Keeling plot approach and that the soil probe is able to provide estimates of uncertainty for the isotopic composition of soil gas as well as information pertinent to the soil profile.

Introduction

Accurate measurements of the isotopic signature of soil-respired CO_2 are critical to understanding ecosystem metabolism (Steinmann et al. 2004; Bowling et al. 2002) and geologic processes (Lewicki et al. 2003; Evans et al. 2003) .Yet, a clear technique to sample this flux has not emerged. Current methods for measuring the isotopic signature

of soil respired CO_2 include deploying static chambers to capture the $^{13}CO_2$ gradient evolved from the soil surface over time (Ekblad and Högberg 2000), deploying dynamic chambers connected to an infra red gas analyzer (Bertolini et al. 2006), or sampling a static chamber once the volume headspace is in equilibrium with the soil gas (Mora and Raiche et al. 2007). An alternative to using surface chambers to measure the isotopic signature of soil respired CO_2 is collecting soil gas within wells that penetrate the soil surface and identifying the isotopic composition of respired CO_2 based on a two end-member mixing model (Steinmann et al 2004; Tu and Dawson 2005). If we wish to evaluate estimates of soil respired $^{13}CO_2$ using different measurement approaches, then the variability due to different measuring techniques needs to be minimized. One strategy to minimize differences between methods is to perform controlled experiments with a known CO_2 source, much like what has already been accomplished for soil flux chambers (Widen and Lindroth 2003).

Relatively few comparisons of methods used to measure the isotopic signal of soil respired CO_2 have been made under field conditions (Mortazavi et al. 2004) and even fewer have been compared in a controlled laboratory experiment. The purpose of this study is to test current methods used to identify the isotopic composition of soil efflux in a well-controlled environment. Recent evidence suggests that data from samples of the CO_2 gradient over time within a static chamber may be prone to misinterpretation (Risk and Kellman 2008), and the dynamic chamber is still in a state of development (Bertolini et al. 2006). The gas well method has been tested for reliability of soil $^{13}CO_2$ values (Breeker and Sharp 2008) and CO_2 flux (Risk et al. 2002; DeSutter et al. 2008) but a similar test for reliable estimates of the isotopic signature of the soil flux has not occurred. Thus, we chose to compare the static chamber at equilibrium[7] with a series of stacked gas wells, which we refer to as a soil probe, for this test. The selection of these two methods is reasonable given that 1) we gain both a belowground and aboveground perspective of soil respired $^{13}CO_2$ 2) both methods are similar in measurement assumptions and 3) they are both relatively straightforward in their implementation and analysis.

The fundamental difference between the methods we chose is the location from which $^{13}CO_2$ is sampled: soil CO_2 is collected from the surface using the static chamber

whereas the soil probe samples soil CO_2 at depth in the soil. The two methods are similar in that they assume soil CO_2 efflux is at steady-state; a condition where the isotopic signature of the CO_2 emitting from the soil surface is equal to the isotopic source of respired CO_2 (Amundson et al. 1998). The static chamber at equilibrium is designed to measure the isotopic source of respiration, which is impossible to measure from the soil surface unless the isotopic source is at steady-state. In the case of the soil probe, the estimate of the isotopic signature of the respiration source is systematically enriched in $^{13}CO_2$ as a result of soil gas sampled from within the soil matrix. The enriched soil gas is a function of the molecular rate of diffusion by $^{13}CO_2$, which is slower than that of $^{12}CO_2$, and results in a greater concentration of ^{13}C in the soil. When the soil CO_2 is at isotopic steady-state, the soil probe estimate identifies the source of the isotopic signal of respiration when corrected for this increase in concentration of $^{13}CO_2$ related to diffusion.

To test the static chamber at equilibrium and soil probe methods, we constructed a column filled with sand and plumbed a single CO_2 source of known isotopic value and concentration. We hypothesized that for CO_2 diffusing at steady-state both methods will estimate the correct source gas isotopic composition.

Methods

Soil probe: This method of sampling involves sampling gas for isotopic composition at different depths in the soil. The soil probe contained three isolated wells made from PVC (poly-vinyl chloride). These wells are held at a fixed distance (5, 15 and 30cm) by PVC tubing. Small diameter holes were drilled around the perimeter of each well which allowed for equilibration with the soil gas at depth. A 0.635 cm diameter stainless steel tube was inserted into each well that extends to the soil surface where a stainless steel union was attached resulting in a total volume of $20cm^3$ at the 5cm depth, $23cm^3$ at the 15cm depth, and $27cm^3$ at the 30cm depth . A septum was inserted at the end of the union which allows for sampling with a syringe without atmospheric CO_2 entering the sampled well. The gas sample collected from each well was used in a Keeling plot analysis to identify the isotopic signature of the source gas.

The Keeling mixing model describes a sample of the air in a system as a mixture of two sources of $^{13}CO_2$, the background atmosphere, and the source of respiration (Pataki et al. 2003). In field studies it is assumed that the soil source of respiration is a single, well mixed gas of CO_2 production from microbial and root respiration. For our laboratory experiment, we use a single gas source to meet the assumptions of this model. The Keeling linear mixing model equation that relates the observed ^{13}C to the observed $[CO_2]$ is given in Equation 1.

$$\delta_{obs} = \frac{C_{bg}}{C_{obs}}\left(\delta_{bg} - \delta_s\right) + \delta_s \quad (1)$$

Where C is $[CO_2]$ and the subscripts *obs*, *s*, and *bg* refer to the observed, source and background values. In Equation 1, δ refers to the isotopic value of the component expressed in δ notation:

$$\delta = (R_{sample} / R_{standard} - 1) * 1000‰ \quad (2)$$

Where R is the molar ratio of heavy to light isotopes. The carbon isotope ratio ($\delta^{13}C$) is expressed relative to the standard Vienna Pee Dee belemnite. The Keeling plot method relies on the regression of the isotopic signature and the corresponding CO_2 concentration, the sample concentrations are inverted in order to apply a linear regression model, from a series of samples of a system. The intercept of the regression is the isotopic source of respiration. We used an ordinary least squares regression model for the Keeling plot analysis, this combination has shown to provide accurate estimates of the isotopic signal of respiration (Pataki et al. 2003; Zobitz et al. 2006). For estimates of intercept standard error, we bootstrapped the Keeling plot regression (10,000 iterations) using S-Plus (Insightful Corporation, Seattle, WA, USA).

For this application, the Keeling intercept identifies the isotopic source of CO_2 based on the samples that have been enriched in $^{13}CO_2$ due to kinetic fractionation associated with diffusion (O'Leary 1988). We can correct for this diffusive enrichment by subtracting 4.4‰ from the Keeling intercept but we must also assume the system is at isotopic steady-state. If the CO_2 is not at isotopic steady-state then the concentration of $^{13}CO_2$ and $^{12}CO_2$ could be less than the steady-state concentrations yielding erroneous isotopic ratios and Keeling intercepts.

Static chamber at equilibrium: We used a 10cm diameter PVC chamber fitted with a 0.3 cm swagelock and septum. The bottom of the chamber remained open to allow entry of soil gas when pushed into the sand surface (~ 1cm). The static chamber at equilibrium technique assumes that once in isotopic equilibrium, the isotopic signature of $^{13}CO_2$ in the chamber space is equal to that of the source of respired CO_2.

Sand Column System: The sand column was constructed from 1.3 cm thick PVC pipe with a 30.5 cm diameter. The bottom of the pipe was inserted into a PVC cap and sealed with PVC cement. The column was filled with carbonless quartz sand to a depth of 60 cm. The sand bulk density was 3.22 g cm^{-3} and the sand diffusivity was 0.056 cm^2 s^{-1}. A PVC platform perforated with several 0.3 cm holes held up the column of sand which creates a sandless area approximately 25cm deep at the bottom of the column. A thin layer of glass wool was laid between the platform and sand to prevent the sand from filling the reservoir. Swagelock bulkhead unions were installed into the sides of the sand column to create ports from which to measure the isotope and concentration profiles. The ports between 5 and 30cm served as a control to the soil probe and we expected any effects due to the soil probe to materialize as differences in the concentration and isotopic gradients between the soil probe and side ports. The source gas was plumbed into the reservoir with 0.635 cm diameter Teflon tubing. A swagelock T connection, capped with a septum, was inserted between the regulator and a needle valve. This connection provided a point along the Teflon line to sample the source gas.

Test: We used the sand column to test the soil probe and static chamber methods in their ability to measure the isotopic composition of an isotopic source diffusing through the sand column. The source gas was a house standard of CO_2 mixed with N_2 yielding an isotopic value of -34.2‰ and CO_2 concentration of 3000ppm (± 2%). We hypothesized that for CO_2 diffusing at steady-state both methods will estimate the source gas isotopic composition. At steady-state we expected to observe the theoretical 4.4‰ offset between the source gas and the Keeling intercepts we generated for the soil probe and control ports.

The experiment was run over a 7 hour period during which the static chamber, soil probe and control ports were sampled at 2.5 hours and 7 hours. Source gas was sampled via an in-line T-connector near the tank regulator at 2.5 and 7 hours. For each gas sample, a syringe needle was inserted into a septum and 12 mL of sand column gas was withdrawn. The syringe needle was left in the sampling port for at least 30 seconds to allow for equilibration. The gas samples were then injected into a pre-evacuated (100 militorr) 12 mL exetainer (Labco Exetainer®, High Wycombe, UK). Two samples were withdrawn within three minutes of each other for each depth of the soil probe and control ports and headspace of the static chamber.

We took measures to make sure the gas transport was only diffusive through the sand column. If the transport mechanism was advective, mass flow due to a pressure gradient, then a higher concentration of $^{13}CO_2$ would be present in the isotopic signal of the CO_2 emitting from the surface, violating the assumptions of the tested measurement techniques (i.e. the fractionation factor due to diffusion would be less than the -4.4‰). To avoid advection from a pressure build up in the sand column due to source gas flow, we plumbed a pressure release tube into the reservoir space that terminated into a flask of water. The pressure release tube ensured that the pressure in the reservoir was always close to atmospheric pressure.

Sample analysis: All gas samples were run at the Idaho Stable Isotopes Laboratory (ISIL). A gas autosampler (GC Pal, CTC Analytics, Zwingen, Switzerland) is used to sample CO_2 from the exetainers which is vented to a isotope ratio mass spectrometer (Delta+ XP, ThermoElectron Corp., Bremen, Germany) via a gas interface (Gas Bench II, ThermoElectron Corp., Bremen, Germany). Standardized CO_2 gasses are analyzed every nine samples for assurance of stability, drift correction, and calculation of CO_2 concentration.

Results and Discussion

To test the measurement techniques, CO_2 transport within the sand column was required to be diffusive and at steady-state. The CO_2 concentration gradient was linear from the

sand surface to the bottom reservoir of the sand column (Figures 2.1A & 2.2A), as expected from a purely diffusive system (Camarda et al. 2007), and concentrations predicted by a steady-state model for bulk soil (Cerling et al. 1991) were similar (Figure 2.3), indicating that CO_2 transport was diffusive. To determine if the CO_2 flux was at isotopic steady-state, we compared the gas samples from the control ports collected after 7 hours with a steady-state isotopic model (Amundson et a. 1998) (Figure 2.4). The isotopic values were depleted by at least 1.1‰ with reference to the predicted values, indicating the sand column was at near-steady state. The isotopic gradient in the sand column has a curvilinear pattern, which is what we would expect from a two CO_2 sources mixing (Faure 1986), and the average change in isotopic value over a five hour period is less than 0.60‰.The isotopic values of CO_2 at lower depths in the sand column are more depleted than the predicted values and become more enriched over time. This pattern, as predicted by simulations of CO_2 transport (Amundson et al. 1998), is explained by $^{12}CO_2$ arriving at steady-state before $^{13}CO_2$. Overall, the sand column system did not interfere with the analysis and successfully reproduced a purely diffusive system allowing for future comparisons of measurement techniques.

To evaluate any effects the soil probe might have on the composition of CO_2, we compared samples from the soil probe and samples from the control ports. The isotopic composition and concentrations of CO_2 from the three depths of the soil probe fell on the same concentration and mixing lines (Figures 2.1B & 2.2B) as the control ports, and therefore reflected the same $\delta^{13}CO_2$ signature derived from the Keeling plot (Table 2.1). Thus, the soil probe did not alter the isotopic composition or concentration of soil gas. There was very little variation between the first and second samples taken at each depth (Figures 2.1A & 2.2B) for the soil probe and control ports. This suggests that the probe can equilibrate with the surrounding soil gas within five minutes and may therefore capture diurnal variation in field studies.

The static chamber at equilibrium estimate of the source gas was enriched by 13‰ in our experiment. The concentration and isotopic signature of the CO_2 in the chamber at the 2.5 and 7 hour sampling resembles values of the soil probe at 5 cm (Figures 2.1A & 2.2A). The results from this study agree with the results of Mora and Raich (2007) who found the isotopic composition in the static chamber headspace to

reach equilibrium after an extended period of time, however, the isotopic composition of the gas in the static chamber did not accurately reflect that of the source gas. As depicted by the isotopic and concentration profile, the signal in the static chamber at equilibrium is more likely from soil gas at the depth to which the chamber was inserted. The same conclusions were drawn concerning the insertion depth of the chamber in a similar test of a dynamic chamber method on a sand column (Bertolini et al. 2006). While the chamber value did not equal the isotopic source in our experiment, the chamber value did fall on the same mixing line (Figures 2.1B & 2.2B) derived from the control port samples, indicating the chamber could be used in a Keeling plot with the addition of a sample of the atmosphere (Table 2.1).

For all sampling methods, the Keeling intercepts were enriched with reference to the source gas, but the fractionation factors after seven hours were -2.6 ± 0.1‰, slightly more than half the theoretical value of -4.4‰ (Table 2.1). Figure 2.5 depicts a hypothetical steady-state mixing line that would be approached at steady-state if the theoretical diffusive fraction factor of -4.4‰ applies. We can estimate the time to achieve isotopic stead-state for the sand column, based on our existing data, assuming that the approach to equilibrium follows an exponential function,

$$\Delta_{\delta^{13}C} = 4.4e^{-\left(\frac{1}{\tau}*T\right)} - 4.4 \qquad (3)$$

where τ is the exponential time constant of the system, and T is the time since the beginning of the experiment. A good fit to the data in Table 1 is obtained for τ=8 hours, implying that an approach to steady-state would only occur after ~48 hours. Given well known temporal variability in soil flux rates over a diurnal cycle (Liu et al. 2006; Hibbard et al. 2005) it is unlikely that real-world soil systems ever reach a true isotopic steady-state with respect to diffusion. This means that field studies that employ isotopic methods to fingerprint sources of CO_2 from soils relative to vegetation must consider non steady-state effects.

Although our system did not reach isotopic steady-state over the 7 hours the experiment was conducted, the overall experiment was still able to demonstrate the feasibility of both the static chamber and soil probe techniques. We have shown that the static chamber can be applied when in equilibrium with the soil gas though only through

a Keeling plot approach. However, implementing only two points in a regression for a Keeling plot does not provide enough degrees of freedom for the evaluation of uncertainty in the Keeling intercept. The soil probe we used in this experiment has three wells, but has the potential for multiple wells, to draw samples from within the soil which allows for error estimates of the intercept at the cost of increased mass spectrometer time and labor.

The soil probe has the added benefit of providing samples of soil gas that describe the soil profile. The CO_2 soil profile has been shown to be useful in describing advective and diffusive boundaries (Lewicki et al. 2003), soil flux (Jassal et al. 2005) and the effects of meteorological fluctuations on soil gas transport (Risk et al. 2002; Tackle et al. 2004; Flechard et al. 2007). Davidson et al. (2006), used the soil CO_2 profile to determine soil productivity at different soil depths to discern different contributions to soil respiration. The soil probe could be applied in the same manner to evaluate the isotopic composition of each depth within the soil to provide information regarding isotopic partitioning of soil respiration. For example, in a separate experiment we injected 60 ml of ambient air into the sand column at 30 cm depth and collected five samples over a 25 minute period. These samples were used in a Keeling plot to identify the isotopic signal of soil gas at the 30cm depth. This approach measures the isotopic composition of production at a certain depth. To clarify, the isotopic signal measured here contributes to the isotopic signal of the well mixed source of the entire sand column which is identified via a Keeling plot as the isotopic signal of soil respiration. In this initial test, the difference between the Keeling intercept and control port value was less than 1‰ (-36.0‰ calculated value vs. -35.3‰ control port value at 30cm), indicating that, with further refinement and replication, this technique could be a viable method towards soil component partitioning.

Conclusions

Using both static chamber at equilibrium and soil probe sampling techniques we calculated the same Keeling intercept as the control ports. The soil probe provides additional information through CO_2 soil profiles and estimates of uncertainty for the

Keeling intercept. After 7 hours of diffusive gas transport, CO_2 in the sand column was not at isotopic steady-state, and as a result the apparent fractionation with diffusive transport was not fully expressed. Based on the samplings at 2.5 and 7 hours after initiating the experiment, we calculate an equilibrium exponential time constant of about 8 hours suggesting that the approach to isotopic steady-state with respect to diffusion would take about 48 hours. If our sand column experiment is representative of soil gas diffusion in more complex real-world situation with diurnal cycles of temperature and CO_2 production, our study implies that it is unlikely that these soil systems to ever reach isotopic steady-state with respect to diffusion. This means that field studies that use carbon isotope signatures to fingerprint CO_2 sources on timescales of less than a few days will have to consider the dynamics of carbon fluxes in diffusive systems.

The inferences drawn from the experiment are limited to the imposed conditions of a carbonless sand medium of homogenous physical properties, no moisture content, a single gas source, and a single concentration gradient. However, the soil matrix is complex in physical and biological properties rendering simple laboratory exercises, such as the experiment presented here, a requisite to identifying the optimal method of sampling.

Acknowledgements

Funding for this research was provided by the National Science Foundation (grants DEB 0132737, DEB 0416060) and the Ecoinformatics IGERT at OSU. We thank Renee Brooks, Claire Phillips and two anonymous reviewers for helpful comments on the manuscript. We also thank Benjamin Miller of ISIL and Andrew Ross of the COAS mass spectrometer lab for their assistance in running samples.

References

Amundson, R., L. Stern, T. Baisden and Y. Wang.1998. The isotopic composition of soil and soil-respired CO_2. Geoderma 82(1-3): 83-114.

Bertolini, T., I. Inglima, M. Rubino, F. Marzaioli, C. Lubritto, J. A. Subke, A. Peressotti and M. F. Cotrufo.2006. Sampling soil-derived CO2 for analysis of isotopic composition: a comparison of different techniques. Isotopes in Environmental and Health Studies 42(1): 57-65.

Bowling, D. R., N. G. McDowell, B. J. Bond, B. E. Law and J. R. Ehleringer.2002. ^{13}C content of ecosystem respiration is linked to precipitation and vapor pressure deficit. Oecologia 131(1): 113-124.

Breecker, D. and Z. Sharp.2008. A field and laboratory method for monitoring the concentration and isotopic composition of soil CO_2. Rapid Communications in Mass Spectrometry 22(4): 449-454.

Camarda, M., S. De Gregorio, R. Favara and S. Gurrieri.2007. Evaluation of carbon isotope fractionation of soil CO_2 under an advective-diffusive regimen: A tool for computing the isotopic composition of unfractionated deep source. Geochimica Et Cosmochimica Acta 71(12): 3016-3027.

Cerling, T. E., D. K. Solomon, J. Quade and J. R. Bowman.1991. On the Isotopic Composition of Carbon in Soil Carbon-Dioxide. Geochimica Et Cosmochimica Acta 55(11): 3403-3405.

Davidson, E. A., K. E. Savage, S. E. Trumbore and W. Borken.2006. Vertical partitioning of CO_2 production within a temperate forest soil. Global Change Biology 12(6): 944-956.

DeSutter, T. M., T. J. Sauer, T. B. Parkin and J. L. Heitman.2008. A subsurface, closed-loop system for soil carbon dioxide and its application to the gradient efflux approach. Soil Science Society of America Journal 72(1): 126-134.

Ekblad, A. and P. Högberg .2000. Analysis of delta ^{13}C of CO_2 distinguishes between microbial respiration of added C-4-sucrose and other soil respiration in a C-3-ecosystem. Plant and Soil 219(1-2): 197-209.

Evans, W. C., M. L. Sorey, B. M. Kennedy, D. A. Stonestrom, J. D. Rogie and D. L. Shuster.2001. High CO_2 emissions through porous media: transport mechanisms and implications for flux measurement and fractionation. Chemical Geology 177(1-2): 15-29.

Faure, G.1977. Principles of Isotope Geology. New York, NY, USA, John Wiley and Sons.

Flechard, C. R., A. Neftel, M. Jocher, C. Ammann, J. Leifeld and J. Fuhrer.2007. Temporal changes in soil pore space CO_2 concentration and storage under permanent grassland. Agricultural and Forest Meteorology 142(1): 66-84.

Hibbard, K. A., B. E. Law, M. Reichstein and J. Sulzman.2005. An analysis of soil respiration across northern hemisphere temperate ecosystems. Biogeochemistry 73(1): 29-70.

Jassal, R., A. Black, M. Novak, K. Morgenstern, Z. Nesic and D. Gaumont-Guay.2005. Relationship between soil CO_2 concentrations and forest-floor CO2 effluxes. Agricultural and Forest Meteorology 130(3-4): 176-192.

Lewicki, J. L., W. C. Evans, G. E. Hilley, M. L. Sorey, J. D. Rogie and S. L. Brantley.2003. Shallow soil CO_2 flow along the San Andreas and Calaveras Faults, California. Journal of Geophysical Research-Solid Earth 108(B4).

Liu, Q., N. T. Edwards, W. M. Post, L. Gu, J. Ledford and S. Lenhart.2006. Temperature-independent diel variation in soil respiration observed from a temperate deciduous forest. Global Change Biology 12(11): 2136-2145.

Mora, G. and J. W. Raich.2007. Carbon-isotopic composition of soil-respired carbon dioxide in static closed chambers at equilibrium. Rapid Communications in Mass Spectrometry 21(12): 1866-1870.

Mortazavi, B., J. L. Prater and J. P. Chanton.2004. A field-based method for simultaneous measurements of the $\delta^{18}O$ and $\delta^{13}C$ of soil CO_2 efflux. Biogeosciences 1(1): 1-9.

Ohlsson, K. E. A., S. Bhupinderpal, S. Holm, A. Nordgren, L. Lovdahl and P. Högberg .2005. Uncertainties in static closed chamber measurements of the carbon isotopic ratio of soil-respired CO_2. Soil Biology & Biochemistry 37(12): 2273-2276.

O'leary, M. H., S. Madhavan and P. Paneth.1992. Physical and chemical basis of carbon isotope fractionation in plants. Plant Cell and Environment 15(9): 1099-1104.

Pataki, D. E., J. R. Ehleringer, L. B. Flanagan, D. Yakir, D. R. Bowling, C. J. Still, N. Buchmann, J. O. Kaplan and J. A. Berry.2003. The application and interpretation of Keeling plots in terrestrial carbon cycle research. Global Biogeochemical Cycles 17(1).

Risk, D., L. Kellman and H. Beltrami.2002. Soil CO_2 production and surface flux at four climate observatories in eastern Canada. Global Biogeochemical Cycles 16(4).

Risk, D., L. Kellman and H. Beltrami.2008. A new method for in situ soil gas diffusivity measurement and applications in the monitoring of subsurface CO_2 production. Journal of Geophysical Research-Biogeosciences 113(G2).

Steinmann, K. T. W., R. Siegwolf, M. Saurer and C. Korner.2004. Carbon fluxes to the soil in a mature temperate forest assessed by ^{13}C isotope tracing. Oecologia 141(3): 489-501.

Takle, E. S., W. J. Massman, J. R. Brandle, R. A. Schmidt, X. H. Zhou, I. V. Litvina, R. Garcia, G. Doyle and C. W. Rice.2004. Influence of high-frequency ambient pressure pumping on carbon dioxide efflux from soil. Agricultural and Forest Meteorology 124(3-4): 193-206.

Tu, K. and T. Dawson.2005. Partitioning Ecosystem Respiration Using Stable Carbon Isotope Analyses of CO_2. Stable Isotopes and Biosphere-Atmoshpere Interactions. J J. R. Ehleringer, D.E. Pataki, L.B. Flanagan (eds). San Francisco, Ca, USA, Elsevier.

Widen, B. and A. Lindroth.2003. A calibration system for soil carbon dioxide efflux measurement chambers: Description and application. Soil Science Society of America Journal 67(1): 327-334.

Zobitz, J. M., J. P. Keener, H. Schnyder and D. R. Bowling.2006. Sensitivity analysis and quantification of uncertainty for isotopic mixing relationships in carbon cycle research. Agricultural and Forest Meteorology 136(1-2): 56-75.

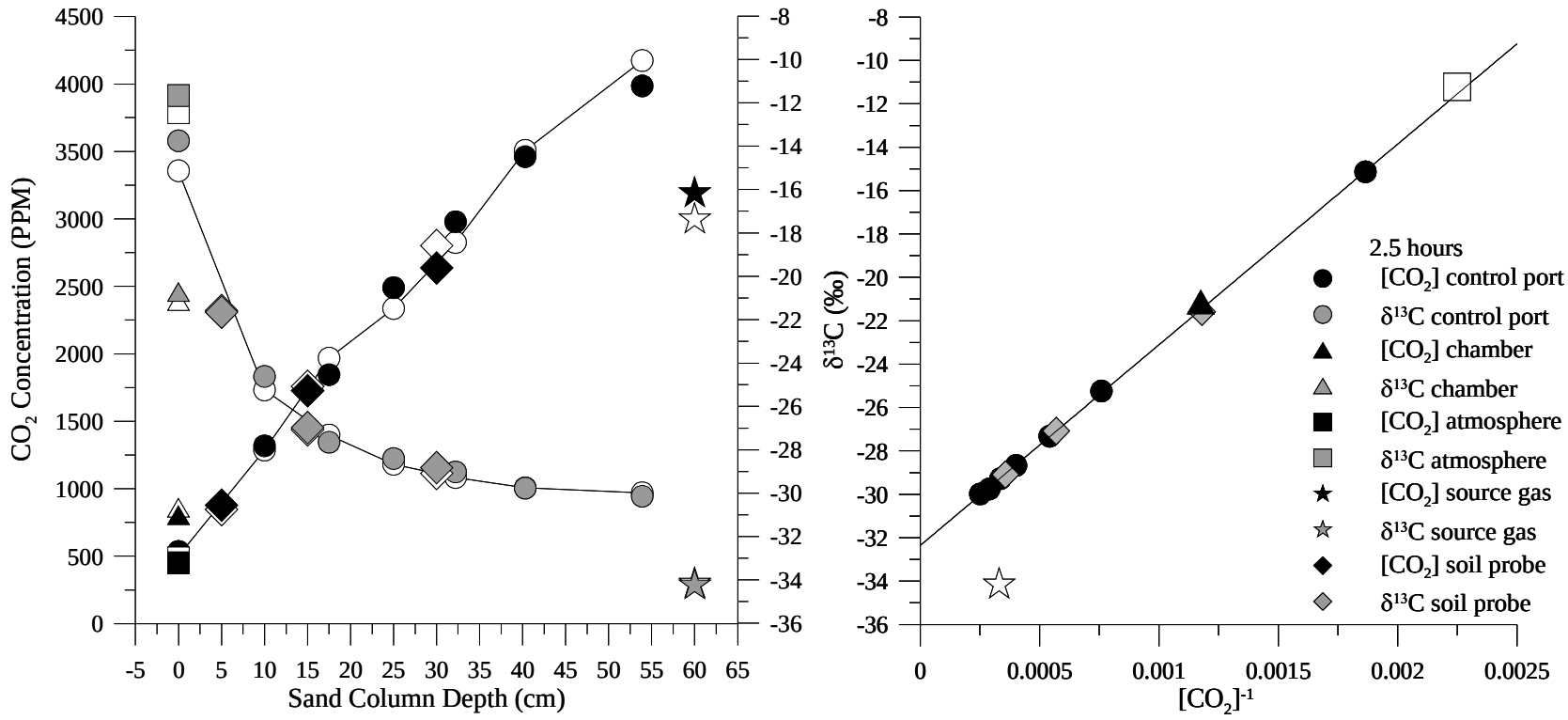

Figure 2.1: Sand column concentration and isotopic profiles after 2.5 hours of diffusion. A) Concentration (black) and ^{13}C (grey) gradient after 2.5 hours of diffusion of a known gas source in a 60cm column of quartz sand. The trend line refers to the bulkheads. Two gas samples were withdrawn at each depth, the solid symbol is one sample and the open symbol is the other. B) Keeling plot of bulkhead gas samples for the concentration and isotopic data. The soil probe, static chamber and atmospheric sample were not included in calculating the mixing line.

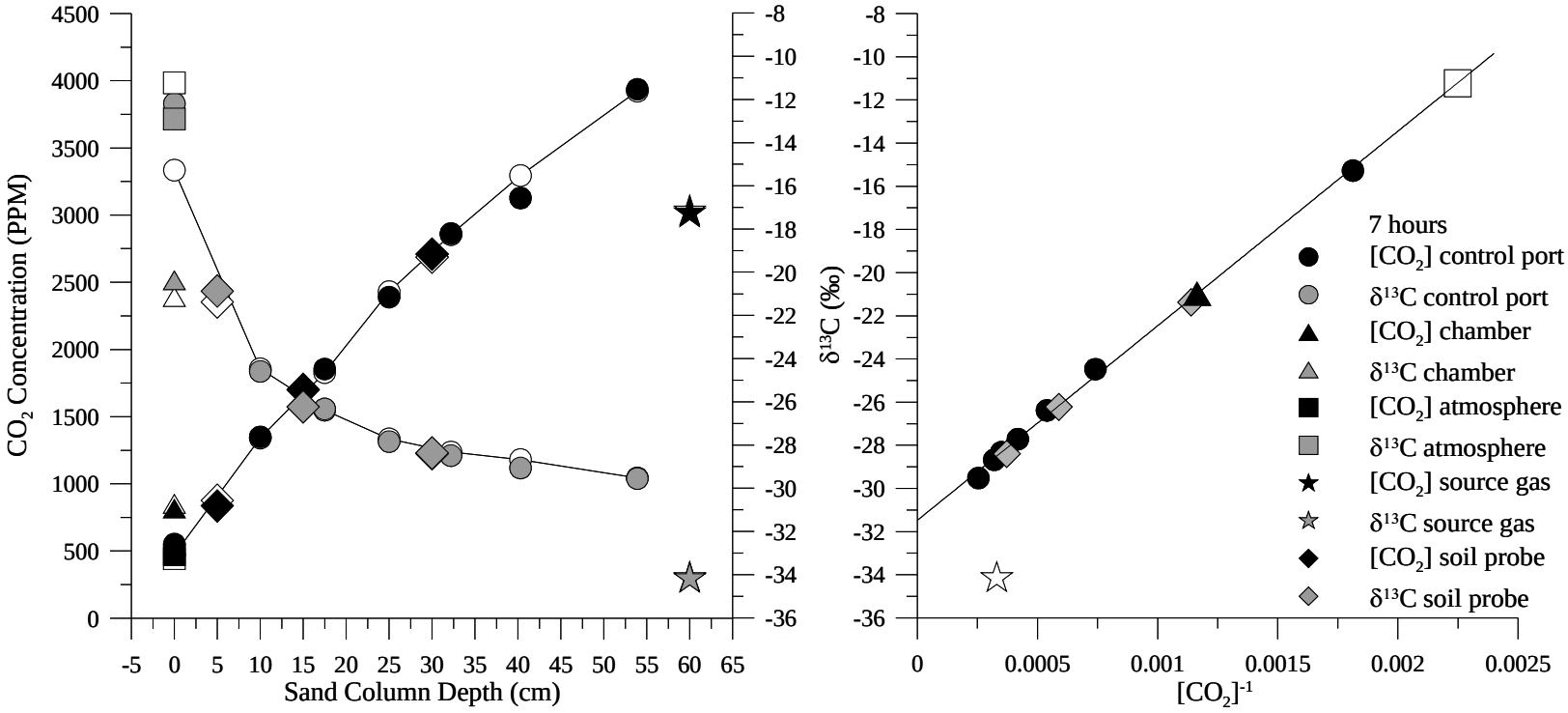

Figure 2.2: Sand column concentration and isotopic profiles after 7 hours of diffusion. A) Concentration (black) and ^{13}C (grey) gradient after 7 hours of diffusion of a known gas source in a 60cm column of quartz sand. The trend line refers to the bulkheads. Two gas samples were withdrawn at each depth, the solid symbol is one sample and the open symbol is the other. B) Keeling plot of bulkhead gas samples for the concentration and isotopic data. The soil probe, static chamber and atmospheric sample were not included in calculating the mixing line.

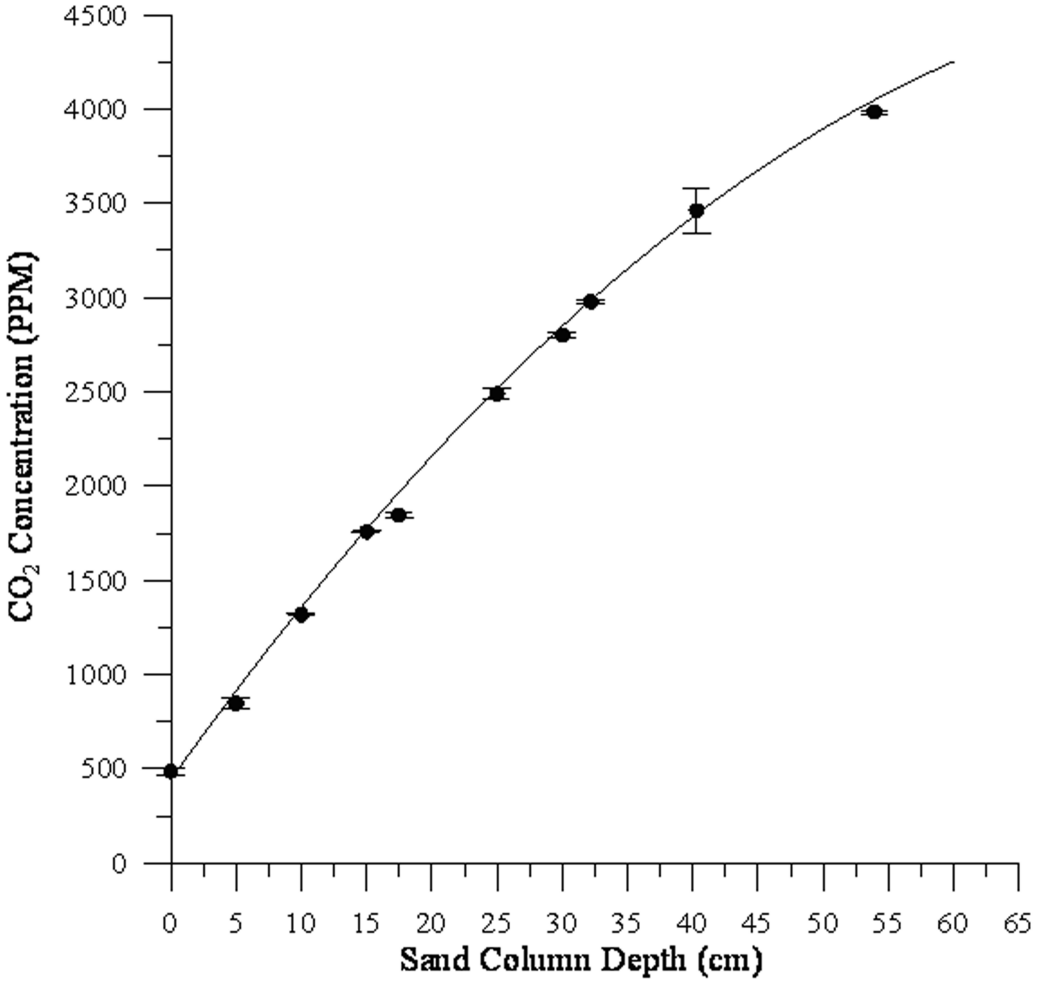

Figure 2.3 Predicted sand column CO_2 profile concentrations. Measured sand column CO_2 concentration values versus concentration values predicted by the steady-state model of Cerling et al. (1991) for a rate of production of 2.5×10^{-12} mol $m^{-3}s^{-1}$ and lower flux boundary of 85cm.

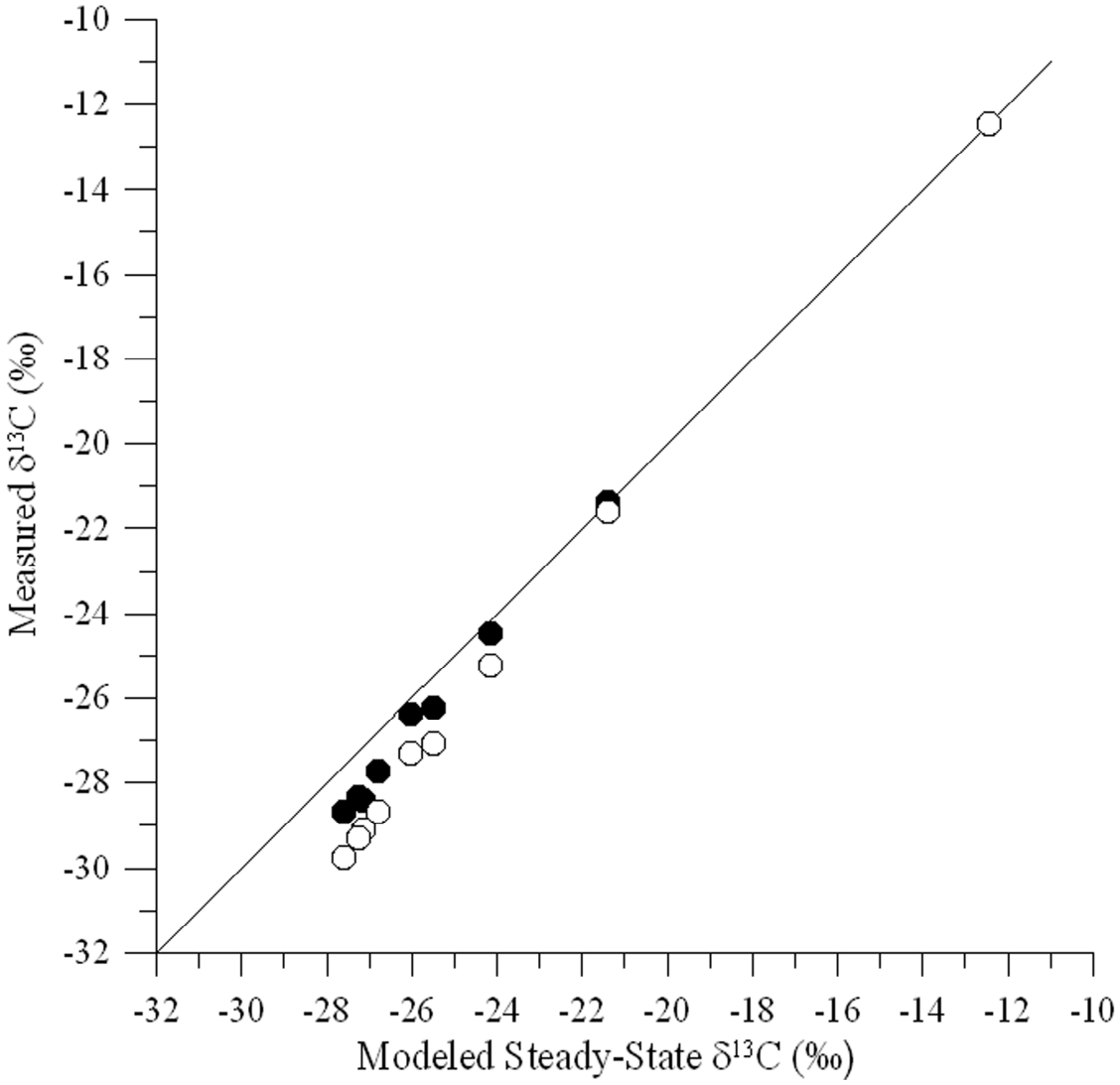

Figure 2.4: Predicted sand column isotopic profile. Measued sand column $^{13}CO_2$ values versus isotopic values predicted by the steay-state model of Amundson et al. (1998) for a rate of production of 2.5 x 10^{-12} mol $m^{-3}s^{-1}$ and lower flux boundary of 85cm.

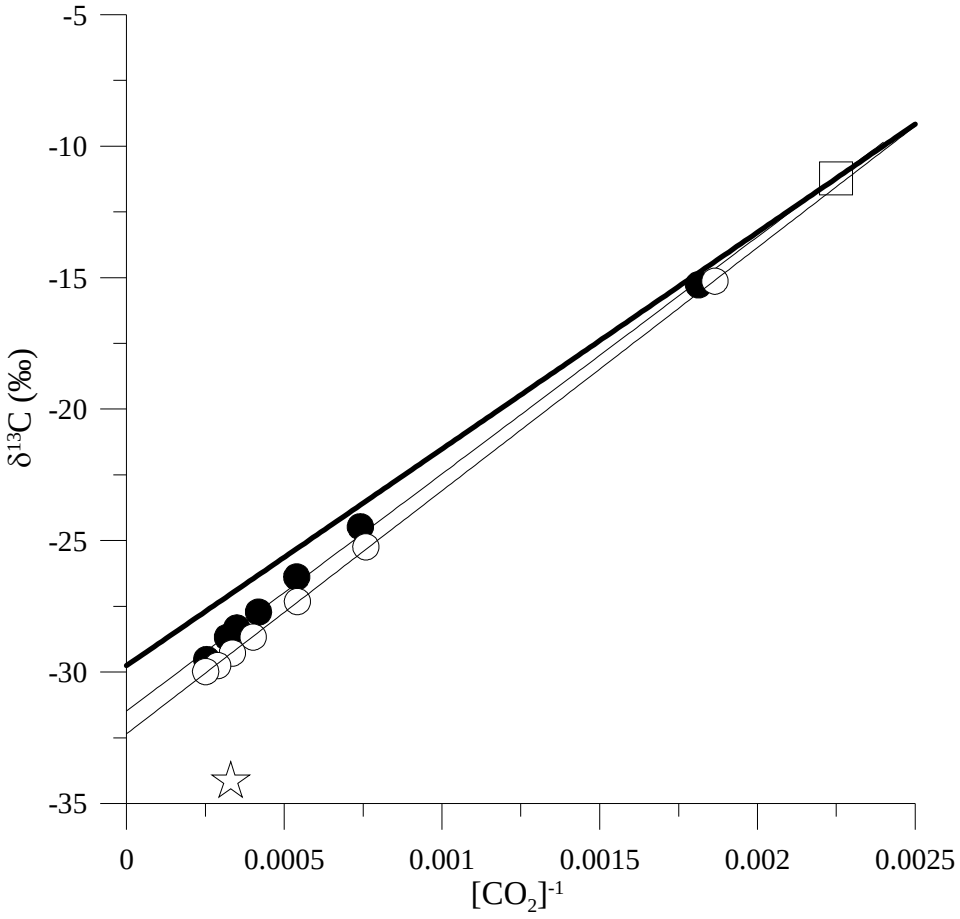

Figure 2.5: Keeling mixing lines of control port samples after 2.5h (open symbols) and 7 h (filled symbols) of diffusion of a known gas source in a 60cm column of quartz sand. The square symbol is the atmospheric value and the bold line is the theoretical mixing line that is needed to achieve a 4.4‰ offset from the gas source (star).

Table 2.1: Keeling intercept values (‰) for the soil probe, static chamber and control ports. The standard errors calculated from bootstrapping the Keeling plot (10,000 iterations) are in parenthesis. The Keeling intercepts are uncorrected since the sand column was at near steady-state. Fractionation factors (Δ) represent the difference between the source gas and the Keeling intercept. The static chamber Keeling intercept was calculated with two samples which did not allow for an estimate of intercept error.

Sampling Method	Keeling intercept 2.5 hours (‰)	Δ (‰)	Keeling intercept 7 hours (‰)	Δ (‰)
Control Ports	-32.5 (0.13)	-1.7	-31.6 (0.12)	-2.6
Soil Probe	-32.4 (0.05)	-1.8	-31.6 (0.14)	-2.6
Static Chamber	-32.2 NA	-2.0	-32.0 NA	-2.2

Chapter 3 Bias and uncertainty of ^{13}C isotopic mixing models applied to experimental conditions in small vs. large CO_2 concentration regimes

Zachary Kayler, Lisa Ganio, Mark Hauck, Thomas Pypker, Elizabeth W. Sulzman, Alan Mix and Barbara J. Bond.

Prepared for Submission to Oecologia

Abstract

Two-component mixing models are used to identify the isotopic signal of respiration ($\delta^{13}C_R$). While reports on the accuracy and precision of $\delta^{13}C_R$ of ecosystems exist, there is a paucity of studies concerning the $\delta^{13}C_R$ of soil, foliage or tree boles, where the [CO_2] values and ranges tend to be several orders of magnitude greater. Using a simulation approach, we show that it is important to distinguish between large (> 1000 μmol mol^{-1}) and small (< 100 μmol mol^{-1}) CO_2 concentration regimes when applying a mixing model (Keeling plot or Miller-Tans) and regression approach (ordinary least squares or geometric mean regression) combination to isotopic data. We found the combination of geometric mean regression and the Miller-Tans mixing model to provide the most accurate and precise estimate of $\delta^{13}C_R$ when the range of [CO_2] is equal to or greater than 1000 μmol mol^{-1}. The patterns of model bias and uncertainty for this concentration regime were primarily driven by CO_2 concentration ([CO_2]) error, but were markedly improved to estimates within 1‰ when the concentration range was 5000 μmol mol^{-1} and greater. For small concentration regimes, the Keeling or Miller-Tans model used with ordinary least squares resulted in the least biased estimate of $\delta^{13}C_R$ when concentration error was small (<1 μmol mol^{-1}). However, for large concentration error levels we found the ordinary least squares estimate could have a positive bias. The geometric mean regression bias was negative when the isotopic error was large and [CO_2] error was small. The bias was positive when the isotopic error was low and [CO_2] error was large. We found Keeling plot estimates of $\delta^{13}C_R$ in small [CO_2] regimes will improve if samples are uniformly distributed over the inverted concentration range.

Introduction

Significant advancement toward understanding ecosystem carbon metabolism has been accomplished through the analysis of the carbon isotopic signature of respired CO_2 ($\delta^{13}C_R$). For example, measurements of $\delta^{13}C_R$ of forest ecosystems have been used to explore the seasonal and short-term effects of moisture stress on ecosystem respiration

(Bowling et al. 2002; McDowell et al. 2004; Pypker et al. 2008), the close coupling between above-ground and below-ground carbon metabolism (Steinmann et al. 2004, Ekblad et al. 2005, Scartazza et al. 2004), the contributions of autotrophic versus heterotrophic respiration (Högberg et al. 2001) and the effects of tree age on forest metabolism (Fessenden and Ehleringer 2002).

The carbon isotopic signal of respiration is the ratio of $^{13}C/^{12}C$ of CO_2 produced from the oxidation of organic carbon molecules that occurs in cells of organisms from the ecosystem, soil or tissue of study. At ecosystem scales, it is difficult, if not impossible to acquire representative samples of respired CO_2 directly. Keeling (1958) introduced a clever approach that involves analysis of multiple samples of ambient air mixed with respired CO_2 in different proportions. Carbon dioxide concentrations ($[CO_2]$) and carbon isotope composition of multiple samples are plotted against each other, resulting in a mixing hyperbola from which a mixing equation can be derived when the data are transformed to be linear (Faure 1977). Regression models are typically used with mixing models to determine the parameters of the mixing equation. In general, this mixing model and regression approach involves two assumptions: 1) there are only two sources of $^{13}CO_2$: the source of respiration and the background signal, and 2) the isotope ratios of the source and background do not change over the measurement period (Pataki et al. 2003).

In most terrestrial ecosystems, the proportion of respired CO_2 relative to the atmospheric background is small; thus the CO_2 concentration of samples is typically near that of the ambient atmosphere and the range of $[CO_2]$ values ($[CO_2]_{range}$) collected in any given sample period is usually less than 100 μmol mol^{-1}. In contrast, the $[CO_2]_{range}$ is typically around 500 μmol mol^{-1} for samples collected from foliar respiration (Xu et al. 2004), 1,000 - 10,000 μmol mol^{-1} from soil respiration studies (Ohlsson et al. 2005; Mortazavi et al. 2004), and 20,000 - 30,000 μmol mol^{-1} from studies concerning human respiration and car exhaust (Affek and Eiler 2006). Because both the $[CO_2]_{range}$ as well as the sample values of $[CO_2]$ vary dramatically in these different applications, and because the $[CO_2]_{range}$ may affect the uncertainty and precision of regression analyses, we distinguish between "small " $[CO_2]_{range}$ and "large" $[CO_2]_{range}$ regimes in this study.

Two mixing models are typically used to estimate $\delta^{13}C_R$ in ecological studies, the Keeling plot and the Miller-Tans model (Miller and Tans 2003) (these are further described in the methods section). Rigorous comparisons have been conducted to determine whether one or the other model is preferable when applied to small $[CO_2]_{range}$ regimes; in most cases the uncertainty and precision of the two models are similar (Pataki et al. 2003, Zobitz et al. 2006), and by convention Keeling plots are primarily used (Tu and Dawson 2005). Researchers also commonly apply the Keeling mixing model to large $[CO_2]_{range}$ regime; however, rigorous comparisons of the models have not been conducted for cases when the range of CO_2 values is broad. Our primary objective of this study was to compare the two models for large $[CO_2]_{range}$ situations.

The best mixing model will produce the most accurate and precise estimate of $\delta^{13}C_R$, where accuracy is defined as the nearness of a measurement to the true value, and precision is defined as the degree to which repeated measurements yield the same value (Zar 1999). Thus, the optimal mixing model will minimize the effect of the variation due to both measurement error and the natural heterogeneity of the system (genetic variation, spatial and temporal heterogeneity, etc) such that the estimate is accurate within 1‰ (O'Leary 1992). This level of accuracy will be able to detect true variability in seasonal patterns of $\delta^{13}C_R$ of forest ecosystem respiration that varies on the order of 3 to 4‰ seasonally (Fessenden and Ehleringer 2002; Pypker et al. 2008), soil and tree bole respiration which varies 1 to 3‰ (Maunoury et al. 2007; Mortazavi et al. 2004), and foliar respiration that can have seasonal differences can be up to 10‰ (Prater et al. 2006; Xu et al. 2004).

Previous studies have analyzed the uncertainty and precision of estimates of $\delta^{13}C_R$ when mixing models are applied to small $[CO_2]_{range}$ systems (Pataki et al. 2003, Zobitz et al. 2006). From this research we have learned that the choice of the regression approach used with either of the mixing models can impact the estimate of $\delta^{13}C_R$. The ordinary least squares (OLS) and geometric mean regression (GMR) are the regression models typically used with either of the mixing models (Pataki et al. 2003; Zobitz et al. 2006). The OLS and GMR estimator have fundamentally different assumptions about error in the independent and dependent variables. When OLS is used to estimate regression parameters, the uncertainty of the estimators relies on the assumption that the

independent variable in the regression ($[CO_2]$ for Miller-Tans and $1/[CO_2]$ for Keeling) is measured without error. Because there are errors associated with both the independent and dependent variables in Keeling Plot analyses, Pataki et al. (2003) suggested using GMR with the mixing model. However, Bowling et al. (2003) found GMR produces estimates of $\delta^{13}C_R$ that are negatively biased; this was subsequently confirmed by Zobitz et al. (2006). Due to this bias in small $[CO_2]_{range}$ regimes, both Bowling et al.(2003) and Zobitz et al.(2006) recommended the Keeling-OLS mixing model.

The accuracy and precision of mixing models applied to large $[CO_2]_{range}$ regimes may not be similar for small $[CO_2]_{range}$ regimes. Previous studies have shown that the larger concentration gradient (i.e., greater range of x values), should reduce the uncertainty of estimates of $\delta^{13}C_R$ (Ohlsson et al. 2005), but estimates of $\delta^{13}C_R$ in large $[CO_2]_{range}$ have not been discussed in the context of measurement or sampling error. It is often assumed that a larger range of $[CO_2]$ values also implies that a smaller number of samples could be used while maintaining a given level of uncertainty and precision in estimates of $\delta^{13}C_R$. Indeed, researchers typically use a much smaller number of samples for each regression analysis in studies of foliar or soil respiration (large $[CO_2]_{range}$ regimes) than in studies of ecosystem respiration (Tu and Dawson 2005), allowing them to estimate $\delta^{13}C_R$ both spatially and temporally. However, this tradeoff between the $[CO_2]_{range}$ and the sample size has not been investigated.

Complicating this tradeoff further is the degree of measurement error in both $[CO_2]$ and the $\delta^{13}C$ values. The precision of the $[CO_2]$ measurements by infrared gas analyzers is on the order of 0.1 to 1 $\mu mol\ mol^{-1}$ (Miller and Tans 2003, Hauck 2006). The gas standards used to calibrate gas analyzers, however, are typically accurate within 2% or greater of the target value, which represents an error of potentially several hundred $\mu mol\ mol^{-1}$ in large $[CO_2]_{range}$ regimes and should therefore be included in the analysis of mixing model performance. The precision of isotopic measurements is largely determined by the method of analysis (i.e. isotope ratio mass spectrometer, tunable diode laser, etc); and while the precision of each machine varies from laboratory to laboratory, a reasonable upper level estimate of the uncertainty of these instruments is on the order of 0.2‰ or less.

The goal of this study was to evaluate how factorial combinations of two mixing models and two regression approaches (Keeling-OLS, Miller-Tans-OLS, Keeling-GMR, Miller-Tans- GMR) compare in small $[CO_2]_{range}$ vs. large $[CO_2]_{range}$ regimes, with different combinations of pertinent variables ($[CO_2]_{range}$, $[CO_2]$ error, $\delta^{13}C$ error and *n*) that are realistic for experimental applications in each of the two regimes (Figure 1). Our approach was to conduct a series of simulations using artificial datasets. From these simulations we report 1) how the bias and uncertainty of estimates of $\delta^{13}C_R$ in large concentration and small concentration regimes differ, 2) which simulation input variables influence $\delta^{13}C_R$ bias and uncertainty, and 3) which mixing and regression model produces the least bias and uncertainty when applied to samples from large $[CO_2]_{range}$ systems.

Methods

Mixing models

The two mixing models we examined are based on the conservation of mass, describing a sample as a mixture of two sources of $^{13}CO_2$: the background atmosphere and the source of respiration. The Keeling linear mixing model equation that relates the observed $\delta^{13}C$ to the observed $[CO_2]$ is given in Equation 1.

$$\delta_{obs} = \frac{C_{bg}}{C_{obs}}\left(\delta_{bg} - \delta_s\right) + \delta_s \qquad \text{(eq.1)}$$

Where C is $[CO_2]$ and the subscripts *obs*, *s*, and *bg* refer to the observed, source and background values, respectively. In Equation 1, δ refers to the isotopic value of the component expressed in δ notation: $\delta = (R_{sample} / R_{standard} - 1) * 1000‰$, where R is the molar ratio of heavy to light isotopes. The carbon isotope ratio ($^{13}C/^{12}C$) is expressed relative to the standard Vienna Pee Dee Belemnite. The estimate of source $\delta^{13}C_R$ is obtained as the intercept of this linear model, regressing δ_{obs} vs. $1/[CO_2]$.

Using the same principles of conservation of mass, Miller and Tans (2003) derived a different linear mixing model equation, given in Equation 2.

$$\delta_{obs} C_{obs} = \delta_s C_{obs} - C_{bg}(\delta_{bg} - \delta_s) \qquad \text{(eq.2)}$$

In this case, $\delta^{13}C_R$ is estimated as the slope of the regression line of $\delta_{obs} \times [CO_2]_{obs}$ vs. $[CO_2]$ rather than the intercept of δ vs. $1/[CO_2]$, as in eq. 1.

Regression Approaches

The OLS model is:

$$y = \alpha + \beta x + \varepsilon \quad \text{(eq. 3)}$$

Where α is the intercept, β is the slope, x= $[CO_2]$ data, y= $\delta^{13}C$ data and ε is a normally distributed term from a distribution with mean zero and variance σ^2. The slope of the line is estimated by minimizing the sum of squared vertical deviations from the observed data to the estimated line.

$$\hat{\beta} = \frac{\sum (x_i - \bar{x})(y_i - \bar{y})}{\sum (x_i - \bar{x})^2} \text{(eq. 4)}$$

The intercept of OLS is estimated as:

$$\hat{\alpha} = \overline{Y} - \hat{\beta}\overline{X} \quad \text{(eq. 5)}$$

Estimates for standard errors of the OLS slope and intercept are based on the normality assumption of the ε_i.

Geometric mean regression assumes there is a measurement error associated with the independent variable as well as the dependent variable. GMR is a special case of orthogonal regression (OR) in which orthogonal deviation from the regression line are minimized, not vertical deviations. GMR has the formula:

$$y_{gmr} = \alpha_{gmr} + \beta_{gmr}(X + \delta) + \varepsilon \quad \text{(eq. 6)}$$

Where x, y, α, β and ε are defined as before, and δ is the normally distributed term from a distribution with mean zero and variance σ_x^2. The slope is estimated as the sample standard deviation of Y divided by the sample standard deviation of X:

$$\hat{\beta}_{gmr} = \frac{S_Y}{S_x} \quad \text{(eq. 7)}$$

and takes the sign (+ or -) of the linear correlation coefficient (r). The GMR slope can also be estimated as the geometric mean of the OLS slope from *y* regressed on *x* and the OLS slope of *x* regressed on *y*. The GMR intercept is estimated as:

$$\hat{\alpha}_{gmr} = \overline{Y} - \hat{\beta}_{gmr}\overline{X} \quad \text{(eq. 8)}$$

There are no provisions for estimating standard errors for GMR regression.

Simulation variables ($[CO_2]_{range}$, $[CO_2]$ error, $\delta^{13}C$ error and sample size):

To examine the impacts of the two mixing models and the two regression approaches, we generated "artificial" datasets that were based on a "known" value of $\delta^{13}C_R$. For each artificial dataset, paired values of $[CO_2]$ and $\delta^{13}C$ were generated with varying ranges of $[CO_2]$, error in $[CO_2]$ values, error in $\delta^{13}C$ values, and sample size, in a factorial design (Figure 1). A separate set of artificial datasets were generated to be representative of conditions involving small $[CO_2]_{range}$ (i.e., those typical of applications involving ecosystem respiration) and large $[CO_2]_{range}$ measurement regimes (i.e., those typical of applications involving leaf and soil respiration).

For each of the two concentration regimes we used three $[CO_2]$ ranges. For the small $[CO_2]$ regimes we used 10, 40 and 100 μmol mol^{-1} and for the large $[CO_2]_{range}$ regime series we used $[CO_2]$ ranges of 1,000, 5,000, and 10,000 μmol mol^{-1}. The initial concentration point used for all ranges was 380 μmol mol^{-1}. We used three values for sample size. For the small $[CO_2]_{range}$ regime we used n=5, 13, and 21. These values span the range of what is considered a conservative sample size for ecosystem respiration (Zobitz et al. 2006). For the large concentration regime we used n= 3, 5, and 10. These values are based on soil respiration methods (Steinmann et al. 2004; Kayler et al. 2008).

To generate the artificial data sets we calculated concentration and isotopic values from a mixing-model characteristic of each regime. We call these values of concentration, isotopic composition, and $\delta^{13}C_R$ "truth" in the sense that these values form the base to which we add the prescribed error defined previously. Furthermore, the estimates of $\delta^{13}C_{R\text{-}s}$ from the "truth" models allow us to evaluate the accuracy of the mixing model estimate of $\delta^{13}C_R$ calculated from the simulated dataset. Ecosystem respiration "truth" values were generated from a Keeling plot regression model based on typical night time respiration values encountered in the central Cascades of Oregon, USA resulting in a slope of 7500 ‰ $[CO_2]^{-1}$ and intercept of -26‰ (Hauck 2006). In the case of large $[CO_2]_{range}$ regimes, the "truth" values were calculated from a typical soil respiration Keeling plot from the same location with a slope of 10754‰ $[CO_2]^{-1}$ and a corresponding intercept of -25‰.

Using the regression model from each regime (ecosystem respiration and soil respiration), we generated *n* "truth" [CO_2] values at equally spaced points in [CO_2] space, as opposed to 1/[CO_2] space, that encompassed the concentration range. We did not randomly select points in the concentration range of CO_2 to avoid additional sampling variation into the investigation that a random selection of points would induce. We wanted the effect of $[CO_2]_{range}$ to remain fixed for any combination of conditions and if we used random samples then the $[CO_2]_{range}$ could potentially get smaller in some of the simulated datasets.

From the "truth" [CO_2] values we generated datasets that contained predetermined levels of error in the [CO_2] and $\delta^{13}C$ sample values. We chose levels of error that reflect a range of sampling conditions from ideal to poor. We used standard deviations for [CO_2] of 0.1, 0.5, 1, 2, 3 and 5 μmol mol^{-1} for the small $[CO_2]_{range}$ regime. The values of 0.1 μmol mol^{-1} and 1 μmol mol^{-1} represent the uncertainty of gas standards for ambient conditions and the precision of a field auto sampler (Hauck 2006). The 5 μmol mol^{-1} value captures variation beyond the instrument precision and represents a hypothetical maximum variation of about 1% for the small $[CO_2]_{range}$ regime. Standard deviations used for the large $[CO_2]_{range}$ regime were 0.1, 1, 15, 45, 75, and a maximum of 100 μmol mol^{-1}, which represents variation of about 1% for the highest concentration value we used in the simulation for this regime. We generated normally distributed errors from a normal distribution with mean 0 and standard deviation equal to the desired simulation standard deviation of [CO_2] and then added the simulated errors to the true [CO_2] values. This constituted one set of CO_2 concentration values with error.

We used [CO_2] values generated from the truth models to produce $\delta^{13}C$ truth values (i.e. values of $\delta^{13}C$ without error). We used three levels of $\delta^{13}C$ variation (standard deviation of 0.01, 0.05, and 0.2‰) for both the large and small concentration series. These values represent the typical precision of isotope ratio mass spectrometers and gas analyzer technology (Miller and Tans 2003; Los Gatos Research (www.lgrinc.com)). We generated $\delta^{13}C$ errors from a normal distribution with mean 0 and standard deviation equal to the desired simulation standard deviation for $\delta^{13}C$ and added each error term to the true $\delta^{13}C$ values to produce $\delta^{13}C$ values with error. Thus, for a given set of conditions

we had *n* pairs of [CO_2] plus error and $\delta^{13}C$ plus error values over the specified concentration range.

We repeated the process above 10,000 times, generating 10,000 x-y data pairs of size *n*. For each simulated dataset, we fit each of the 4 models and estimated the isotopic composition of respiration. We thus obtained four distributions with 10,000 estimates $\delta^{13}C_R$ for each set of experimental conditions; for each distribution we calculated the mean value and the standard deviation. We repeated this process for each of the 81 different combinations of experimental conditions. We refer to the difference between the mean value of the simulated distribution and the "true" value as the "mixing model bias". We refer to the standard deviations of the simulated distributions as "mixing model uncertainty".

Results and Discussion

Increasing $[CO_2]_{range}$ consistently improved the accuracy and precision of the $\delta^{13}C_R$ estimate for all model and regression combinations for both the small and large $[CO_2]_{range}$ regime. However, increasing the sample size consistently led to a more biased and yet more precise estimate. This tradeoff of accuracy and precision is especially relevant at small $[CO_2]_{ranges}$ and is just one example of how the two concentration regimes responded differently in the simulations. In addition to this tradeoff, there is considerable variation in the magnitude of mixing model bias and uncertainty in response to the different levels of simulated errors and sample size (Figures 3.2-3.5), justifying a separate discussion for each regime.

Small [CO_2] regime:

When used with the OLS regression approach, the Keeling and Miller-Tans models produced similarly biased estimates of $\delta^{13}C_R$ (Table 3.1) which is consistent with previous studies (Pataki et al. 2003; Zobitz et al. 2006; Ohlsson et al. 2005). However, when used with the GMR regression approach, there is a distinct difference in the pattern of bias between the mixing models, a relationship that has not been previously discussed

in the literature (Figure 3.2). The largest difference in $\delta^{13}C_R$ estimates between the Keeling and Miller-Tans models was 3.4‰ and the Keeling model consistently produced more negatively biased estimates of $\delta^{13}C_R$ with respect to the Miller-Tans model. This difference in estimates has also been observed by Hemming et al. (2005), who found differences up to 0.84‰ in their study, but in the case of Hemming et al. it is difficult to know which model is more accurate without knowledge of the error in $[CO_2]$ and $\delta^{13}C$ measurements. As Figure 3.2 exemplifies, if we assume that the $\delta^{13}C$ error is small then the Keeling-GMR estimate will provide a more accurate estimate of $\delta^{13}C_R$ and conversely, if the error in ^{13}C is large, on the order of 0.2 ‰, then the Miller-Tans model is more accurate at low levels of $[CO_2]$ error. The difference in estimates between the two models decreases with larger $[CO_2]_{range}$ although it is probably best to avoid this discrepancy by using OLS with either the Keeling or Miller-Tans model.

The bias of small $[CO_2]_{range}$ regimes is highly influenced by the relative levels of $\delta^{13}C$ error and $[CO_2]$ error, levels of error that are addressed differently by each regression approach due to their underlying assumptions. GMR assumes that error is present in both the x and y variables of the regression. If the variance of the error distribution is similar for both x and y, which is usually assumed in the use of GMR (Legendre and Legendre 1998; McArdle 2003), then the GMR estimate has a small bias. This relationship is seen in Figure 3.2, where the bias plane crosses zero as the $[CO_2]$ error and $\delta^{13}C$ error change at an optimal rate. In ecosystem respiration research, we often assume that $[CO_2]$ error is low relative to the measurement of $\delta^{13}C$ (Zobitz et al. 2006) and reports in the literature have shown the negative bias of GMR in this case (Bowling et al. 2003). However, field research is not able to consider the full range of potential error variance and by using our simulation approach we have shown that GMR can have both a negative and positive bias. When we simulated estimates using the largest level of $[CO_2]$ error and smallest level of $\delta^{13}C$ error, the bias was consistently positive and conversely, the bias was negative when the isotopic error was large and the $[CO_2]$ error was small. At a small $[CO_2]_{range}$, a positive bias is possible with GMR when $[CO_2]$ error is as little as 1 μmol mol^{-1}.

A positive bias also occurred with the OLS estimator. In general the OLS regression (with either the Keeling or Miller-Tans mixing models) produced a systematic positive bias that increased with $[CO_2]$ error. The smallest OLS bias resulted when the smallest level of CO_2 error, 0.1 μmol mol^{-1}, was used in the simulation. A bias in excess of 1‰ is possible at $[CO_2]$ accuracies on the order of 1 μmol mol^{-1} and a small concentration range. It is often assumed that $[CO_2]$ sampling error is very low (Zobitz et al. 2006) and while gas sampling technologies are very precise there is still room for error due to uncertainty in the $[CO_2]$ of standard gasses and problems in gas collection (Griffis et al. 2004; O'Leary et al. 1992). In this case, there is a large potential for a positive bias in the $\delta^{13}C_R$ estimate. An increase in concentration range and $[CO_2]$ accuracy decreases this potential positive bias with OLS; in our simulation the maximum bias at the $[100]_{range}$ was 0.42‰. When $[CO_2]_{range}$ is small we show the bias can be as great as 14‰; although, the bias is improved to within 2.5‰ with a moderate increase in the concentration range (40 μmol mol^{-1} in this study). It has been recommended that a concentration range of 75 μmol mol^{-1} will provide $\delta^{13}C_R$ estimates of adequate certainty (< 1‰) for $\delta^{13}C_{R\text{-}eco}$ (Pataki et al. 2003), although most published ranges are on the order of 60 μmol mol^{-1} (Hemming et al. 2005; Pataki et al. 2003).

This positive bias in the OLS regression estimates can be partly understood by the assumptions behind the approach. The estimated slope of the OLS regression is the ratio between the estimated covariance of *x* and *y* and the sum of squared deviation of x from its mean (see eq. 4). For OLS we assume that measurements of *x* are made without error. This assumption works well when $[CO_2]$ measurement error is low; however, when random error is introduced, variation in x causes the estimated covariance between x and y to be less than the expected covariance value, causing the estimated slope to be too small and ultimately resulting in a regression slope closer to zero (McArdle 2003). In the case of small $[CO_2]_{range}$ regimes, a mixing model with a regression slope closer to zero translates to a positively biased estimate of its isotopic signal.

Similar to the model bias results, the OLS approach used with either the Keeling or Miller-Tans mixing model produced the most precise estimates of $\delta^{13}C_R$ (Table 3.2). For all models, the standard deviation of the model estimates improved with an increase in the concentration range and sample size (Figure 3.4). We found a dynamic interaction

between $[CO_2]$ error and $\delta^{13}C$ error toward explaining model precision. Precision decreased linearly with an increase in ^{13}C error when the level of $[CO_2]$ error was low. Conversely, when ^{13}C error was low the standard deviations increased logarithmically with $[CO_2]$ error and appeared to reach a maximum within the range of $[CO_2]$error levels we used. Intermediate values of ^{13}C and $[CO_2]$ error led to greater standard deviations that were primarily driven by the level of ^{13}C error. The precision of $\delta^{13}C_R$ estimates will therefore improve with large $[CO_2]_{range}$ and, given the steep linear relationship with model uncertainty, accurate measures of $\delta^{13}C$.

Large $[CO_2]$ regimes:

Overall, the bias of the estimates for the simulated large $[CO_2]_{range}$ regimes was small with a range of -0.004 to 0.173‰ on average (Table 3.1). When the results are classified by concentration regime, sample size, $[CO_2]$ error, $\delta^{13}C$ error and mixing model combination then patterns in bias are present. The greatest absolute bias occurred with the Keeling mixing-model used with either regression approach while the minimum absolute bias occurred with the Miller-Tans mixing model implemented with the GMR regression approach. Importantly, for large $[CO_2]_{range}$ regimes the performance of the mixing model- regression combination does not behave similar to small $[CO_2]_{range}$ regimes.

In contrast to the small $[CO_2]_{range}$ regimes, the Keeling and Miller-Tans models used with the OLS regression did not yield equivalent results and the Keeling estimate, in general, had the greatest bias. In Figure 3.7, the increase in Keeling bias used with both regression models is shown in relation to the different levels of $[CO_2]$ and $\delta^{13}C$ error. The GMR approach was consistently the least biased when the sample size was greater than three. When we compare the Miller-Tans and the Keeling model applied with the GMR approach (Figure 3.8) we can see that the Keeling model is both the most positively and negatively biased estimator when sample size is equal to three or ten. The level of $[CO_2]$ error was the primary driver of bias and precision in the simulations in contrast to the small $[CO_2]_{range}$ regime where the interaction of both $[CO_2]$ and ^{13}C error influenced model bias.

The precision of the model estimate was greatly influenced by the concentration range (Table 3.2). For a $[CO_2]_{range}$ greater or equal to 5000 μmol mol^{-1}, the maximum standard deviation was 1.13‰ or less and for a $[CO_2]_{range}$ of 1000 μmol mol^{-1} the maximum standard deviation was 4.17‰. Similar to the patterns in bias, precision was primarily driven by $[CO_2]$ error (Figure 3.5). Overall, the Miller-Tans mixing model implemented with the GMR regression approach consistently produced the most precise estimate of $\delta^{13}C_R$.

Sample Size Effect:

Pataki et al. (2003), reported that simply increasing sample size does not improve the estimate of $\delta^{13}C_R$. We found for all simulations the $\delta^{13}C_R$ bias actually increased with the number of samples used in the mixing model. This phenomenon occurred at most levels of $[CO_2]$ error we used in our simulations. We hypothesized this phenomenon was an artifact from generating datasets of size *n* equidistantly across the determined $[CO_2]_{range}$ in $[CO_2]$ space rather than $1/[CO_2]$ space; the dimension used for Keeling plots. Data generated equidistantly in CO_2 space are not equidistantly distributed across the range in $1/[CO_2]$, instead there are more data points toward the source endpoint (i.e., infinite $[CO_2]$) of the mixing model.

We ran simulations where data were generated equidistantly in $1/[CO_2]$ space and analyzed similarly to our previous simulations (Figures 3.9 & 3.10). We found the Keeling-OLS plot bias of $\delta^{13}C_R$ for small $[CO_2]_{range}$ regimes to decrease significantly to within 5‰ from a maximum bias of 11.4‰ when data were generated in $[CO_2]$ space. There was essentially no effect on the Keeling-GMR or the Miller-Tans models. The effect on the large $[CO_2]_{range}$ showed a contrasting pattern to the small $[CO_2]_{range}$ where bias increased from a maximum of 1.75‰ to over 4‰ when we simulated $\delta^{13}C_R$ using data from $1/[CO_2]$ space. The negative bias was absent from all of the large $[CO_2]_{range}$ model combinations except the Miller-Tans GMR model and even this bias was reduced from -0.2‰ to < - 0.1‰. These results are consistent with our previous simulations that illustrate the inherent differences between the small $[CO_2]_{range}$ and large $[CO_2]_{range}$ regimes, but we were unable to determine the nature of the increase of bias with sample size.

To investigate this pattern further, we ran simulations for both small and large concentration regimes at the greatest $[CO_2]$ error, concentration range (100 μmol mol^{-1}, 10,000 μmol mol^{-1}) and varied the sample size from 3 to 500. The bias as a function of sample size reached an asymptote for both concentration regimes (Figure 3.11). In the case of the small concentration regime, the maximum bias of the estimate was 14.6‰ less negative than the true value; for the case of a $[CO_2]$ error of 0.01 there is functionally no bias. The maximum bias was much smaller (approximately 0.25‰) for the large concentration regime under analogous conditions (i.e. large $[CO_2]$ error and large concentration range).

Recommendations:

For relatively small $[CO_2]_{range}$ regimes, OLS is consistently the least biased estimator when $[CO_2]$ error is low, conditions for which GMR will generally have a negative bias. Because small $[CO_2]_{range}$ regimes, like ecosystem respiration, have a limited concentration range it is important to have estimates of $[CO_2]$ accurate within 1 μmol mol^{-1} and then the accuracy and precision of $\delta^{13}C_R$ will improve with better measurement of $\delta^{13}CO_2$. Fortunately, the calibration gasses available today for atmospheric conditions are very accurate and infra red gas analyzers can achieve a high level of precision justifying OLS as the regression model of choice to achieve the least biased estimate of $\delta^{13}C_{R\text{-}eco}$ with the least uncertainty.

Zobitz et al. (2006) reported that measurement with a small $\delta^{13}C$ error is essential to achieve estimates of $\delta^{13}C_R$ with acceptable bias and uncertainty. Their analyses were restricted to conditions similar to those we used for simulations of small $[CO_2]_{range}$ regimes, and in contrast to their results we found that estimates of $\delta^{13}C_R$ for large $[CO_2]_{range}$ regimes were improved by minimizing $[CO_2]$ error rather than minimizing $\delta^{13}C$ error. We consider the error levels used in our simulations to be conservative. The $[CO_2]$ error was on the order of 1-2% for the large $[CO_2]_{range}$ regimes. Our study illustrates that uncertainty in calibration gas could potentially have a significant impact on $\delta^{13}C_R$ estimates. Thus, researchers conducting studies involving large $[CO_2]_{range}$ regimes should strive to use standard gases with small $[CO_2]$ uncertainty. For instance, gases from

NOAA have an uncertainty that are within 5 μmol mol^{-1} of ambient concentrations while gas concentrations above 500 μmol mol^{-1} are expected to decrease in uncertainty at about a rate of 0.01% (Duane Kitzis *personal communication*). Not all standards are equal, for instance gases available through industrial distributors are commonly accurate to ±2% of the target value and even secondary or field standards have been shown to drift up to 5 μmol mol^{-1} over time (Griffis et al. 2004). In large $[CO_2]_{range}$ applications, the actual error encountered in measuring the $[CO_2]$ may be larger than the reported precision of the instrument due to the uncertainty in the standard gasses or additional measurement error incurred during sampling. Therefore, it is prudent to expect a relatively high $[CO_2]$ error in large $[CO_2]_{range}$ regimes, in which case the Miller-Tans-GMR mixing model had the smallest range in bias for the range of simulated conditions.

Bias and uncertainty were relatively insensitive to $\delta^{13}C$ error in large $[CO_2]_{range}$ regimes, most likely due to the overwhelming influence of $[CO_2]$ error on $\delta^{13}C_R$. However, the estimates of $\delta^{13}C_R$ did vary with *n*. With low *n* (n=3) $\delta^{13}C_R$ is negatively biased, although the absolute range of the bias is small. For $n>3$, the range of the bias increased with increasing *n*, indicating that a priority should be placed on increasing $[CO_2]_{range}$ and reducing $[CO_2]$ error rather than increasing *n* to improve the bias and uncertainty of $\delta^{13}C_R$.

In large $[CO_2]_{range}$ regimes (>5000 μmol mol^{-1}), mixing model bias was < 1‰ and for all models the standard deviations were at most 1.2‰. For $[CO_2]_{range}$ near 1000 μmol mol^{-1}, model bias can be greater than 1‰ and the standard deviation of the estimate can be up to 4‰. In this case, the Miller-Tans-GMR model was the best estimator because it had the smallest range in values of bias and uncertainty. The Miller-Tans-GMR mixing model is arguably the model of choice for large $[CO_2]_{range}$ regimes in general, given the uncertainty of measuring $[CO_2]$ accurately and the model's tendency to produce the estimate with the least bias under all of the conditions we imposed.

Conclusions

There are inherent differences between small and large $[CO_2]$ regimes regarding measurement assumptions, the interaction between $[CO_2]$ and ^{13}C error, and mixing

model performance, differences that warrant separate recommendations for measuring $\delta^{13}C_R$. Our simulation results are consistent with those of Zobitz et al. (2006), which recommends the use of the Keeling-OLS combination for ecosystem respiration. For systems with large $[CO_2]_{range}$ (e.g. soil, tree bole, foliar respiration), many of the model combinations are functionally unbiased, however the Miller-Tans-GMR mixing model is the least biased and most precise at moderate concentration ranges for situations when error is present in either $\delta^{13}C$ or $[CO_2]$ values.

References

Affek, H. P. and J. M. Eiler.2006. Abundance of mass 47 CO_2 in urban air, car exhaust, and human breath. Geochimica Et Cosmochimica Acta 70(1): 1-12.

Bowling, D. R., N. G. McDowell, B. J. Bond, B. E. Law and J. R. Ehleringer.2002. ^{13}C content of ecosystem respiration is linked to precipitation and vapor pressure deficit. Oecologia 131(1): 113-124.

Bowling, D. R., S. D. Sargent, B. D. Tanner and J. R. Ehleringer.2003. Tunable diode laser absorption spectroscopy for stable isotope studies of ecosystem-atmosphere CO_2 exchange. Agricultural and Forest Meteorology 118(1-2): 1-19.

Ekblad, A., B. Bostrom, A. Holm and D. Comstedt. 2005. Forest soil respiration rate and $\delta^{13}C$ is regulated by recent above ground weather conditions. Oecologia 143(1): 136-142.

Faure, G. 1977. Principles of Isotope Geology. New York, NY, USA, John Wiley and Sons.

Fessenden, J. E. and J. R. Ehleringer.2002. Age-related variations in $\delta^{13}C$ of ecosystem respiration across a coniferous forest chronosequence in the Pacific Northwest. Tree Physiology 22(2-3): 159-167.

Griffis, T. J., J. M. Baker, S. D. Sargent, B. D. Tanner and J. Zhang.2004. Measuring field-scale isotopic CO_2 fluxes with tunable diode laser absorption spectroscopy and micrometeorological techniques. Agricultural and Forest Meteorology 124(1-2): 15-29.

Hauck, M. J. 2006. Isotopic Composition of Respired CO_2 in a Small Watershed: Development and Testing of an Automated Sampling System and Analysis of First Year Data. Maters Thesis: Forest Science. Corvallis, Oregon State University: 115.

Hemming, D., D. Yakir, P. Ambus, M. Aurela, C. Besson, K. Black, N. Buchmann, R. Burlett, A. Cescatti, R. Clement, P. Gross, A. Granier, T. Grunwald, K. Havrankova, D. Janous, I. A. Janssens, A. Knohl, B. K. Ostner, A. Kowalski, T. Laurila, C. Mata, B. Marcolla, G. Matteucci, J. Moncrieff, E. J. Moors, B. Osborne, J. S. Pereira, M. Pihlatie, K. Pilegaard, F. Ponti, Z. Rosova, F. Rossi, A. Scartazza and T. Vesala.2005. Pan-European delta C-13 values of air and organic matter from forest ecosystems. Global Change Biology 11(7): 1065-1093.

Högberg , P., A. Nordgren, N. Buchmann, A. F. S. Taylor, A. Ekblad, M. N. Högberg , G. Nyberg, M. Ottosson-Lofvenius and D. J. Read.2001. Large-scale forest girdling shows that current photosynthesis drives soil respiration. Nature 411(6839): 789-792.

Kayler, Z. E., E. W. Sulzman, J. D. Marshall, A. Mix, W. D. Rugh and B. J. Bond.2008. A laboratory comparison of two methods used to estimate the isotopic composition of soil $\delta^{13}CO_2$ efflux at steady state. Rapid Communications in Mass Spectrometry 22(16): 2533-2538.

Keeling, C. D.1958. The concentration and isotopic abundances of atmospheric carbon dioxide in rural areas. Geochimica Et Cosmochimica Acta 13: 322-334.

Legendre, P. and L. Legendre (1998). Numerical Ecology. Amsterdam, Elsevier.

Maunoury, F., D. Berveiller, C. Lelarge, J. Y. Pontailler, L. Vanbostal and C. Damesin.2007. Seasonal, daily and diurnal variations in the stable carbon isotope composition of carbon dioxide respired by tree trunks in a deciduous oak forest. Oecologia 151(2): 268-279.

McArdle, B. H.2003. Lines, models, and errors: Regression in the field. Limnology and Oceanography 48(3): 1363-1366.

McDowell, N. G., D. R. Bowling, A. Schauer, J. Irvine, B. J. Bond, B. E. Law and J. R. Ehleringer.2004. Associations between carbon isotope ratios of ecosystem respiration, water availability and canopy conductance. Global Change Biology 10(10): 1767-1784.

Miller, J. B. and P. P. Tans.2003. Calculating isotopic fractionation from atmospheric measurements at various scales. Tellus Series B-Chemical and Physical Meteorology 55(2): 207-214.

Mortazavi, B., J. L. Prater and J. P. Chanton.2004. A field-based method for simultaneous measurements of the $\delta^{18}O$ and $\delta^{13}C$ of soil CO_2 efflux. Biogeosciences 1(1): 1-9.

Ohlsson, K. E. A., S. Bhupinderpal, S. Holm, A. Nordgren, L. Lovdahl and P. Högberg .2005. Uncertainties in static closed chamber measurements of the carbon isotopic ratio of soil-respired CO_2. Soil Biology & Biochemistry 37(12): 2273-2276.

O'Leary, M. H., S. Madhavan and P. Paneth.1992. Physical and Chemical Basis of Carbon Isotope Fractionation in Plants. Plant Cell and Environment 15(9): 1099-1104.

Pataki, D. E., J. R. Ehleringer, L. B. Flanagan, D. Yakir, D. R. Bowling, C. J. Still, N. Buchmann, J. O. Kaplan and J. A. Berry.2003. The application and interpretation of Keeling plots in terrestrial carbon cycle research. Global Biogeochemical Cycles 17(1).

Prater, J. L., B. Mortazavi and J. P. Chanton.2006. Diurnal variation of the $\delta^{13}C$ of pine needle respired CO_2 evolved in darkness. Plant Cell and Environment 29(2): 202-211.

Pypker, T. G., M. Hauck, E. W. Sulzman, M. H. Unsworth, A. C. Mix, Z. E. Kayler, D. Conklin, A. Kennedy, H. R. Barnard, C. Phillips and B.J. Bond.2008. Toward using $\delta^{13}C$ of ecosystem respiration to monitor canopy physiology in complex terrain. Oecologia 158(3):399-410.

Scartazza, A., C. Mata, G. Matteucci, D. Yakir, S. Moscatello and E. Brugnoli.2004. Comparisons of $\delta^{13}C$ of photosynthetic products and ecosystem respiratory CO_2 and their response to seasonal climate variability. Oecologia 140(2): 340-351.

Steinmann, K. T. W., R. Siegwolf, M. Saurer and C. Korner.2004. Carbon fluxes to the soil in a mature temperate forest assessed by ^{13}C isotope tracing. Oecologia 141(3): 489-501.

Tu, K. and T. Dawson (2005). Partitioning Ecosystem Respiration Using Stable Carbon Isotope Analyses of CO2. Stable Isotopes and Biosphere-Atmosphere Interactions J. R. Ehleringer, D.E. Pataki, L.B. Flanagan. San Francisco, Ca, USA, Elsevier.

Xu, C., Guang-hui Lin, Kevin L. Griffin, Raymond N. Sambrotto.2004. Leaf respiratory CO_2 is ^{13}C enriched relative to leaf organic components in five species of C3 plants. New Phytologist 163: 499-505.

Zar, J. H. (1999). Biostatistical Analysis. New Jersey, USA, Simon and Schuster.

Zobitz, J. M., J. P. Keener, H. Schnyder and D. R. Bowling.2006. Sensitivity analysis and quantification of uncertainty for isotopic mixing relationships in carbon cycle research. Agricultural and Forest Meteorology 136(1-2): 56-75.

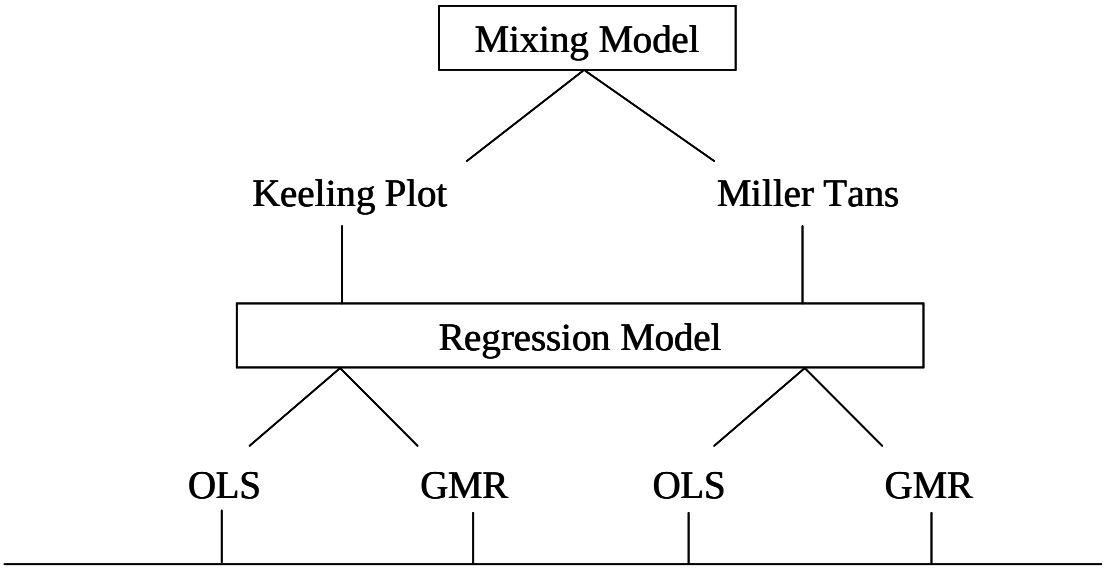

Regime type	Small $[CO_2]_{range}$	Large $[CO_2]_{range}$
Input Variable Name	Input Variable Values	
CO_2 concentration error (ppm)	0.1, 1, 2, 3, 5	0.1, 15, 45, 75, 100
$\delta^{13}C$ error (‰)	.01, 0.5, 0.2	.01, 0.5, 0.2
sample size	5, 13, 21	3, 5, 10
concentration range (ppm)	10, 40, 100	1000, 5000, 10000
truth model $\delta^{13}CO2$ (‰)	-25	-26

Figure 3.1 Diagram illustrating the different mixing and regression model combinations tested for bias and uncertainty. The table lists the different measurement errors, sample size and concentration ranges we used in our simulation of small and large $[CO_2]$ concentration regimes.

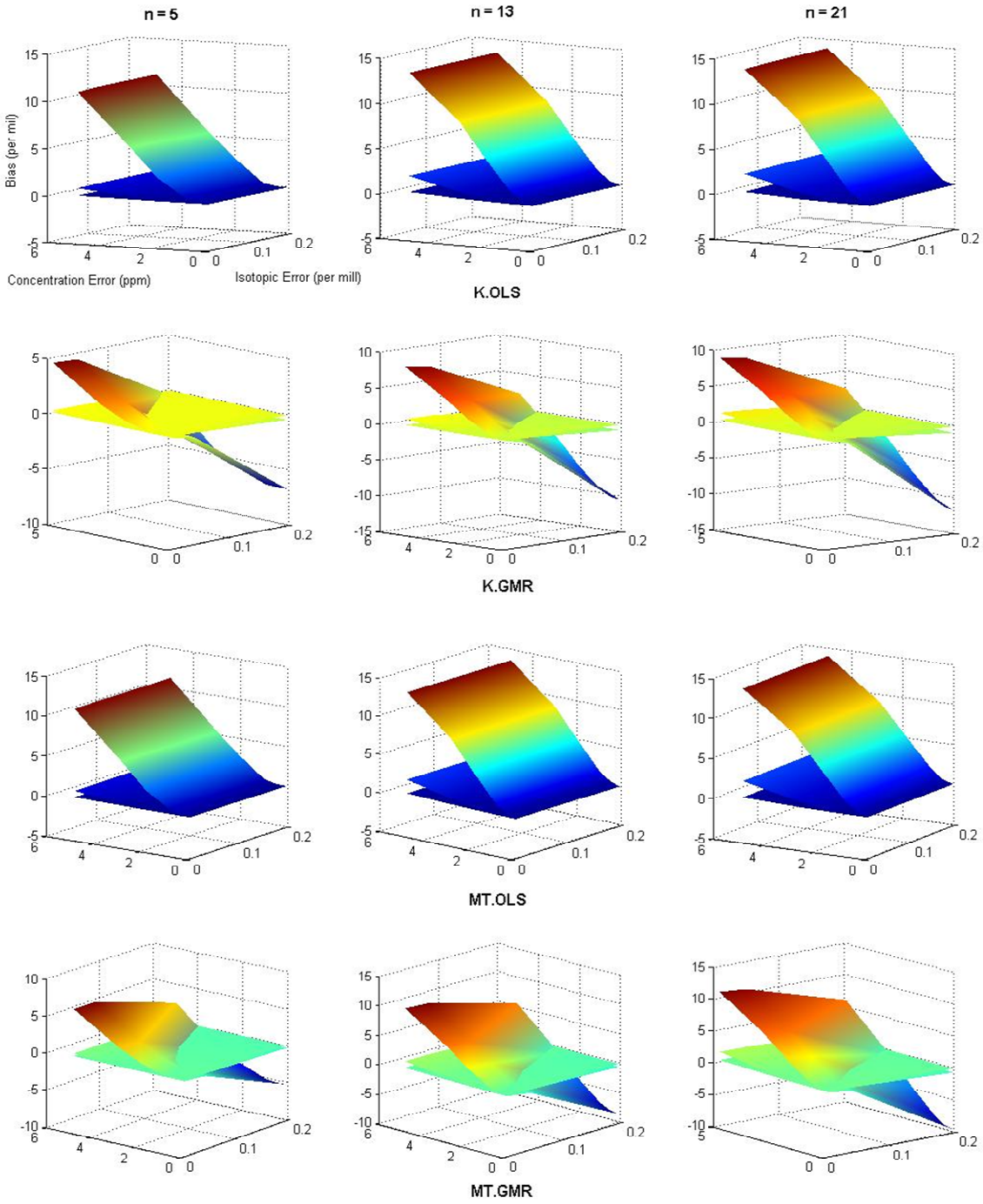

Figure 3.2. Small $[CO_2]_{range}$ model bias for the Keeling (K) and Miller-Tans (MT) mixing model in combination with ordinary least squares (OLS) and geometric mean regression (GMR) approaches. The concentration error (x-axis), isotopic error (y-axis) and bias (z-axis) forms the response surface for each concentration level: from top to bottom 10, 40, and 100 μmol mol^{-1}. The sample size used in the simulation is at the top of each column.

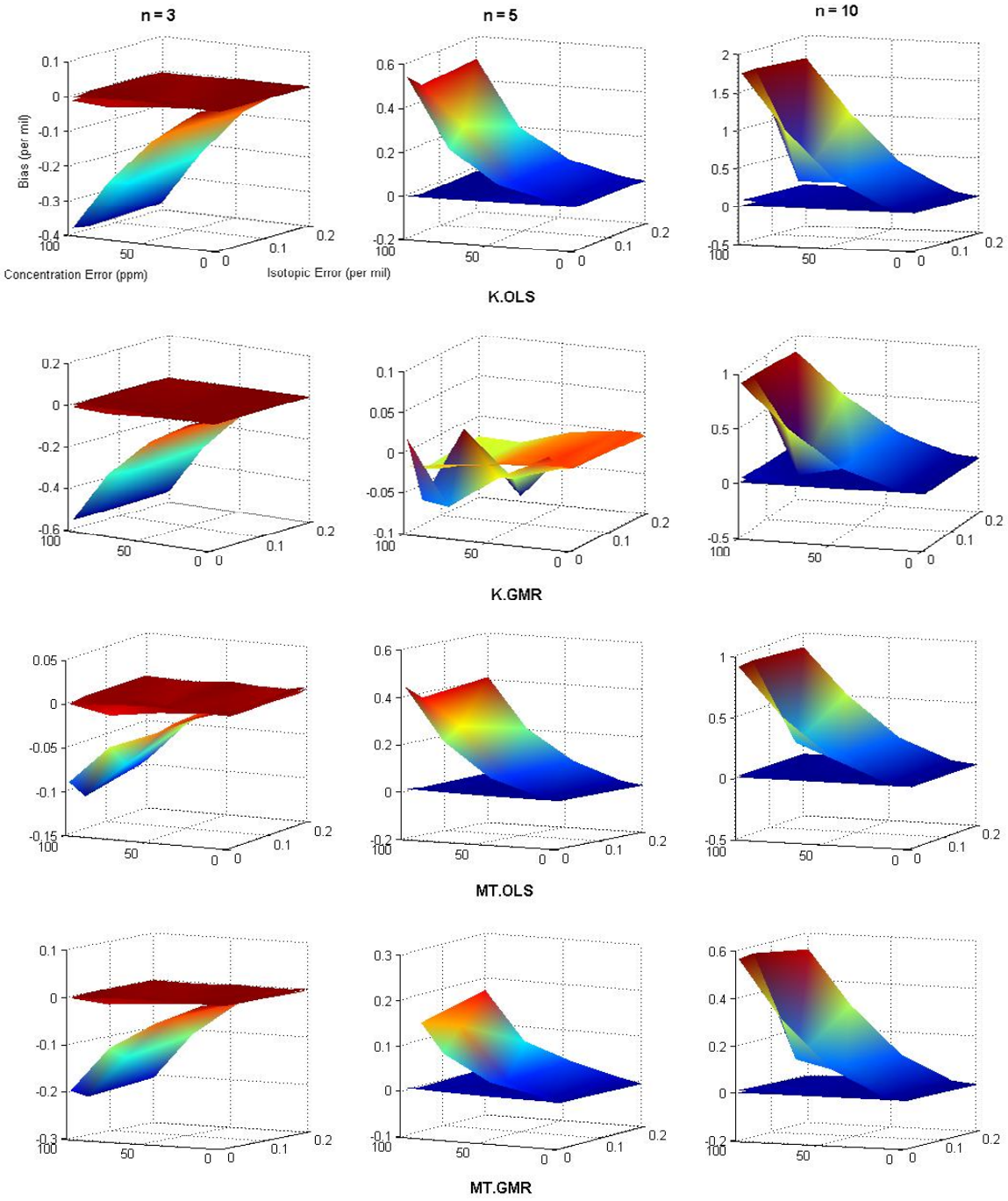

Figure 3.3. Large $[CO_2]_{range}$ model bias for the Keeling (K) and Miller-Tans (MT) mixing model in combination with ordinary least squares (OLS) and geometric mean regression (GMR) approaches. The concentration error (x-axis), isotopic error (y-axis) and bias (z-axis) forms the response surface for each concentration level: from top to bottom 1000, 5000, and 10,000 μmol mol^{-1}. The sample size used in the simulation is at the top of each column.

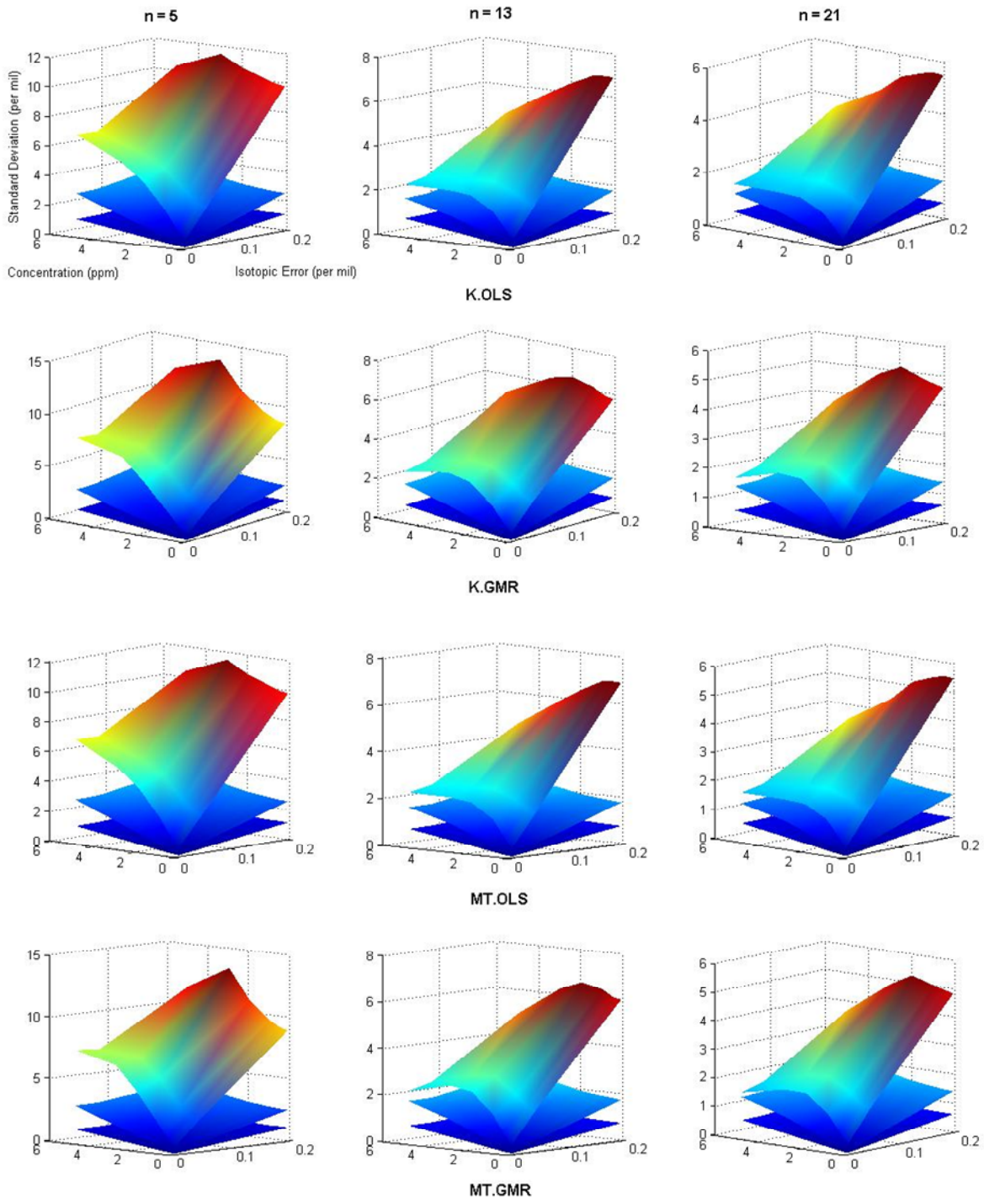

Figure 3.4. Small $[CO_2]_{range}$ model standard deviation for the Keeling (K) and Miller-Tans (MT) mixing model in combination with ordinary least squares (OLS) and geometric mean regression (GMR) approaches. The concentration error (x-axis), isotopic error (y-axis) and standard deviation (z-axis) forms the response surface for each concentration level: from top to bottom 10, 40, and 100 μmol mol^{-1}. The sample size used in the simulation is at the top of each column.

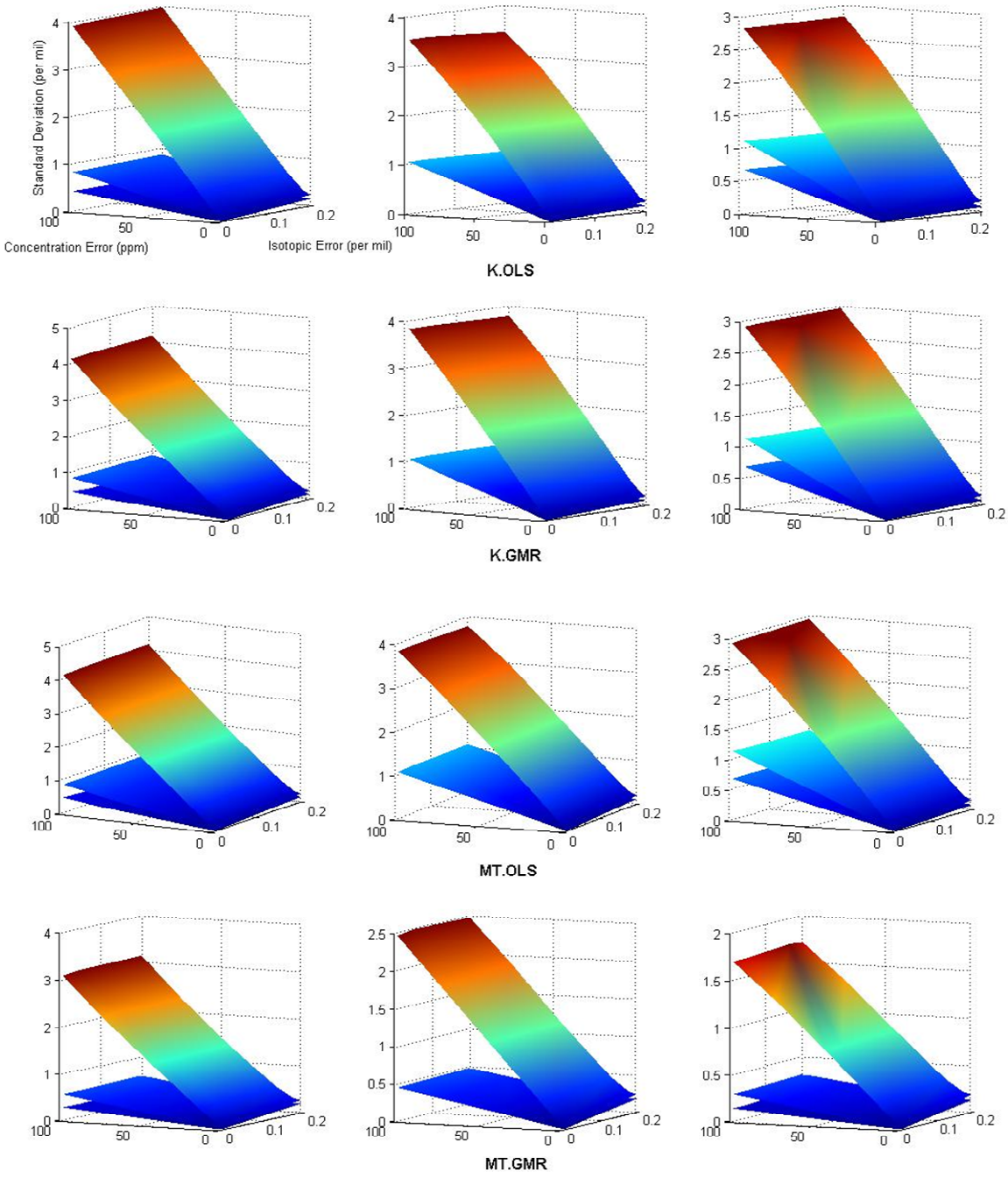

Figure 3.5. Large $[CO_2]_{range}$ model standard deviation for the Keeling (K) and Miller-Tans (MT) mixing model in combination with ordinary least squares (OLS) and geometric mean regression (GMR) approaches. The concentration error (x-axis), isotopic error (y-axis) and standard deviation (z-axis) forms the response surface for each concentration level: from top to bottom 1000, 5000, and 10,000 μmol mol^{-1}. The sample size used in the simulation is at the top of each column.

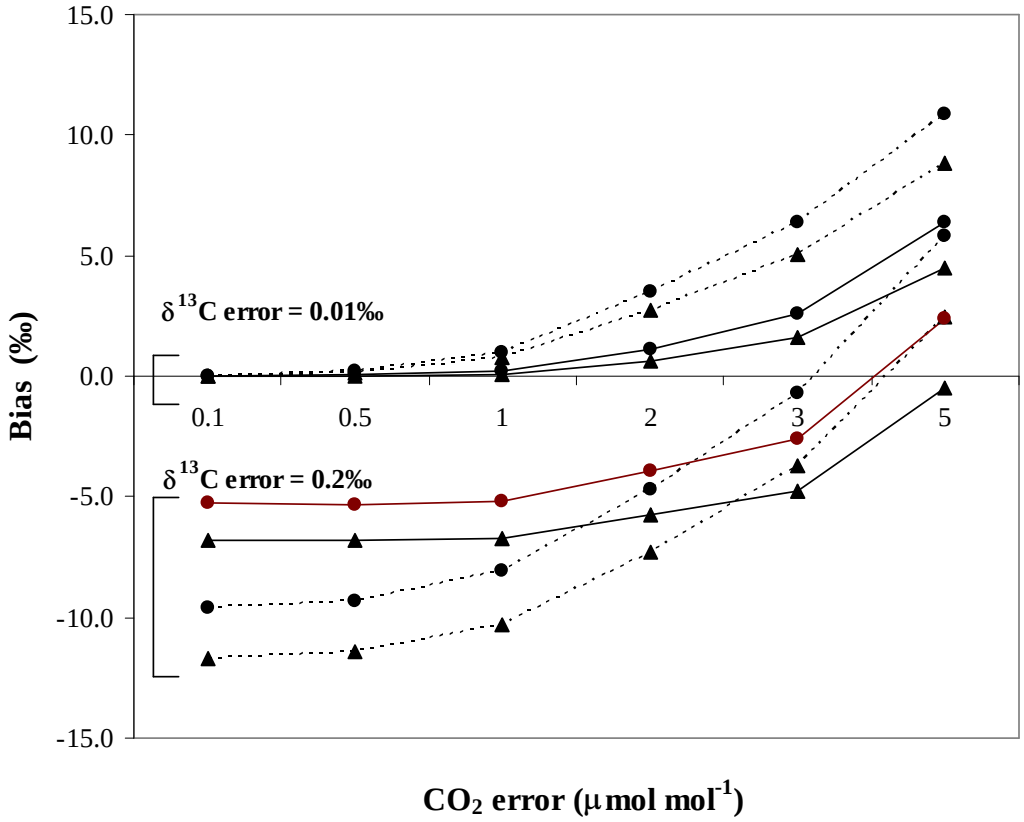

Figure 3.6. Patterns of $\delta^{13}C_R$ bias simulated from Miller-Tans (circle) and Keeling (triangle) models used with GMR. Bias is depicted as a function of $[CO_2]$ error (x-axis) and varying levels of ^{13}C error (0.01‰ and 0.2‰), sample size (n = 5 (solid line) and 21 (dashed line)),with a $[CO_2]_{range}$ of 10 μmol mol^{-1}.

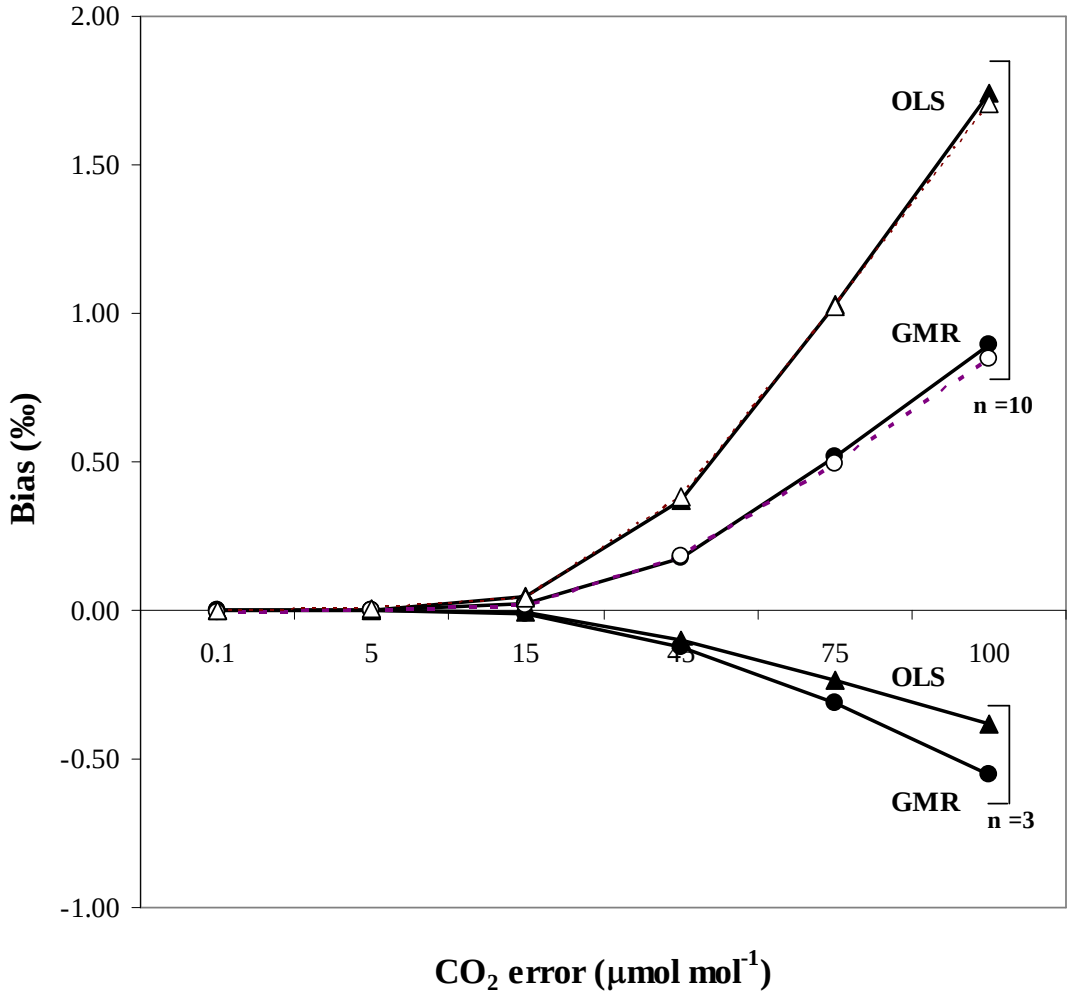

Figure 3.7 Large $[CO_2]_{range}$ regime patterns of $\delta^{13}C_R$ bias resulting from the Keeling mixing model used with the OLS and GMR regression approach. $[CO_2]$ error levels are listed along the x-axis, bias along the y-axis and varying levels of ^{13}C error (0.01‰ (solid line and symbols) and 0.2‰ (dashed line and open symbols)), sample size (n = 3 and 10), for a $[CO_2]_{range}$ of 1000 μmol mol^{-1}.

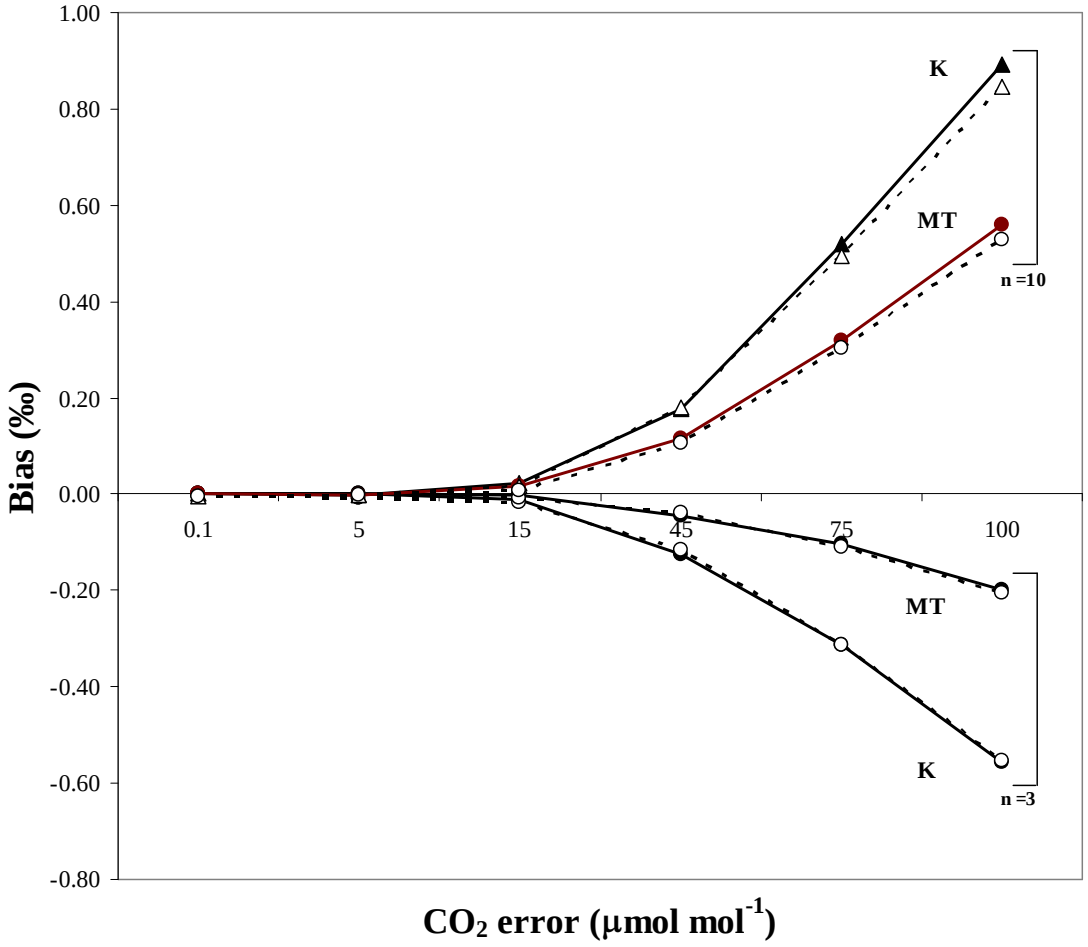

Figure 3.8 Large $[CO_2]_{range}$ regime patterns of $\delta^{13}C_R$ bias resulting from the Keeling and Miller-Tans mixing models used with the GMR regression approach. CO_2 error levels are listed along the x-axis, bias along the y-axis and varying levels of ^{13}C error (0.01‰ and 0.2‰), sample size (n = 3 and 10), for a $[CO_2]_{range}$ of 1000 µmol mol^{-1}.

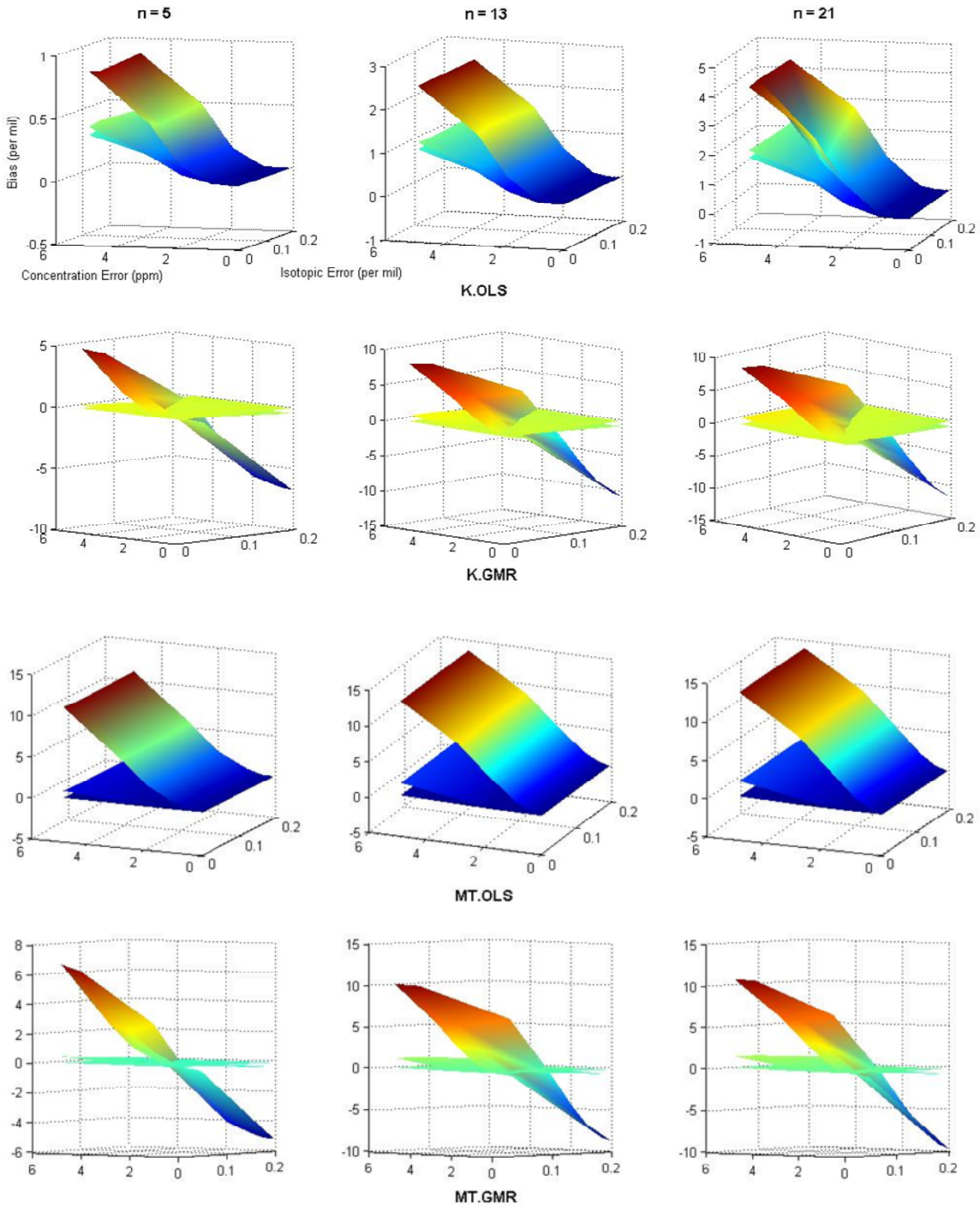

Figure 3.9 Results from generating simulation data sets in $1/[CO_2]$ space for the small $[CO_2]_{range.}$ Model bias is depicted for the Keeling (K) and Miller-Tans (MT) mixing model in combination with ordinary least squares (OLS) and geometric mean regression (GMR) approaches. The concentration error (x-axis), isotopic error (y-axis) and bias (z-axis) forms the response surface for each concentration level: from top to bottom 10, 40, and 100 μmol mol^{-1}. The sample size used in the simulation is at the top of each column.

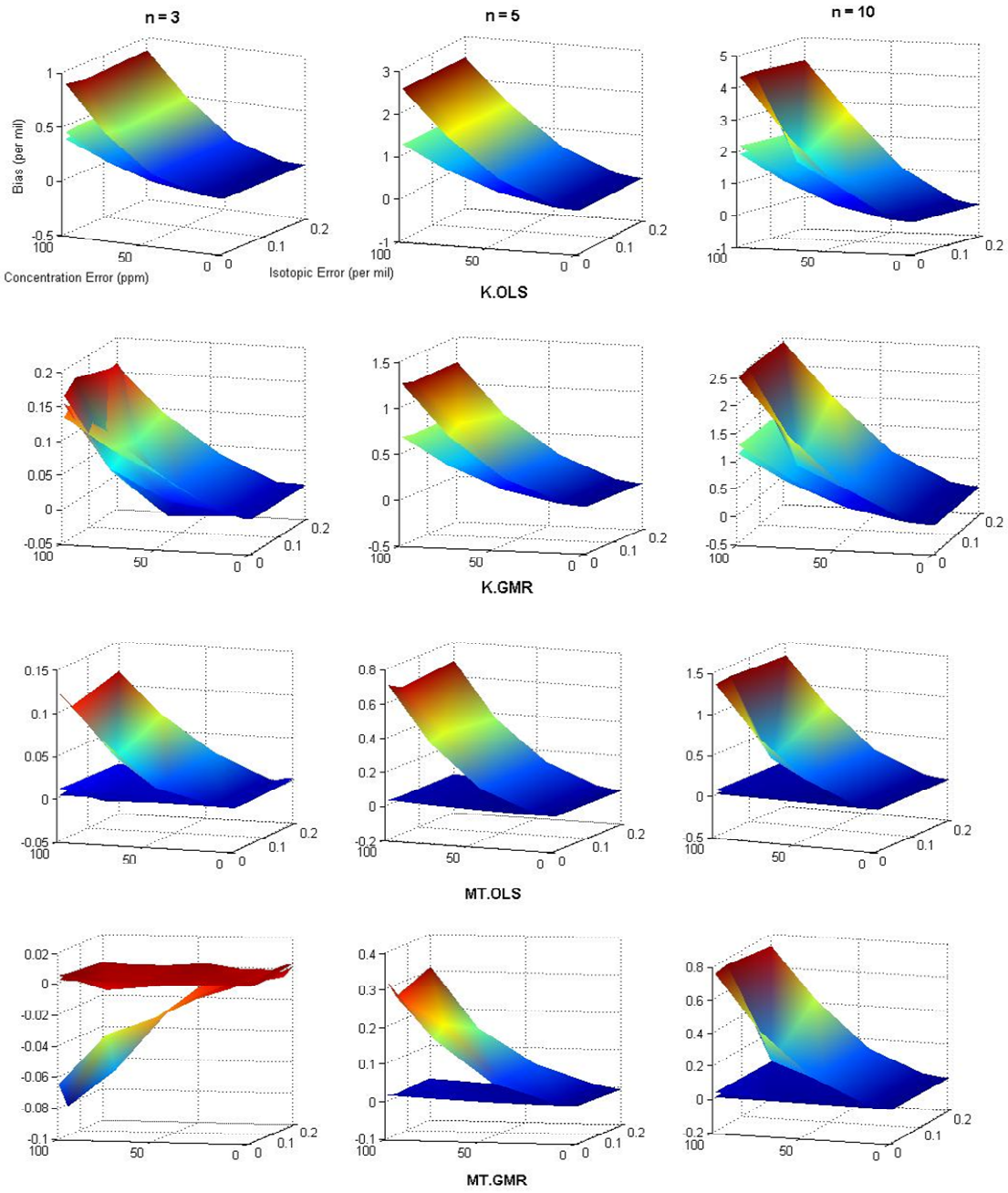

Figure 3.10 Results from generating simulation data sets in $1/[CO_2]$ space for the large $[CO_2]_{range.}$ Model bias is depicted for the Keeling (K) and Miller-Tans (MT) mixing model in combination with ordinary least squares (OLS) and geometric mean regression (GMR) approaches. The concentration error (x-axis), isotopic error (y-axis) and bias (z-axis) forms the response surface for each concentration level: from top to bottom 10, 40, and 100 μmol mol^{-1}. The sample size used in the simulation is at the top of each column.

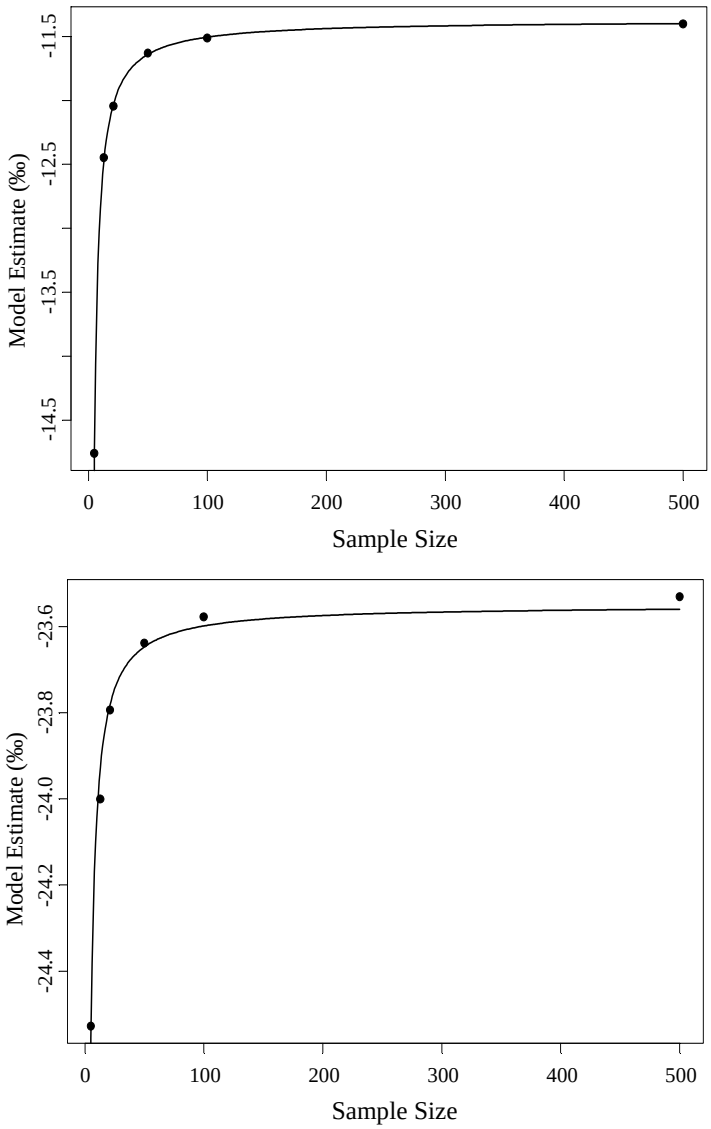

Figure 3.11.Mixing model estimates of $\delta^{13}C_R$ as a function of sample size for the small (top) and large [CO_2] (bottom) regimes. A Michaelis-Menton function was fit to the results to estimate the maximum estimate.

		K.GMR			K.OLS			MT.GMR			MT.OLS		
regime	range	min	average	max	min	average	max	min	average	max	min	average	max
Small $[CO_2]_{range}$	10	-11.7270	-0.7959	8.8065	0.0004	4.3980	13.9683	-9.6095	0.4759	10.8502	0.0005	4.3968	13.9659
	40	-1.0354	-0.0707	1.1590	-0.0263	0.4908	2.4412	-0.7635	0.0830	1.5140	-0.0277	0.4884	2.4311
	100	-0.2059	-0.0252	0.1920	-0.0161	0.0769	0.4201	-0.1399	0.0055	0.2552	-0.0181	0.0746	0.4058
Large $[CO_2]_{range}$	1000	-0.5570	0.0171	0.8954	-0.3895	0.1686	1.7542	-0.2184	0.0477	0.5697	-0.1131	0.1164	0.9168
	5000	-0.0309	-0.0034	0.0367	-0.0234	0.0030	0.0859	-0.0122	-0.0003	0.0125	-0.0109	0.0015	0.0183
	10000	-0.0087	-0.0012	0.0101	-0.0073	0.0004	0.0228	-0.0048	-0.0003	0.0035	-0.0024	0.0005	0.0061

Table 3.1: Bias of $\delta^{13}C_R$ estimates simulated from different mixing model (Keeling (K) and Miller-Tans (MT)) and regression approach (ordinary least squares (OLS) and geometric mean regression (GMR)) combinations for small $[CO_2]_{range}$ and large $[CO_2]_{range}$ regimes.

		K.GMR			K.OLS			MT.GMR			MT.OLS		
regime	range	min	average	max	min	average	max	min	average	max	min	average	max
Small $[CO_2]_{range}$	10	0.3145	4.1495	13.3686	0.3146	4.0125	11.4296	0.3146	4.1307	13.3470	0.3145	4.0125	11.4286
	40	0.0795	1.3509	4.0057	0.0795	1.3237	3.8395	0.0795	1.3463	3.9793	0.0796	1.3216	3.8356
	100	0.0333	0.5622	1.5666	0.0333	0.5608	1.5559	0.0334	0.5580	1.5500	0.0334	0.5566	1.5414
Large $[CO_2]_{range}$	1000	0.0085	1.4986	4.1650	0.0085	1.4403	3.9456	0.0099	1.0109	3.1452	0.0099	0.9938	3.0845
	5000	0.0044	0.4256	1.1355	0.0044	0.4203	1.1055	0.0070	0.2165	0.6147	0.0070	0.2164	0.6144
	10000	0.0038	0.2432	0.6856	0.0038	0.2408	0.6724	0.0068	0.1344	0.3503	0.0068	0.1344	0.3503

Table 3.2: Standard deviation of $\delta^{13}C_R$ estimates simulated from different mixing model (Keeling (K) and Miller-Tans (MT)) and regression approach (ordinary least squares (OLS) and geometric mean regression (GMR)) combinations for small $[CO2]_{range}$ and large $[CO_2]_{range}$ regimes.

Chapter 4 Estimating the contribution of new and old carbon sources to soil respired $^{13}CO_2$ constrained by ^{13}C of tree and soil organic matter.

Abstract:

A primary goal of measuring the carbon isotopic signal of soil respiration is to discover the carbon source that is being oxidized. We measured the isotopic signature of aboveground and belowground carbon sources in a stand of Douglas-fir trees in the Pacific Northwest in an effort to determine the carbon source of soil respiration ($\delta^{13}C_{R\text{-}s}$). In addition to determining the carbon source of $\delta^{13}C_{R\text{-}s}$, there is a clear need to assess whether or not the assumptions concerning the measurement and analysis of the carbon source of soil respiration are appropriate given the variability in carbon sources and soil properties in forest ecosystems. To do this we designed a series of field experiments to investigate the impact of soil gas transport on estimates of $\delta^{13}C_{R\text{-}s}$. We compared estimates of $\delta^{13}C_{R\text{-}s}$ derived from aboveground and belowground techniques to observe the degree of isotopic fractionation due to gas transport. In addition to the field estimates, to determine the influence of advection on belowground transport we implemented diffusion and advection-diffusion models that predict $^{13}CO_2$ concentrations in the soil profile. To further explore the role of advection, we induced a large negative pressure gradient (-4kPa) at the soil surface to observe changes in $\delta^{13}C_{R\text{-}s}$. Soil gas transport during the experiment was primarily by diffusion and the belowground estimate of $\delta^{13}C_{R\text{-}s}$ was enriched on average by 3.8 to 4.0‰ with respect to the source estimates from the transport models, indicating that the soil ^{13}C was at semi-steady-state. The advection-diffusion model was more accurate than a model based solely on diffusion in predicting the isotopic samples from the soil profile. We found a maximum difference of -2.36‰ between the belowground and aboveground estimates of $\delta^{13}C_{R\text{-}s}$, the aboveground estimate was enriched relative to the belowground estimate. There was -1‰ difference between the aboveground estimate under diffusive and advective conditions and this value may represent an upper boundary of the effects of advection on the apparent fractionation of ^{13}C. We found that aboveground measurements may be particularly susceptible to atmospheric incursion, which may produce $\delta^{13}C_{R\text{-}s}$ estimates that are enriched in ^{13}C. The partitioning results attributed 69 to 98% of soil respiration to a

source with a highly depleted isotopic signature that we interpreted to have come from dissolved organic carbon which may be an important driver of early-growing-season carbon dynamics in Douglas-fir ecosystems.

Introduction

The largest terrestrial pool of carbon is soil (Amundson 2001) and soil respiration is the second largest flux of carbon globally, approximately an order of magnitude greater than the combined flux of fossil fuel and deforestation (Schimel et al. 1995). We have entered a period of great uncertainty with regards to the global climate and it is crucial that we develop a thorough understanding of the physical and biological controls of the evolution and egress of soil CO_2. Soil respiration is the efflux of CO_2 from the soil surface and is classically partitioned into: 1) autotrophic respiration, respiration by organisms that respire self-assimilated carbon, and 2) heterotrophic respiration, respiration of carbon by organisms that are not able to anabolize their own high energy oxidative substrate (Luo and Zhou 2006; Hanson et al. 2000). Partitioning of soil respiration into these two components is functionally relevant given that each flux responds differently to temperature (Boone et al. 1998; Pregitzer et al. 2000; Epron et al. 2001), soil moisture (Scott-Denton et al. 2006, Pendall et al. 2004) and CO_2 fertilization (Pregitzer et al. 2006). While these respiratory categories are conceptually justified, it is difficult to deconstruct the many sources of respiration in the soil with current methods (Hanson et al. 2000; Subke et al. 2006).

Part of the difficulty in identifying sources of carbon for soil respiration lies in the degree to which roots, mycorrhizae and soil bacteria are intertwined within the soil, a characteristic of the rhizosphere that is characterized more easily by tracking "new" carbon, or recent photosynthetic assimilates, and "old" carbon sources rather than separating each respiring organism (Högberg and Read 2006). Natural abundance stable carbon isotopes can be used as a non-intrusive method to identify new and old carbon sources (Dawson et al. 2002; Tu and Dawson 2005). This approach uses the naturally distinct isotopic signatures, or concentration ratio of $^{13}C/^{12}C$, of organic matter from leaves to soil. Recent assimilates tend to have low ratios of $^{13}C/^{12}C$, while older soil organic matter (SOM) tends to have high ratios of the two isotopes (Ehleringer et al.

2000; Bowling et al. 2008). These ratios are expressed in delta notation (δ) where $\delta^{13}C = (R_{sample}/ R_{VPDB} -1) \times 1000‰$ and R is the molar ratio of $^{13}C/^{12}C$ and VPDB is the Vienna Pee Dee Belemnite isotopic standard. Past research has shown the isotopic signature of bulk C3 leaf organic matter ranges from -20 to -35‰ (Dawson et al. 2002) while soil organic matter (SOM) is on average 2‰ enriched in ^{13}C relative to the bulk leaf signal (Bowling et al. 2008). Thus, by sampling the isotopic signature of potential soil respiration sources, it is possible to determine the relative contribution of new and old carbon by deconvoluting the isotopic signature of soil respired CO_2 ($\delta^{13}C_{R-s}$) (Ekblad et al. 2001; Steinmann et al. 2004; Millard et al. 2008; Takahashi et al. 2008; Kodama et al. 2008). A critical assumption behind this strategy is the magnitude of the isotopic signature between the pools must be large enough such that potential contributors can be identified (i.e. >1‰; O'Leary (1984)).

The potentially small difference between soil respiration isotopic sources requires an accurate measurement of $\delta^{13}C_{R-s}$ which presents its own unique challenges. Current methods to estimate $\delta^{13}C_{R-s}$ can be categorized into those made aboveground via closed or open top chambers (Ekblad and Högberg 2000; Ohlsson et al. 2005; Takahashi et al. 2008) and those made belowground that use samples from the soil [CO_2] profile (Kayler et al. 2008; Steinmann et al. 2004). Both methods make key assumptions concerning soil respiration 1) CO_2 transport through the soil is only by diffusion and 2) soil CO_2 flux is at steady-state (Cerling et al. 1991; Amundson et al. 1998).

Transport solely by diffusion is critical to estimates of $\delta^{13}C_{R-s}$ because diffusion leads to a kinetic fractionation of ^{13}C and ^{12}C. Isotopic fractionation is broadly defined as a process that results in abundances of heavier isotopes in the substrate being different from the abundances of the heavy isotopes in the product. The fractionation that occurs during diffusion of $\delta^{13}C$ is a function of the differences in molecular mass of the two isotopes. The difference in mass results in different rates of molecular diffusion with ^{13}C diffusing at a slower rate relative to ^{12}C. Thus, there are two species of CO_2 moving through the soil and when sampled in the soil profile there is an apparent increase in the concentration of ^{13}C due to the slower rate of diffusion. The end result is a sample of gas from the soil that is enriched in ^{13}C relative to the $\delta^{13}CO_2$ source. Therefore, estimates of $\delta^{13}C_{R-s}$ made from gas samples of the soil profile must be corrected by 4.4‰, the amount

that estimates of $\delta^{13}C_{R\text{-}s}$ will be enriched because of fractionation due to diffusion of CO_2 (Craig 1953).

The second assumption, soil CO_2 flux is at isotopic steady-state, is important for both surface and belowground methods of $\delta^{13}C_{R\text{-}s}$ estimates. When CO2 fluxes in the soil are at isotopic steady-state, the isotopic signal leaving the soil surface is equal to the isotopic source of respiration by definition (Amundson et al. 1998). This means that for measurements made at the soil surface, such as with a chamber, a correction for fractionation due to diffusion is unnecessary. If respiration is not at isotopic steady-state then there is a disequilibrium between the source isotopic signature and the CO_2 emitted through the profile and to the surface. Such a phenomenon might occur with a shift in the dominant carbon substrate being respired for instance. Amundson et al. (1998) showed that such a change from a background signal of 8‰ to a soil isotopic signal of -26‰ could take up to 30 h to come to equilibrium through simulations. Kayler et al. (2008) calculated a time to equilibration of approximately 48 h for nearly the same conditions in a laboratory experiment.

Yet another cause of uncertainty in estimates of $\delta^{13}C_{R\text{-}s}$ is soil gas transport that is not only by diffusion but also by advection, which does not cause fractionation. Advection, or mass flow of CO_2 because of pressure gradients, as a transport mechanism has been suggested in many studies of different ecosystem types (Takle et al. 2004; Risk et al. 2002; Flechard et al. 2007). These observations have led to advection-diffusion transport models that have been verified where geologic sources predominate soil CO_2 flux (Camarda et al. 2007; Lewicki et al. 2003). If gas transport within soil is not solely by diffusion then the correction due to diffusion becomes uncertain, and a correction less than 4.4 ‰ may apply. In this case, ^{13}C and ^{12}C are moved through the soil at nearly the same rate, diminishing the effect of kinetic fractionation resulting from diffusion. However, only a few studies have addressed the influence of advection on the $\delta^{13}C_{R\text{-}s}$; indeed, most reports apply a correction that solely reflects diffusive gas transport (Steinmann et al. 2004; Mortazavi et al. 2004).

There is a need to assess whether or not the assumptions concerning the measurement and analysis of $\delta^{13}C_{R\text{-}s}$ are appropriate given the variability in carbon sources and soil properties in forest ecosystems. During a single day in the early growing

season of 2006, we performed a series of field experiments to investigate the impact of soil gas transport on estimates of $\delta^{13}C_{R\text{-}s}$. To accomplish this we sampled soil gas belowground using a soil probe (Kayler et al. 2008) and aboveground using a mini-tower (Mortazavi et al. 2004) to estimate $\delta^{13}C_{R\text{-}s}$. We hypothesized that there would not be a difference between the two estimates when the soil probe estimate was corrected for kinetic fractionation due to diffusion. We also used the isotopic data from the soil profile in a steady state model (Amundson et al. 1998) of $^{13}CO_2$ based on transport solely by diffusion and a model that accounts for both advection and diffusion (Camarda et al. 2007). We also considered that advection may be difficult to detect and so to further explore the potential influence of advection on aboveground estimates of $\delta^{13}C_{R\text{-}s}$, we induced a negative pressure gradient on the soil surface. Finally, we put the estimates of $\delta^{13}C_{R\text{-}s}$ in an ecological context by comparing the estimated source of respiration with the isotopic signature of carbon in soluble extracts from leaves and phloem as well as the isotopic signature of bulk soil organic matter. Then, using an isotope mixing model, we determined the contribution of new and old carbon sources to $\delta^{13}C_{R\text{-}s}$ for a Douglas-fir stand in the Pacific Northwest.

Methods

Site description The experiment was conducted within a 96 ha watershed ('watershed 1'), located in the H J Andrews Experimental Forest (HJA) in the western Cascades of central Oregon, USA (44.2 °N, 122.2 °W) (see Pypker et al. 2007 for a detailed description). We chose a subplot near the base of the watershed on the south facing slope. Over a 90 minute period on May 2, 2006 we sampled soil respiration and $\delta^{13}C_{R\text{-}s}$ twice. We also collected samples of foliage, phloem and soil organic matter.

The soil has Andic properties and a loamy to silt loam texture. The organic layer is just 2 cm thick and is composed of primarily recognizable litter fragments with almost no discoloring and no signs of amorphous Oa materials. The A horizon extends to a depth of 9 cm where a diffuse AB transition occurs and extends to 30cm; beyond this the B horizon extends to a depth of 42cm.

Soil moisture and temperature Approximately 20 meters away, soil moisture (Echo-20, Decagon Devices, Pullman, WA) and soil temperature (Model 107 temperature probe, Campbell-Scientific Inc.) were measured at 5, 30 and 100 cm depths. Calibration equations that were specific to HJA soils were used to convert the millivolt signal from the soil moisture sensors to volumetric water content (Czarnomski et al. 2005). Figure 4.1 shows soil moisture and temperature for 15 days prior to sampling.

Soil probe This method involves sampling gas for isotopic composition at different depths in the soil. The soil probe contains three isolated wells made from PVC (poly-vinyl chloride). These wells are held at a fixed distance (5, 15 and 30cm) by PVC tubing. The soil probe is further described in Kayler et al. (2008).

We prefilled exetainers with N_2 in a glove box, allowing us to leave the septum on the exetainer unpunctured. To sample gas we used a gas-tight, 3-way ball valve (Whitey, Swagelok, USA) that was fitted with (in order) a hand vacuum pump (Mityvac, Lincoln Indust. Corp., USA), a double-ended needle that received an exetainer (Labco Ltd., UK) prefilled with N_2, and a double-ended needle that connected to the soil probe septum. This allowed for two positions of the valve: in one direction the exetainer was connected in line with the hand pump and when the valve was turned in the opposite direction, the exetainer was in line with the soil probe to sample soil gas. In the field, a N_2 filled exetainer was first connected in line with the hand pump which allowed us to draw a vacuum (-27 kPa) within the exetainer. Then, with the exetainer still under vacuum, we inserted the second double needle into a septum of the soil probe and turned the valve to allow the flux of soil gas from the probe into the exetainer. We waited 30s to allow for equilibration then detached the exetainer and sealed the puncture of the exetainer septa with silicone sealant. The samples were then transported back to the laboratory and analyzed within 24 hours. A standard gas was sampled in the field to ensure no fractionation occurred during sampling, transport or storage.

The gas sample collected from each well was used in a two end-member isotopic mixing model to identify the isotopic signature of the source gas. We used the Miller-Tans (2003) mixing model which describes a sample of the air in a system as a mixture of two sources of $^{13}CO_2$: the background atmosphere and the source of respiration. In field

studies it is assumed that the soil source of respiration is a single, well mixed gas of CO_2 production from microbial and root respiration. The Miller-Tans mixing formula is given in equation 1:

$$\delta_{obs} C_{obs} = \delta_s C_{obs} - C_{bg} (\delta_{bg} - \delta_s) \quad (1)$$

Where C is $[CO_2]$ and the subscripts *obs*, *s*, and *bg* refer to the observed, source and background values. In this case, $\delta^{13}C_{R\text{-}s}$ is estimated as the slope calculated from a geometric mean regression. In Equation 1, δ refers to the isotopic value of the component expressed in δ notation:

$$\delta = (R_{sample} / R_{standard} - 1) * 1000‰ \quad (2)$$

where R is the molar ratio of heavy to light isotopes. The carbon isotope ratio ($\delta^{13}C$) is expressed relative to the standard Vienna Pee Dee belemnite.

For this application, the Miller-Tans slope identifies the isotopic source of CO_2 based on the samples that have been enriched in $^{13}CO_2$ due to kinetic fractionation associated with diffusion. We can correct for this diffusive enrichment by subtracting 4.4‰ from the mixing model estimate, but we must also assume the system is at isotopic steady-state.

Mini-tower The mini-tower is a one meter tall PVC cylinder with 10 swagelocks ports fitted with septa for collection of gas samples above the soil surface. We attached a $1m^2$ rubber sheet around the bottom of the mini-tower where it contacts the soil surface to prevent atmospheric incursion into the soil and to avoid disturbing the vertical CO_2 flux that may occur due to placement of the mini-tower (i.e. a lateral flux that may develop within the soil that would in effect go around the mini-tower footprint). The estimate of $\delta^{13}C_{R\text{-}s}$ was calculated using the Keeling plot method (Keeling 1958). The Keeling plot method relies on the regression of the isotopic signature and the corresponding CO_2 concentration from a series of samples. The sample concentrations are inverted in order to apply a linear regression model where the intercept of the regression (i.e. infinite CO_2 concentration) is the source of respiration. We used an ordinary least squares regression model for the Keeling plot analysis: this combination has been shown to provide accurate estimates of the isotopic signal of respiration (Chapter 2). For estimates of intercept

standard error, we bootstrapped the Keeling plot regression (10,000 iterations) using S-Plus (Insightful Corporation, Seattle, WA, USA).

We installed the mini-tower in the center of the plot without removing the litter layer. We placed weights on the rubber sheet to create a temporary seal between the tower and litter surface. We first sampled the mini-tower for diffusive gas transport. We let the soil gas diffuse into the mini-tower for 45 minutes, after which we sampled the mini-tower from the bottom to the top. We used the same method to sample gas as used for the soil probe. We induced advection after this initial sampling by inserting a rigid rubber disk with a slightly larger diameter than the mini-tower to the bottom of the tower. We then pulled the disk up with an attached handle to generate a vacuum in the tower (-4 kPa), thereby pulling soil CO_2 into the mini-tower. Leaving the rubber disk at the top of the mini-tower, we then proceeded to sample for CO_2 concentration and ^{13}C as described previously. Following the first diffusion and induced advection sampling, we waited another 45 minutes and repeated the sampling process.

Steady state isotopic models:

Diffusion based model Diffusion of CO_2 at steady state is described by Fick's first law:

$$D_s \frac{\partial^2 C}{\partial z^2} = -\phi \qquad (3)$$

where D_s is the bulk diffusion coefficient of soil ($cm^2\ s^{-1}$), C= the concentration of CO_2 at a given depth in the soil profile (mol cm^{-3}), z = depth in the soil profile (cm) and ϕ = production of CO_2 (mol $cm^{-3}\ s^{-1}$). Cerling (1984) developed a production-diffusion model of $^{13}CO_2$ based on the observation that the ^{12}C and ^{13}C diffuse along their own concentration gradients. In the review of isotopes of soil C and CO_2, Amundson et al. (1998) tested a similar model through simulations:

$$R^{13}_{(z)} = \frac{\frac{\phi R^{13}_S}{D^{13}_S}\left(Lz - \frac{z^2}{2}\right) + C_{atm} R^{13}_{atm}}{\frac{\phi}{D_s}\left(Lz - \frac{z^2}{2}\right) + C_{atm}} \qquad (4)$$

The model describes the isotopic ratio of ^{13}C to ^{12}C of a gas sample in the profile withdrawn from depth z. The model assumes that bulk CO_2 production and concentration represent ^{12}C given that it is the most relative abundant isotope of terrestrial carbon (98.9%). The isotopic ratio of $^{13}CO_2$ is a function of the production rate, the isotopic ratio of the source (R^{13}_S), and the diffusion coefficient of $^{13}CO_2$ (bulk soil D_s / 1.0044 which accounts for the greater mass of ^{13}C and its subsequent slower diffusivity). The upper boundary for the model (z=0) is the atmospheric isotopic signature and the lower boundary is the lower limit of respiration (z=L).

We measured soil respiration using a portable infrared gas analyzer (Li-6250, LI-COR Inc, Lincoln, NE) incorporated into a photosynthesis system (Li-6200) and attached to a closed, dynamic soil respiration chamber (Li-6200-09). The chamber was placed on a 10cm diameter by 5 cm tall PVC collar that was installed 2cm into the mineral soil. We used the production value estimated from the gas analyzer and fit the isotopic and concentration profile samples to the above diffusion model. We used a non-linear regression to determine Ds, L and $\delta^{13}C_{R\text{-}s}$.

Advection-Diffusion model. Gas transport that includes both advection and diffusion at steady state is described by Darcy's law and Fick's first law of diffusion:

$$\upsilon \frac{\partial C}{\partial z} - D_s \frac{\partial^2 C}{\partial z^2} = 0 \qquad (5)$$

where the symbols are similar to the diffusion model and υ= the Darcy velocity. Camarda et al. (2007) developed an isotopic steady state model for CO_2 flux described by both advection and diffusion for a single dimension:

$$R(z) = \frac{\left[{}^{13}CO_2\right]_{atm} + \frac{\left[{}^{13}CO_2\right]_{Z_2} - \left[{}^{13}CO_2\right]_{atm}}{e^{\frac{\upsilon}{D^{13}CO_2} z_2} - 1}\left(e^{\frac{\upsilon}{D^{13}CO_2} z} - 1\right)}{\left[{}^{12}CO_2\right]_{atm} + \frac{\left[{}^{12}CO_2\right]_{Z_2} - \left[{}^{12}CO_2\right]_{atm}}{e^{\frac{\upsilon}{D^{12}CO_2} z_2} - 1}\left(e^{\frac{\upsilon}{D^{12}CO_2} z} - 1\right)} \qquad (6)$$

The model describes the steady isotopic profile from a generic depth z_2 (m) to the soil surface, where [$^xCO_2$] = the concentration of either ^{13}C or ^{12}C for the gas sample (vol %), $D^{13}CO_2$= the diffusion coefficient of $^{13}CO_2$ as described above for the diffusion model

(m^2 s^{-1}), and υ = Darcy velocity (m s^{-1}). For this steady state model the pressure gradient and gas velocity that describe υ are assumed to be constant with depth.

The approach is similar to the diffusion model in that both isotopes are modeled independently. The concentration of each isotope is calculated from samples withdrawn from the soil profile by the formulas:

$$\left[{}^{13}CO_2\right]_z = \frac{A\left[CO_2\right]_z}{1+A} \quad , \quad \left[{}^{12}CO_2\right]_z = \frac{\left[CO_2\right]_z}{1+A} \qquad (7)$$

Where A= R_{PDB} x (($\delta^{13}CO_2)_z$ /1000 + 1). The model assumes that the source of $\delta^{13}C_{R\text{-}s}$ is equivalent to the isotopic value at z= -∞.

We used the D_s calculated from the diffusion model to fit the above model to the isotopic and concentration profiles from the soil profile at our site and estimated υ and $\delta^{13}C_{R\text{-}s}$.

Tree Tissue Samples The most recent form of carbon deposited into soil comes from tree tissues. The isotopic signal of recently-fixed photosynthates (assumed to be represented by the isotopic composition of leaf sugars) in leaves could therefore represent “new” carbon sources to soil respiration. However, the isotopic composition of leaf sugars may not be the same as the isotopic signal of carbon that is respired by roots. We sampled tree phloem carbon to better represent the carbon the isotopic signature of carbon respired by roots. Current-year foliage from the three nearest trees was collected using a shot gun. Phloem was sampled from the same trees by using a tree corer to bore into the tree. The phloem sample was separated from xylem and bark in the field. Both foliage and phloem samples were placed in a cooler filled with ice until they were transported back to the laboratory where they were stored in a 0 degree C freezer until they were prepared for isotopic analysis.

To estimate the isotopic signature of bulk Douglas-fir foliage that reflects newly photosynthesized carbon, we analyzed the isotopic signature of carbon extracted from the foliage using hot water (Gessler et al. 2004; Brandes et al. 2006). We incubated 100mg of ground foliage in 1.5ml of millipure water at 100 deg C for 3minutes to precipitate proteins. Following the incubation we pipette the supernatant into 8ml glass vials. We

froze the supernatant in a -70 deg freezer for at least six hours after which the samples were placed in a freeze drier for at least three days.

SOM Samples Soil organic matter samples were taken from the site at 5, 15 and 30cm depth, the same depths from which soil gas samples were taken. The samples were air dried, then ground to a fine powder for isotopic analysis.

Isotopic Analysis For $\delta^{13}C$ analysis of CO_2 samples, we used a Finnigan/MAT DeltaPlus XL isotope ratio mass spectrometer interfaced to a GasBench II automated headspace sampler at the College of Oceanic and Atmospheric Sciences isotope facility, Oregon State University. The GasBench-II is a continuous flow interface that allows injections of several aliquots of a single gas sample into a mass spectrometer for automated isotope determinations of small gas samples. Exetainers of sampled gas were loaded onto a Combi-PAL auto-sampler attached to the GasBench. Helium pushed the sample air out of the exetainer and into the mass spectrometer. A typical analysis consisted of three gas standards (tank CO_2-He mixtures), five sample replicates and an additional 2 gas standards for every sample. The CO_2 concentration of each sample was calculated from the peak volt area produced by the mass spectrometer analysis of each sample.

The carbon isotope composition of organic matter was measured at the Idaho Stable Isotope Laboratory, where samples were run on a continuous-flow stable isotopic analyses utilizing the Finnigan-MAT, Delta plus isotope ratio mass spectrometer (IRMS). The tree and soil organic matter samples were flash-combusted using CE Instrument's NC 2500 elemental analyzer, interfaced through the Conflo II and sent to the IRMS. Analysis of internal laboratory standards ensured that the estimates of the organic isotopic were accurate to within 0.1‰.

Component Contributions We used the IsoSource stable isotope mixing model described by Phillips and Gregg (2003) to determine the partition contribution to $\delta^{13}C_{R\text{-}s}$ of the SOM at three depths, the foliage and phloem hot water extracts, and in the case of the mini-tower analyses an additional atmospheric component (Table 4.1). We then aggregated the SOM samples *a posteriori* (Phillips et al. 2005) into a group that

represented old carbon sources while foliage and phloem extracts represented independent groups of new carbon sources. For the IsoSource analyses of the mini-tower date, we grouped the foliage and phloem into an aboveground source, the SOM into a belowground source and we included an atmospheric component which represented a third source by itself. We used software settings of 0.1‰ tolerance, 1% intervals and used a component precision of 0.1‰. The output of the model is expressed as the percent frequency of all possible solutions and we report the range of proportions for each source.

Results

Soil probe and profile models The soil gas CO_2 concentration had a range of approximately 5000 μmol mol^{-1} with a corresponding isotopic range of 7‰ as depicted by the isotopic and concentration profiles (Figure 4.2). A difference in concentration of 1500 μmol mol^{-1} was apparent between soil probe 3 at 30cm and the two other probes. The effect of this difference was small as the average of the mixing model estimate was -25.6‰ (Table 4.1 and 4.2; Figure 4.3). The Miller-Tans mixing model estimate of $\delta^{13}C_{R\text{-}s}$ from the soil probes was on average 3.8‰ (0.2 se) enriched relative to the diffusive model source estimate and 4.0‰ (0.6 se) with respect to the advection-diffusion estimate (Table 4.1).

The soil respiration rate was 4.1 μmol m^2s^{-1}.The diffusivity of the soil was on average 8.1 x 10^{-6} m s^{-1} (4.5 x 10^{-6} m s^{-1}se) while the Darcy velocity was on average -2.2 x 10^{-5} m s^{-1} (9.6 x 10^{-6} m s^{-1} se) indicating a flux of atmospheric carbon into the soil profile. Given that there was no indication of advection out of the soil and the similarity in predicted profiles, we adjusted the source estimate of the advection-diffusion model by -4.4‰. The average source of $\delta^{13}C_{R\text{-}s}$ estimated from the steady state diffusive model of the soil probe data was 29.1‰ and 29.3 ‰ from the advection-diffusion model. The variation of the advection-diffusion model was greater than the diffusion model (Table 4.1) and depleted by 0.2‰ on average with a range of -1.88‰ to 1.24‰. The advection-diffusion model more closely predicted the soil profile samples (Figures 4.6 and 4.7).

Mini-tower We sampled the soil respired CO_2 twice within 90 minutes using the mini-tower technique. The concentration gradient between the mini-tower and the background atmosphere was on the order of 375 μmol mol^{-1} with a corresponding isotopic range of 8.5‰ (Figure 4.4). There was a high degree of variability within the mini-tower profiles and distinct geometric gradients did not develop from the soil surface to the top of the mini-tower. We omitted the 4.5cm sample during the first 45 minute sampling from further analysis because it was uncharacteristically depleted with respect to the other samples and most likely experienced fractionation. Despite the variation of the mini-tower profiles the Keeling plot estimates (Figure 4.5) of the $\delta^{13}C_{R\text{-}s}$ were fairly similar, (Table 4.2) yielding a difference of 0.72‰ between the two.

Induced advection Inducted advection within the mini-tower resulted in changes in the concentration and isotopic profiles. The profiles of the first 45 minute sampling were variable, but in comparison to the diffusive mini-tower sampling, the sample concentration values were greater near the soil surface and decreased with height from 30 cm (Figure 4.4). The isotopic values were all depleted relative to the diffusive mini-tower samples, with samples below 21cm having the lowest concentration of ^{13}C. The second advective mini-tower sampling resulted in more consistent profiles where all samples had greater concentration values and depleted isotopic values relative to the diffusive sampling of the mini-tower. The variation in the mini-tower concentration and isotopic profiles resulted in a 0.3‰ between the first and second diffusive mini-tower sampling and a 1‰ difference between the first and second advective sampling (Table4.2).

Organic Matter The isotopic signal of tree and soil samples became increasingly enriched along the plant-soil continuum resulting in a 4.5‰ gradient from tree foliage to soil at 30cm (Table 4.3). The phloem water-soluble extracts were on average 1.6‰ enriched relative to the water soluble extracts of foliage. The isotopic signal of SOM became increasingly enriched with soil depth representing an enrichment of 1.3‰.

Component Contribution The predominate contribution (69-98%) to $\delta^{13}C_{R\text{-}s}$ was from a depleted source that was similar to the isotopic signature of the foliar soluble extracts. In

this analysis we used the average source estimate from the diffusion and advection-diffusion models (-29.2‰) (Figure 4.8). The phloem contribution ranged from 0 to 31% and the contribution from belowground sources ranged from 0 to 16%. The partitioning results were much more diffuse when we implemented the mini-tower source estimate when measured under diffusive conditions (Figure 4.9). In this case the aboveground component (phloem and foliar extracts) contribution ranged from 0 to 78% and the belowground component contribution ranged from 0 to 90%. In partitioning the mini-tower source estimate, we also considered the contribution from the ambient atmosphere which was estimated to range from 8 to 26%.

Discussion

Soil $^{13}CO_2$ transport and measurement: Soil gas transport during the experiment was primarily by diffusion, and the mixing model estimate was enriched on average by 3.8 to 4.0‰ with respect to the source estimates by the transport models, indicating that the soil ^{13}C was at semi-steady-state. The advection-diffusion model tended to more accurately depict the isotopic samples from the soil profile. The Darcy velocities estimated from the model were negative, suggesting a significant influence of the background atmosphere is necessary to achieve the pattern described by our field samples. It is unknown the extent to which the influx of the background atmosphere will affect the fractionation of the source isotopic signal. However, based on the similarity in profiles predicted by the diffusion and advection-diffusion models we can infer that the effect is small.

Based on the isotopic steady-state theory of CO_2 diffusion, the isotopic signature of soil respiration at the surface is equivalent to the isotopic source signature and will therefore be depleted by 4.4‰ relative to the uncorrected mixing model estimate made from belowground samples. We found the maximum difference between the uncorrected belowground estimate of $\delta^{13}C_{R\text{-}s}$ and aboveground techniques to be -2.36‰; where the *aboveground* estimate is enriched relative to the belowground estimate by the soil probe. Mortazavi et al. (2004) found a good agreement between estimates made from the soil profile and the mini-tower they employed and one explanation for our contrasting results may be due to differences in site conditions or mini-tower construction.

The mini-tower estimate may also be different due to an enriched isotopic source that is absent from the belowground samples. The organic matter in the litter layer is one possible location for this source that the mini-tower captures; although the isotopic signature of litter is generally lighter than SOM (Ehleringer et al. 2000, Gleixner 2005). And while the question of whether or not isotopic fractionation occurs during microbial respiration remains to be resolved, the magnitude of this potential fractionation is small, and it cannot explain the difference between our aboveground and belowground estimate of $\delta^{13}C_{R\text{-}s}$ (Schweizer et al.1999; Fernandez and Cadisch 2003; Högberg et al. 2005). Respiration from fungi is another possible source responsible for the enriched signal. Respiration from ectomycorrhizal sporocaps has been shown to be enriched by up to 1‰ (Bostrom et al. 2008); however, no sporocaps were present during the measurement. The soil probe has proved to capture *in-situ* sources (Kayler et al. 2008) and given that isotopic signatures above the soil surface in the litter layer will be depleted with respect to the mini-tower estimate, it is unlikely that an enriched organic source will be found that explains the difference between the two estimates of $\delta^{13}C_{R\text{-}s}$.

The background atmosphere is a highly enriched source relative to the other sources in the soil-plant continuum and it is possible that atmospheric incursion (Livingston et al. 2006) due to natural phenomena or to disturbance during the installation of the mini-tower diluted the source signal estimated by the mini-tower. The advection-diffusion model estimated a negative Darcy velocity, or flux of atmospheric CO_2 into the soil profile. Such atmospheric incursion has been documented in previous soil isotopic studies (Millard et al. 2008; Susfalk et al. 2002; Dudziak and Halas 1996) and may represent up to 26% of the mini-tower estimate as determined by the IsoSource mixing model results.

Transport due to advection, the mass flow due to pressure gradients, may drive heavy atmospheric $^{13}CO_2$ into the soil or withdraw unfractionated soil $^{13}CO_2$ out. The difference between the advective and diffusive sampling of the mini-tower was at most depleted by 1‰. These results were surprising; we expected an enriched $\delta^{13}C_{R\text{-}s}$ which would result from soil gas enriched in ^{13}C pulled up into the mini-tower for sampling. We clearly pulled soil gas into the mini-tower: CO_2 samples were both greater in concentration and depleted in ^{13}C with reference to the diffusive sampling, yielding an

estimate of $\delta^{13}C_{R\text{-}s}$ that was nearly identical to the uncorrected estimate produced by the soil probe. This suggests that the induced advection experiment introduced soil gas that was uncontaminated by the isotopic signature of the background atmosphere. These results taken together with the partitioning results and the evidence of atmospheric incursion illustrate that care must be taken when using aboveground approaches such as closed chambers or open systems such as the mini-tower.

In the advection experiment of this study, we generated a negative pressure of approximately -4 kPa. This value is far greater than the -5 Pa on $\delta^{18}O$ used to model effects on soil respiration (Stern et al. 1999) and -15 Pa induced for a field experiment that investigated the effects of pressure pumping on soil respiration (Takle et al. 2004). Thus, the -1‰ difference between the mini-tower estimate under diffusive and advective conditions may represent an upper bounds of the effects of advection on the apparent fractionation of ^{13}C. With natural fluctuations of pressure that are five orders of magnitude less than the negative pressure we generated, we can infer that gradients due to atmospheric pressure alone will not pull representative soil gas toward the soil surface. We were not able to sample the soil profile during the advection experiment although the profiles proved to be stable given that there was little change in the profiles 45 minutes after the first experiment.

Partitioning the contribution of new and old carbon sources to $\delta^{13}C_{R\text{-}s}$ We calculated that 69 to 98% of the carbon respired from soil was from a depleted isotopic source that was similar to the signature of foliar extracts. The phloem isotopic signature, which we used as a proxy for the carbon substrate of root respiration, was estimated to account for 0 to 31% of respiration indicating that root respiration also contributes to $\delta^{13}C_{R\text{-}s}$ during this period of the growing season. However, even if root respiration accounted for 31% of $\delta^{13}C_{R\text{-}s}$ then 69% of soil respiration came from a source with a highly depleted isotopic signature. The most likely respiratory source of this isotopic signature is dissolved organic carbon (DOC) where carbon is leached from leaves in the tree canopies and decomposing litter (Qualls et al. 1991; McDowell and Likens 1988; Michalzik et al. 2001). To date, the contribution of carbon from DOC to soil respiration is not well

quantified and ranges from low (Neff and Asner 2001) to relatively high (Jones et al. 2008), close to 90% in one case (Jandl and Sollins 1997). Few studies have measured the isotopic composition of DOC from soil, but those that have, report an isotopic signature that is depleted in ^{13}C and is comparable to the signature of foliage at their site (Cleveland et al. 2004; Ziegler and Brisco 2004; Kaiser et al. 2001). The patterns of DOC in this region are dynamic in terms of chemistry, seasonality and carbon sources (Yano et al. 2005; Yano et al. 2004; Lajtha et al. 2005) and further studies are needed to determine the contribution of DOC to $\delta^{13}C_{R\text{-}s}$ during the early growing season.

The isotopic signal of the forest components becomes even more relevant in light of the uncertainty in determining $\delta^{13}C_{R\text{-}s}$. At one end of the plant-soil isotopic continuum, we measured the water soluble extracts of fresh foliage, which had the lightest isotopic signal, consistent with results of leaf material from other forests. If we did not use the phloem isotopic signature as a proxy for root respiration and instead had used the extracts of foliage, we might have mistakenly attributed almost 90% of soil respiration to root respiration. We recognize that the phloem isotopic signal itself is not necessarily the same substrate metabolized by roots and subsequently respired as $^{13}CO_2$ (Badeck et al. 2005; Gottlicher et al. 2006). Quantifying root respiration is difficult, and until we know more about the alterations made to the carbon in phloem during transport, we cannot determine the success of phloem water soluble extracts as a proxy for tree contributions belowground.

Conclusion

We have illustrated the importance of considering: fractionation in the context of soil CO_2 transport, measurement technique and collection of representative sources when using ^{13}C to describe forest soil respiration. We found that aboveground measurements may be particularly susceptible to atmospheric incursion which may produce $\delta^{13}C_{R\text{-}s}$ estimates that are enriched in ^{13}C. We have also shown how the samples of the atmosphere-plant-soil continuum are critical to the analysis of $\delta^{13}C_{R\text{-}s}$. Finally, using ^{13}C as a natural tracer we have provided evidence that DOC as the potential driver of early growing season soil respiration in Douglas-fir ecosystems.

References

Amundson, R., L. Stern, T. Baisden and Y. Wang (1998). The isotopic composition of soil and soil-respired CO_2. Geoderma 82(1-3): 83-114.

Amundson, R. (2001). The carbon budget in soils. Annual Review of Earth and Planetary Sciences 29: 535-562.

Badeck, F. W., G. Tcherkez, S. Nogues, C. Piel and J. Ghashghaie (2005). Post-photo synthetic fractionation of stable carbon isotopes between plant organs - a widespread phenomenon. Rapid Communications in Mass Spectrometry 19(11): 1381-1391.

Boone, R. D., K. J. Nadelhoffer, J. D. Canary and J. P. Kaye (1998). Roots exert a strong influence on the temperature sensitivity of soil respiration. Nature 396(6711): 570-572.

Bostrom, B., D. Comstedt and A. Ekblad (2008). Can isotopic fractionation during respiration explain the C-13-enriched sporocarps of ectomycorrhizal and saprotrophic fungi? New Phytologist 177(4): 1012-1019.

Brandes, E., N. Kodama, K. Whittaker, C. Weston, H. Rennenberg, C. Keitel, M. A. Adams and A. Gessler (2006). Short-term variation in the isotopic composition of organic matter allocated from the leaves to the stem of Pinus sylvestris: effects of photosynthetic and postphotosynthetic carbon isotope fractionation. Global Change Biology 12(10): 1922-1939.

Camarda, M., S. De Gregorio, R. Favara and S. Gurrieri (2007). Evaluation of carbon isotope fractionation of soil CO_2 under an advective-diffusive regimen: A tool for computing the isotopic composition of unfractionated deep source. Geochimica Et Cosmochimica Acta 71(12): 3016-3027.

Carbone, M. S. and S. E. Trumbore (2007). Contribution of new photosynthetic assimilates to respiration by perennial grasses and shrubs: residence times and allocation patterns. New Phytologist 176(1): 124-135.

Cerling, T. E. (1984). The Stable Isotopic Composition of Modern Soil Carbonate and Its Relationship to Climate. Earth and Planetary Science Letters 71(2): 229-240.

Cerling, T. E., D. K. Solomon, J. Quade and J. R. Bowman (1991). On the isotopic composition of carbon in soil carbon-dioxide. Geochimica Et Cosmochimica Acta 55(11): 3403-3405.

Cleveland, C. C., J. C. Neff, A. R. Townsend and E. Hood (2004). Composition, dynamics, and fate of leached dissolved organic matter in terrestrial ecosystems: Results from a decomposition experiment. Ecosystems 7(3): 275-285.

Czarnomski, N., G. W. Moore, T. G. Pypker, J. Licata and B. J. Bond (2005). Precision and accuracy of three alternative instruments for measuring soil water content in two forest soils of the Pacific Northwest. Canadian Journal of Forest Research-Revue Canadienne De Recherche Forestiere 35(8): 1867-1876.

Dudziak, A. and S. Halas (1996). Diurnal cycle of carbon isotope ratio in soil CO_2 in various ecosystems. Plant and Soil 183(2): 291-299.

Ehleringer, J. R., N. Buchmann and L. B. Flanagan (2000). Carbon isotope ratios in belowground carbon cycle processes. Ecological Applications 10(2): 412-422.

Ekblad, A. and P. Högberg (2000). Analysis of $\delta^{13}C$ of CO_2 distinguishes between microbial respiration of added C-4-sucrose and other soil respiration in a C-3-ecosystem. Plant and Soil 219(1-2): 197-209.

Ekblad, A. and P. Högberg (2001). Natural abundance of ^{13}C in CO_2 respired from forest soils reveals speed of link between tree photosynthesis and root respiration. Oecologia 127(3): 305-308.

Epron, D., V. Le Dantec, E. Dufrene and A. Granier.2001. Seasonal dynamics of soil carbon dioxide efflux and simulated rhizosphere respiration in a beech forest. Tree Physiology 21(2-3): 145-152.

Fernandez, I. and G. Cadisch (2003). Discrimination against ^{13}C during degradation of simple and complex substrates by two white rot fungi. Rapid Communications in Mass Spectrometry 17(23): 2614-2620.

Flechard, C. R., A. Neftel, M. Jocher, C. Ammann, J. Leifeld and J. Fuhrer (2007). Temporal changes in soil pore space CO_2 concentration and storage under permanent grassland. Agricultural and Forest Meteorology 142(1): 66-84.

Gessler, A., H. Rennenberg and C. Keitel (2004). Stable isotope composition of organic compounds transported in the phloem of European beech - Evaluation of different methods of phloem sap collection and assessment of gradients in carbon isotope composition during leaf-to-stem transport. Plant Biology 6(6): 721-729.

Gleixner, G. (2005). Stable Isotope Composition of Soil Organic Matter. Stable Isotopes and Biosphere-Atmosphere Interactions. L. B. Flanagan, J. R. Ehleringer and D. E. Pataki. San Francisco, USA, Elsevier: 29-46.

Gottlicher, S., A. Knohl, W. Wanek, N. Buchmann and A. Richter (2006). Short-term changes in carbon isotope composition of soluble carbohydrates and starch: from canopy leaves to the root system. Rapid Communications in Mass Spectrometry 20(4): 653-660.

Hanson, P. J., N. T. Edwards, C. T. Garten and J. A. Andrews (2000). Separating root and soil microbial contributions to soil respiration: A review of methods and observations. Biogeochemistry 48(1): 115-146.

Högberg , P., A. Ekblad, A. Nordgren, A. H. Plamboeck, A. Ohlsson, Bhupinderpal-Singh and M. Hoegber (2005). Factors determining the ^{13}C abundance of soil-respired CO_2 in Boreal Forests. Stable Isotopes and Biosphere-Atmosphere Interactions. L. B. Flanagan, J. R. Ehleringer and D. E. Pataki. San Francisco, USA, Elsevier: 47-68.

Högberg , P. and D. J. Read (2006). Towards a more plant physiological perspective on soil ecology. Trends in Ecology & Evolution 21(10): 548-554.

Jandl, R., P. Sollins (1997). Water-extractable soil carbon in relation to the belowground carbon cycle. Biology and Fertility of Soils 25: 196-201.

Kaiser, K., G. Guggenbergre and W. Zech (2001). Isotopic fractionation of dissolved organic carbon in shallow forest soils as affected by sorption. European Journal of Soil Science 52(4): 585-597.

Kayler, Z. E., E. W. Sulzman, J. D. Marshall, A. Mix, W. D. Rugh and B. J. Bond (2008). A laboratory comparison of two methods used to estimate the isotopic composition of soil $\delta^{13}CO_2$ efflux at steady state. Rapid Communications in Mass Spectrometry 22(16): 2533-2538.

Keeling, C. D. (1958). The concentration and isotopic abundances of atmoshperic carbon dioxide in rural areas. Geochimica Et Cosmochimica Acta 13: 322-334.

Klumpp, K., R. Schaufele, M. Lotscher, F. A. Lattanzi, W. Feneis and H. Schnyder (2005). C-isotope composition of CO_2 respired by shoots and roots: fractionation during dark respiration? Plant Cell and Environment 28(2): 241-250.

Kodama, N., RL Barnard, Y Salmon, C Weston, JP Ferrio, J Holst, RA Werner, M Saurer, H Rennenberg, N Buchmann, A Gessler.2008. Temporal dynamics of the carbon isotope compositin in a *Pinus sylvestris* stand: from newly assimilated organic carbon to respired carbon dioxide. Oecologia 156(4): 737-750.

Lajtha, K., S. E. Crow, Y. Yano, S. S. Kaushal, E. Sulzman, P. Sollins and J. D. H. Spears (2005). Detrital controls on soil solution N and dissolved organic matter in soils: a field experiment. Biogeochemistry 76(2): 261-281.

Lewicki, J. L., W. C. Evans, G. E. Hilley, M. L. Sorey, J. D. Rogie and S. L. Brantley (2003). Shallow soil CO_2 flow along the San Andreas and Calaveras Faults, California. Journal of Geophysical Research-Solid Earth 108(B4).

Livingston, G. P., G. L. Hutchinson and K. Spartalian (2006). Trace gas emission in chambers: A non-steady-state diffusion model. Soil Science Society of America Journal 70(5): 1459-1469.

Luo, Y. and X. Zhou (2006). Soil Respiration and the Environment. San Francisco, Academic Press.

McDowell, W.H. and G.E. Likens (1998). Origin, composition and flux of dissolved organic carbon in the Hubbard Brook Valley. Ecological Monographs 58:177-195.

Michalzik B, K. Kalbitz, J.-H. Park, S. Solinger, E. Matzner (2001). Fluxes and concentrations of dissolved organic carbon and nitrogen – a synthesis for temperate forests. Biogeochemistry 52:173-205.

Millard, P., A. J. Midwood, J. E. Hunt, D. Whitehead and T. W. Boutton (2008). Partitioning soil surface CO_2 efflux into autotrophic and heterotrophic components, using natural gradients in soil $\delta^{13}C$ in an undisturbed savannah soil. Soil Biology & Biochemistry 40(7): 1575-1582.

Miller, J. B. and P. P. Tans (2003). Calculating isotopic fractionation from atmospheric measurements at various scales. Tellus Series B-Chemical and Physical Meteorology 55(2): 207-214.

Mora, G. and J. W. Raich (2007). Carbon-isotopic composition of soil-respired carbon dioxide in static closed chambers at equilibrium. Rapid Communications in Mass Spectrometry 21(12): 1866-1870.

Mortazavi, B., J. L. Prater and J. P. Chanton (2004). A field-based method for simultaneous measurements of the $\delta^{18}O$ and $\delta^{13}C$ of soil CO_2 efflux. Biogeosciences 1(1): 1-9.

Neff, J.C. and G.P. Asner (2001). Dissolved organic carbon in terrestrial ecosystems: synthesis and a model. Ecosystems 4:29-48.

Ohlsson, K. E. A., S. Bhupinderpal, S. Holm, A. Nordgren, L. Lovdahl and P. Högberg .2005. Uncertainties in static closed chamber measurements of the carbon isotopic ratio of soil-respired CO_2. Soil Biology & Biochemistry 37(12): 2273-2276.

Pendall, E., S. Bridgham, P. J. Hanson, B. Hungate, D. W. Kicklighter, D. W. Johnson, B. E. Law, Y. Q. Luo, J. P. Megonigal, M. Olsrud, M. G. Ryan and S. Q. Wan (2004). Below-ground process responses to elevated CO_2 and temperature: a discussion of observations, measurement methods, and models. New Phytologist 162(2): 311-322.

Phillips, D. L. and J. W. Gregg (2003). Source partitioning using stable isotope: coping with too many sources. Oecologia 136: 261-269.

Phillips, D. L., S. D. Newsome and J. W. Gregg (2005). Combining sources in stable isotope mixing models: alternative methods. Oecologia 144(4): 520-527.

Pregitzer, K. S., J. A. King, A. J. Burton and S. E. Brown (2000). Responses of tree fine roots to temperature. New Phytologist 147(1): 105-115.

Pregitzer, K., W. Loya, M. Kubiske and D. Zak (2006). Soil respiration in northern forests exposed to elevated atmospheric carbon dioxide and ozone. Oecologia 148(3): 503-516.

Pypker, T. G., M. H. Unsworth, A. C. Mix, W. Rugh, T. Ocheltree, K. Alstad and B. J. Bond (2007). Using nocturnal cold air drainage flow to monitor ecosystem processes in complex terrain. Ecological Applications 17(3): 702-714.

Qualls R.G., B.L. Haines, W.T. Swank (1991). Fluxes of dissolved organic nutrients and humic substances in a deciduous forest. Ecology 72:254-266.

Risk, D., L. Kellman and H. Beltrami (2002). Soil CO_2 production and surface flux at four climate observatories in eastern Canada. Global Biogeochemical Cycles 16(4).

Schimel, D. S. (1995). Terrestrial Ecosystems and the Carbon-Cycle. Global Change Biology 1(1): 77-91.

Schweizer, M., J. Fear and G. Cadisch (1999). Isotopic (^{13}C) fractionation during plant residue decomposition and its implications for soil organic matter studies. Rapid Communications in Mass Spectrometry 13(13): 1284-1290.

Steinmann, K. T. W., R. Siegwolf, M. Saurer and C. Korner (2004). Carbon fluxes to the soil in a mature temperate forest assessed by ^{13}C isotope tracing. Oecologia 141(3): 489-501.

Stern, L., W. T. Baisden and R. Amundson (1999). Processes controlling the oxygen isotope ratio of soil CO_2: Analytic and numerical modeling. Geochimica Et Cosmochimica Acta 63(6): 799-814.

Subke, J. A., I. Inglima and M. F. Cotrufo (2006). Trends and methodological impacts in soil CO_2 efflux partitioning: A metaanalytical review. Global Change Biology 12(6): 921-943.

Susfalk RB, W. C., DW Johnson, RF Walker, P Verburg, S FU.2002. Lateral Diffusion and atmospheric CO_2 mixing compromise estimates of rhizoshpere respiration in a forest soil. Canadian Journal of Forest Research 32(6): 1005-1015.

Takahashi, Y., N. Liang, R. Hirata and T. Machida (2008). Variability in carbon stable isotope ratio of heterotrophic respiration in a deciduous needle-leaf forest. Journal of Geophysical Research-Biogeosciences 113(G1).

Takle, E. S., W. J. Massman, J. R. Brandle, R. A. Schmidt, X. H. Zhou, I. V. Litvina, R. Garcia, G. Doyle and C. W. Rice (2004). Influence of high-frequency ambient pressure pumping on carbon dioxide efflux from soil. Agricultural and Forest Meteorology 124(3-4): 193-206.

Yano, Y., K. Lajtha, P. Sollins and B. A. Caldwell (2004). Chemical and seasonal controls on the dynamics of dissolved organic matter in a coniferous old-growth stand in the Pacific Northwest, USA. Biogeochemistry 71(2): 197-223.

Yano, Y., K. Lajtha, P. Sollins and B. A. Caldwell (2005). Chemistry and dynamics of dissolved organic matter in a temperate coniferous forest on Andic soils: Effects of litter quality. Ecosystems 8(3): 286-300.

Ziegler, S. E. and S. L. Brisco (2004). Relationships between the isotopic composition of dissolved organic carbon and its bioavailability in contrasting Ozark streams. Hydrobiologia 513(1-3): 153-169.

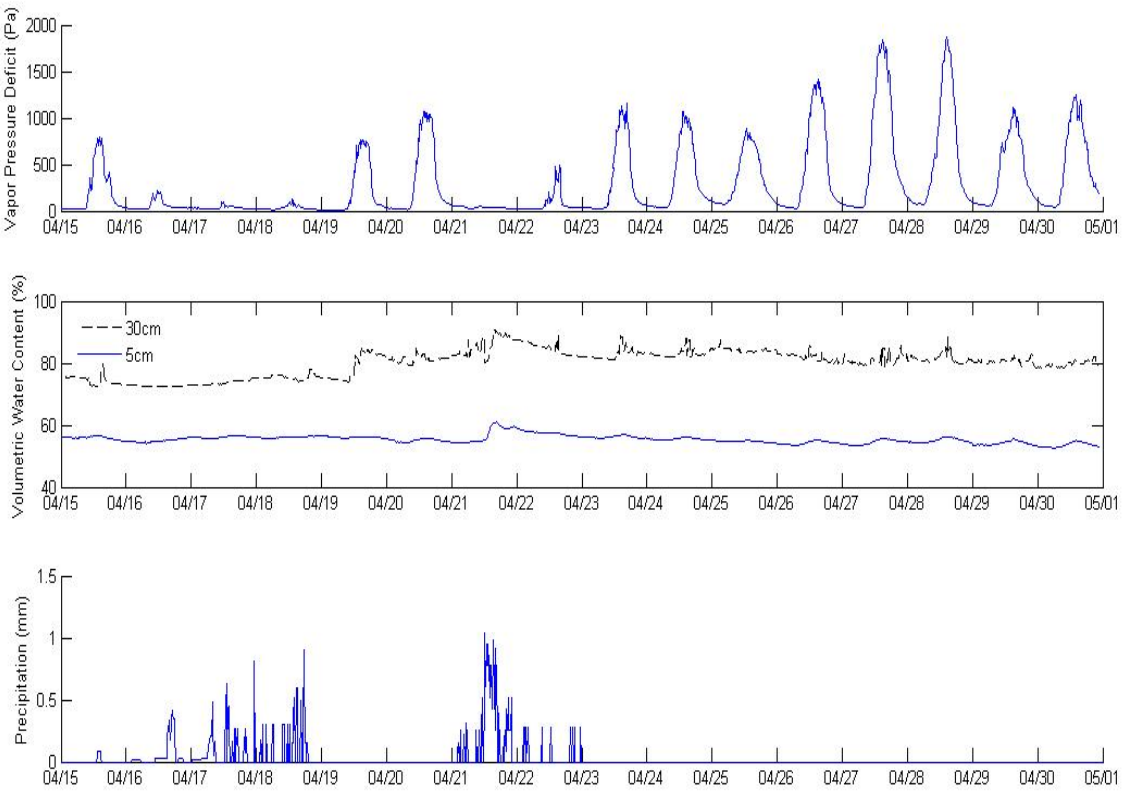

Figure 4.1 Vapor pressure deficit, soil moisture, and precipitation for 15 days prior to the sampling date in WS1 of the H.J. Andrews.

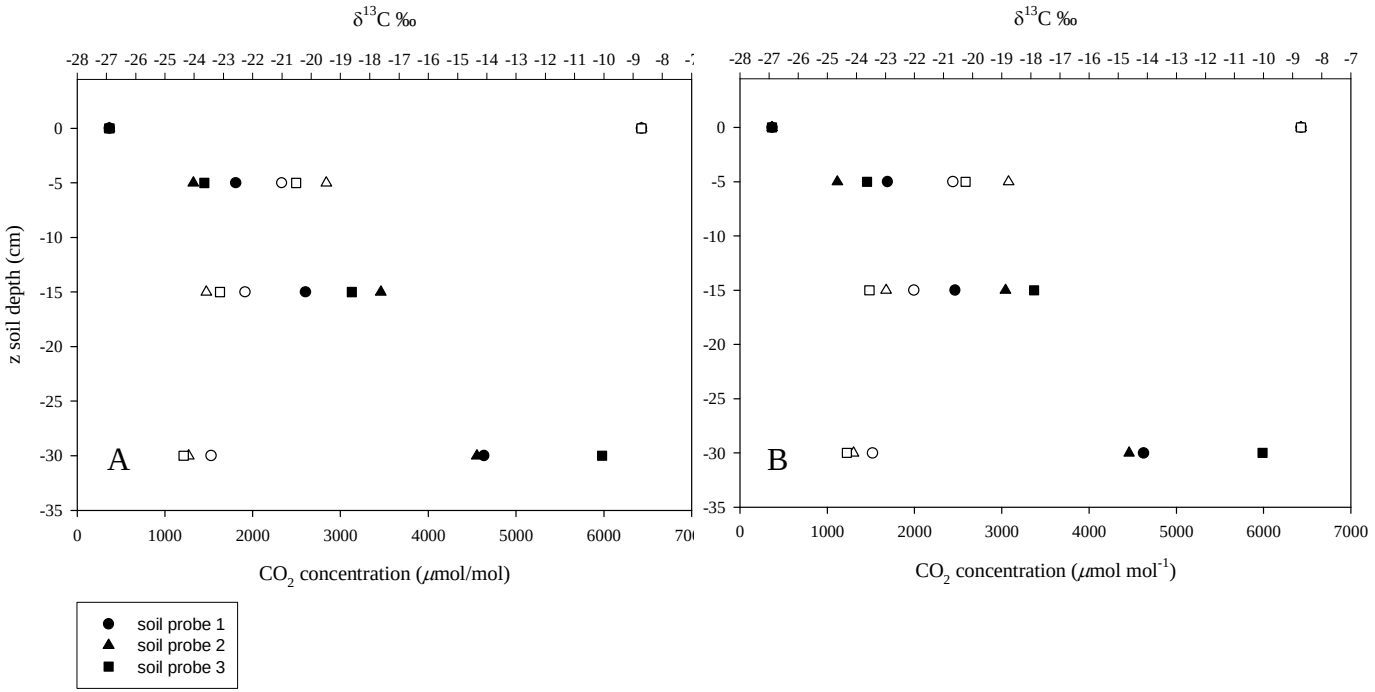

Figure 4.2 Soil CO_2 concentration and isotopic profiles at time 45 (A) and 90 (B) minutes during sampling period. Open symbols are isotope values and closed symbols are concentration values.

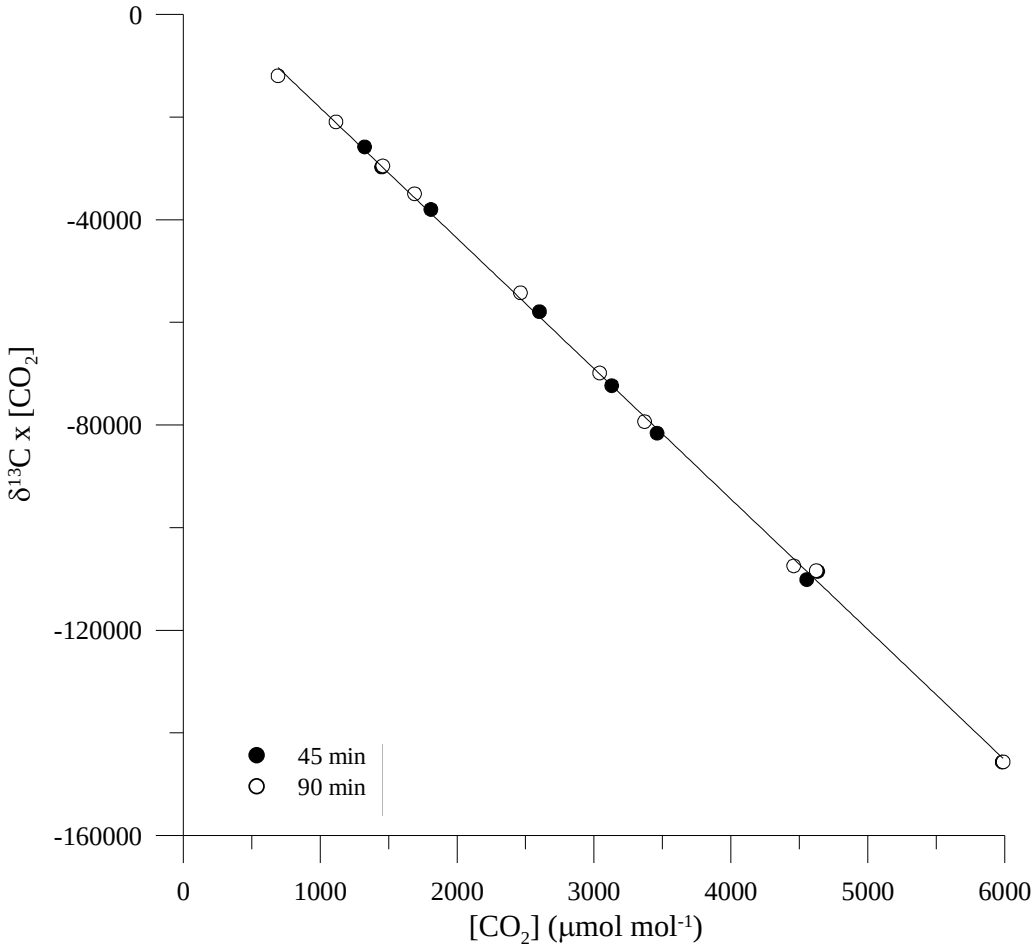

Figure 4.3 Miller-Tans mixing line of soil probe samples. Both sets of soil gas samples are depicted on the same line derived from a geometric mean regression.

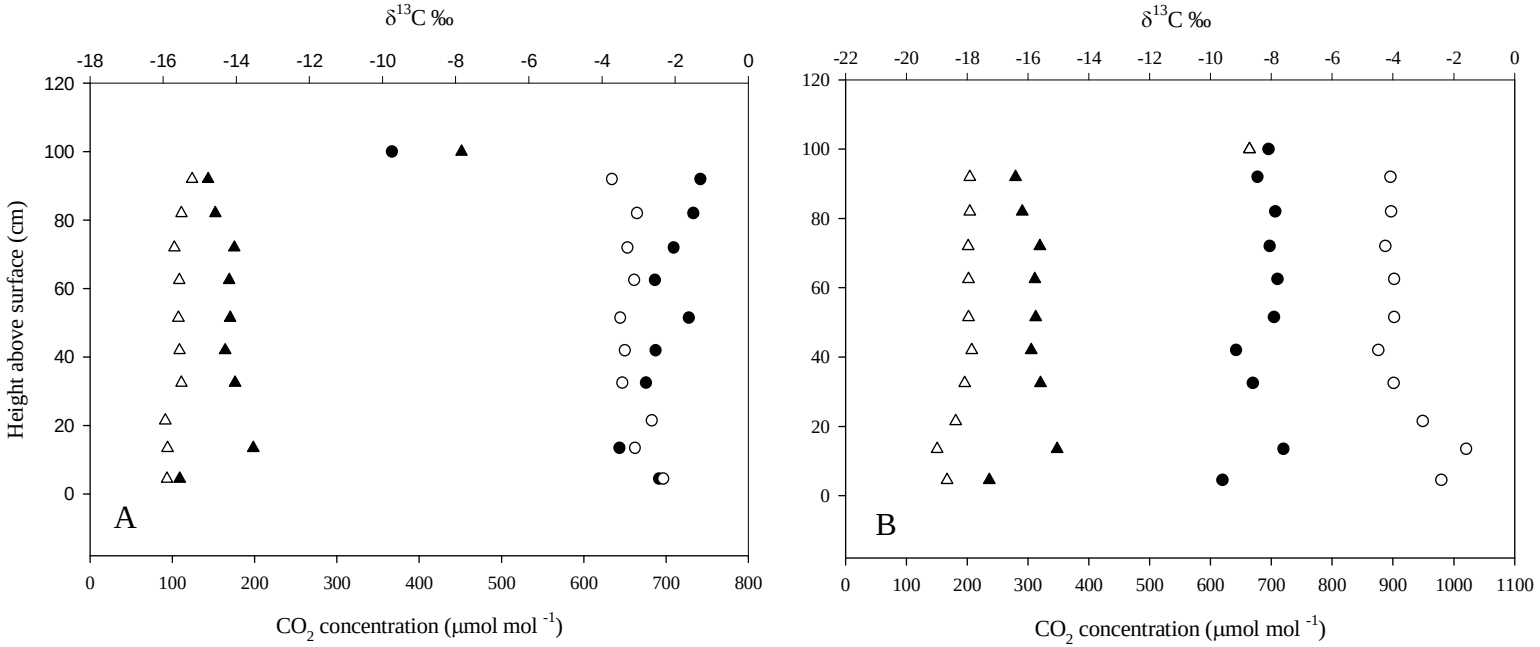

Figure 4.4 Mini-tower CO_2 concentration (circles) and isotopic (triangles) profiles at time 45 (A) and 90 (B) minutes during the sampling period. Open symbols refer to the samples from the advection experiment.

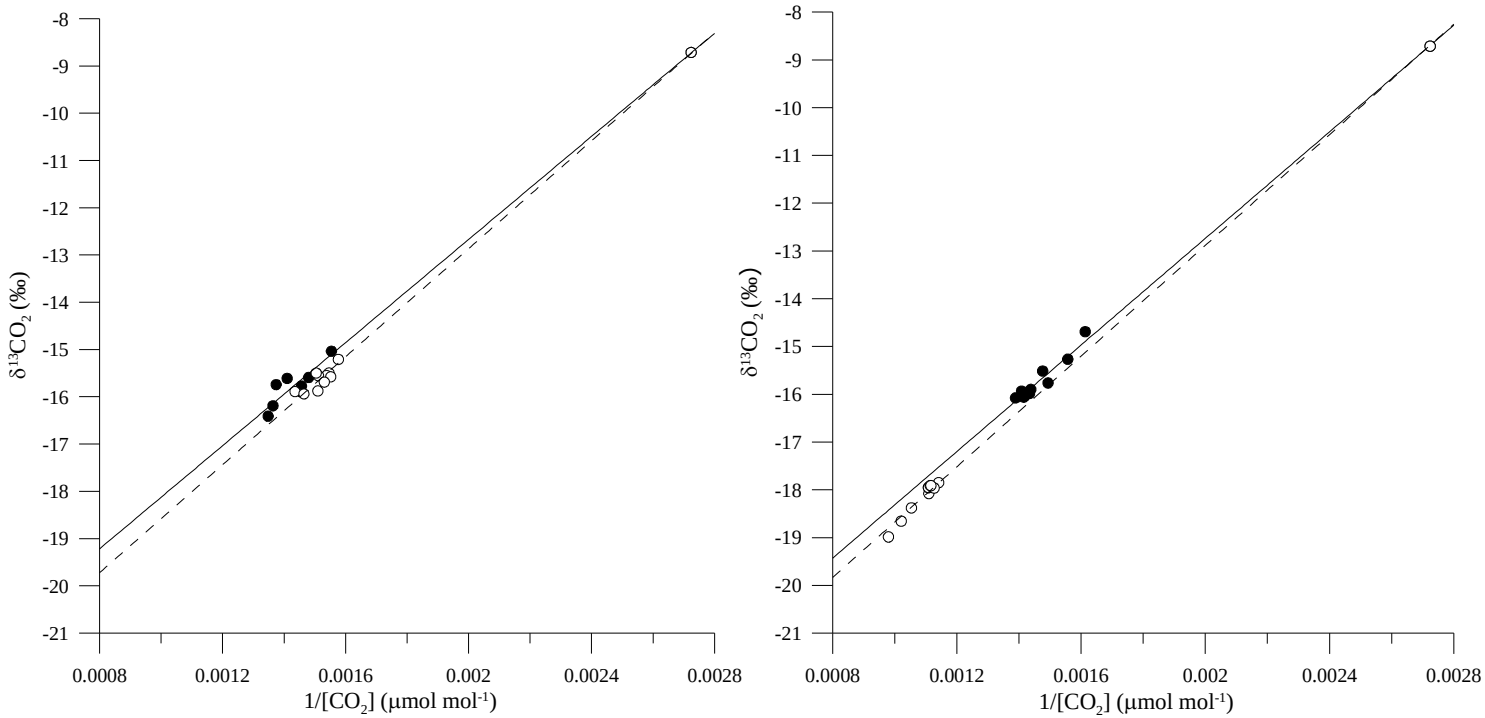

Figure 4.5 Mini-tower Keeling plots. Open symbols refer to samples from the advection experiment.

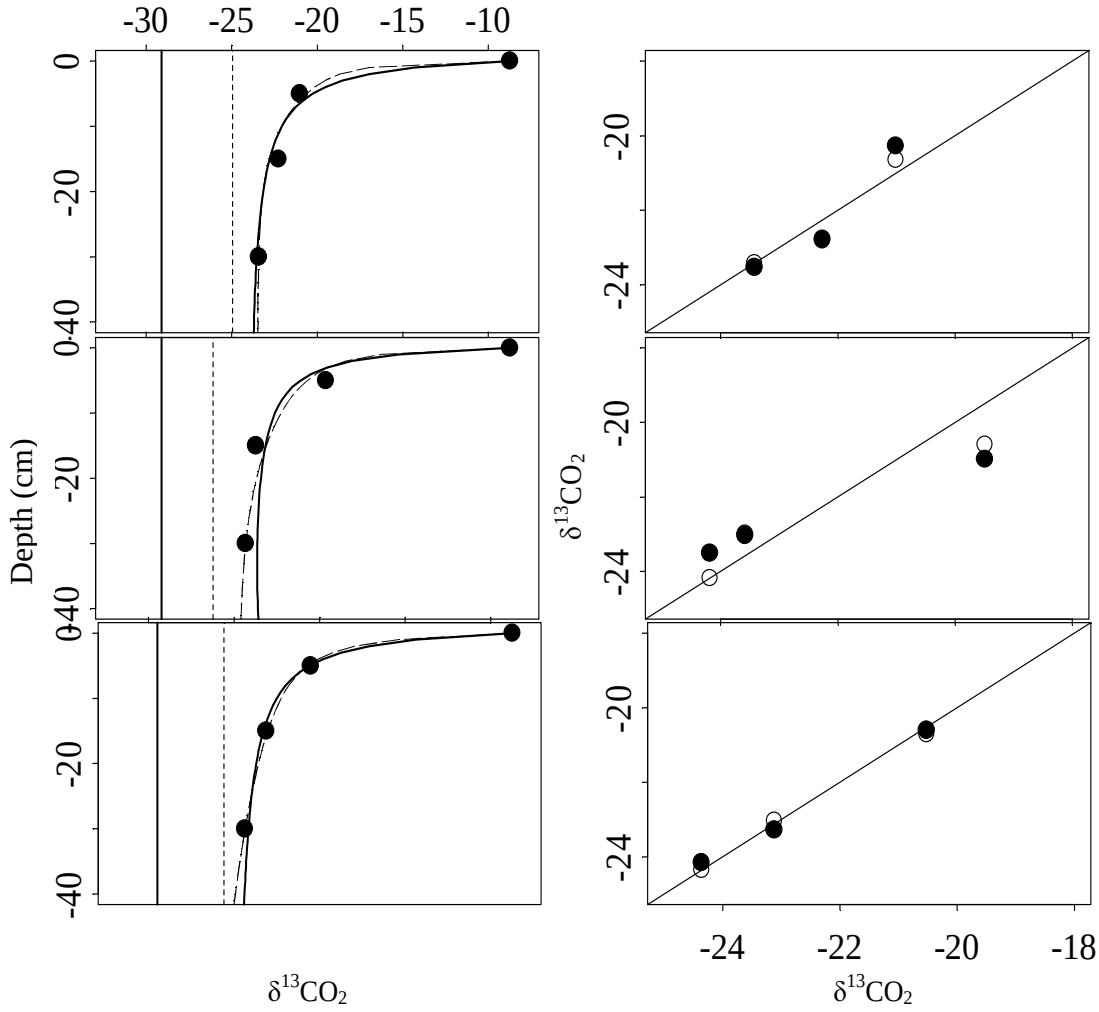

Figure 4.6 Model results for first 45 minute sampling. Three soil probes were sampled during this time (top, middle and bottom).The left column of graphs shows the isotopic soil profile of the first 45 minute sampling period with model fits of steady state diffusion model (solid curve) and advection-diffusion steady state model (dashed curve). The Miller-Tans mixing model estimate (dashed vertical line) and steady state diffusion source estimate (solid vertical line) are shown as a reference. The right column of graphs shows the 1:1 fit of the model predictions (solid symbols = diffusion steady state model, open symbols = advection-diffusion model) and field samples.

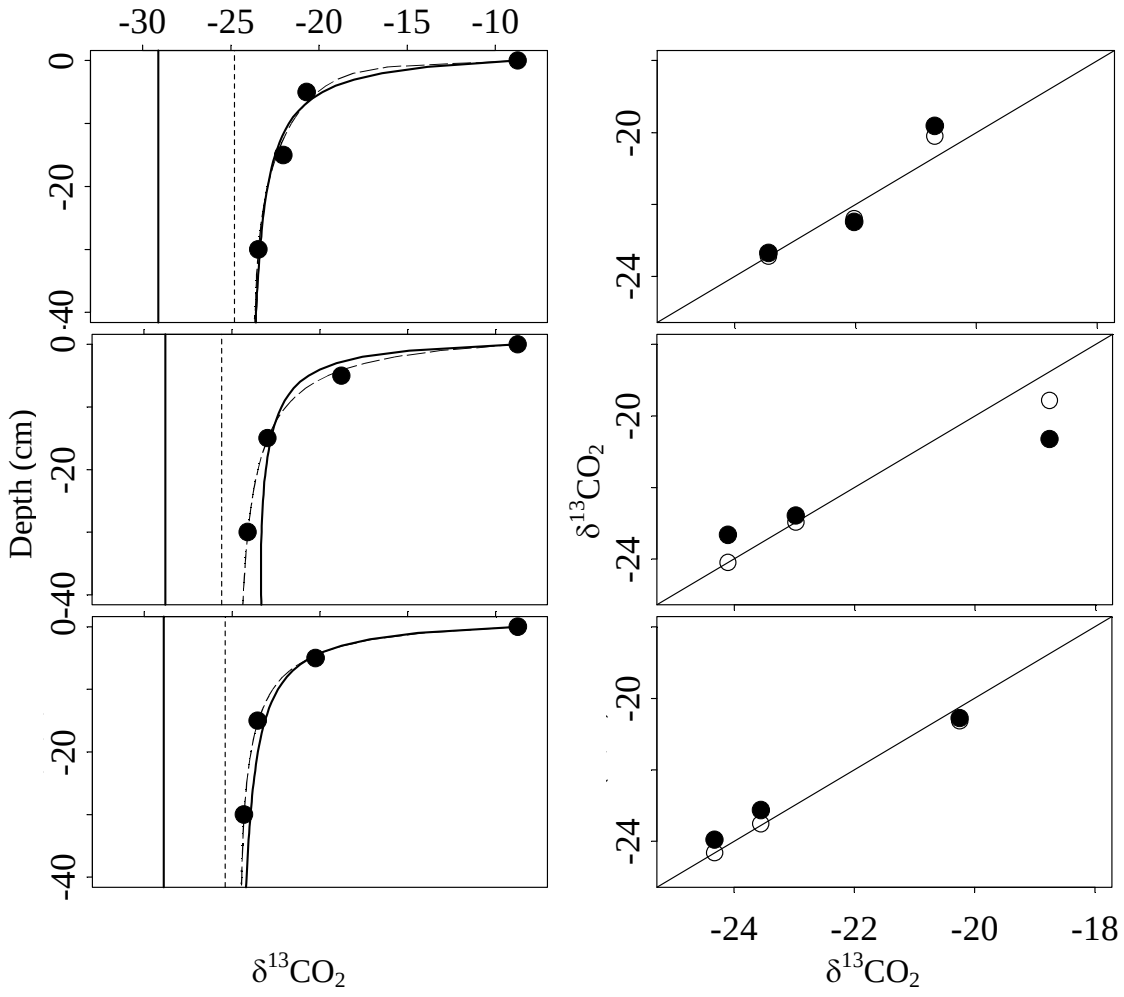

Figure 4.7 Model results for the second 45 minute sampling.The left column of graphs shows the isotopic soil profile of the second 45 minute sampling period with model fits of steady state diffusion model (solid curve) and advection-diffusion steady state model (dashed curve). Three soil probes were sampled during this time (top, middle and bottom).The Miller-Tans mixing model estimate (dashed vertical line) and steady state diffusion source estimate (solid vertical line) are shown as a reference. The right column of graphs shows the 1:1 fit of the model predictions (solid symbols = diffusion steady state model, open symbols = advection-diffusion model) and field samples.

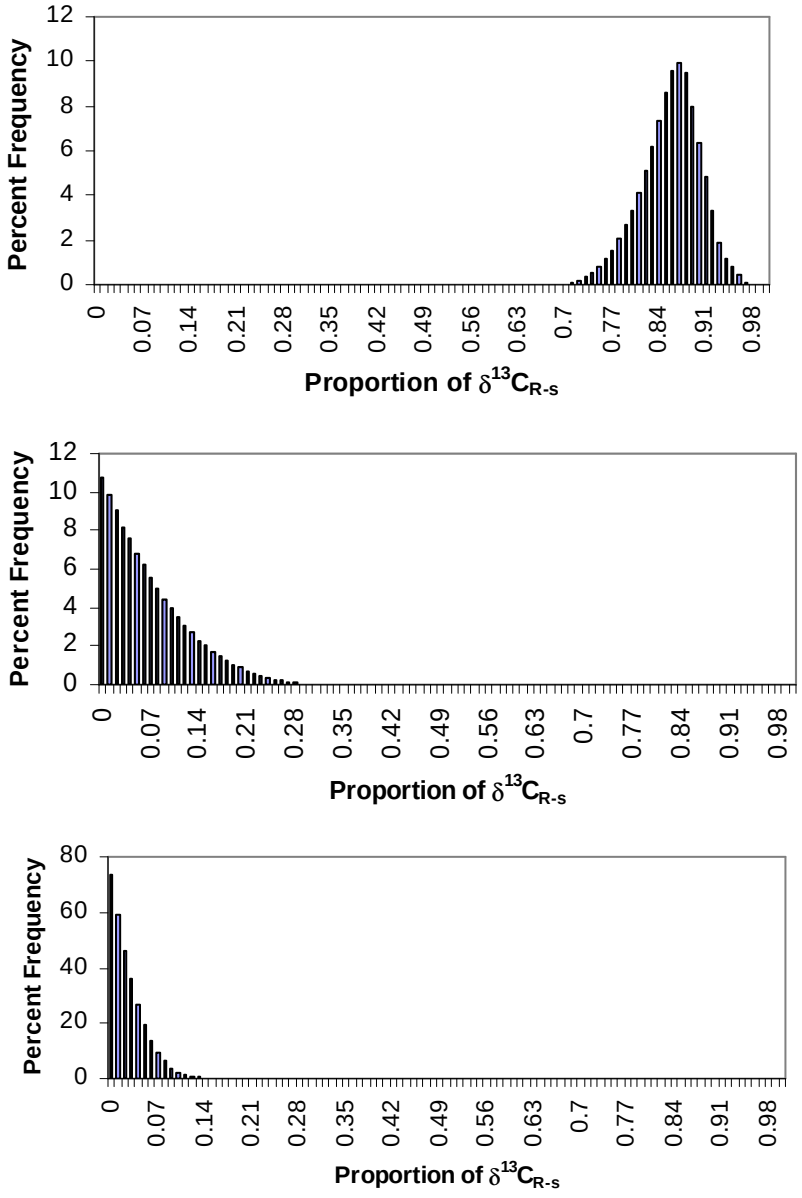

Figure 4.8 Source partitioning results based on $\delta^{13}C_{R-s}$ determined by transport models estimates. Contribution proportions are along the x-axis and percent frequency is along the y-axis. The top figure are the solutions for the contributions of foliage, the middle refers to root contributions and the bottom figure refers to the combined contributions of SOM samples from 5,15,and 30cm.

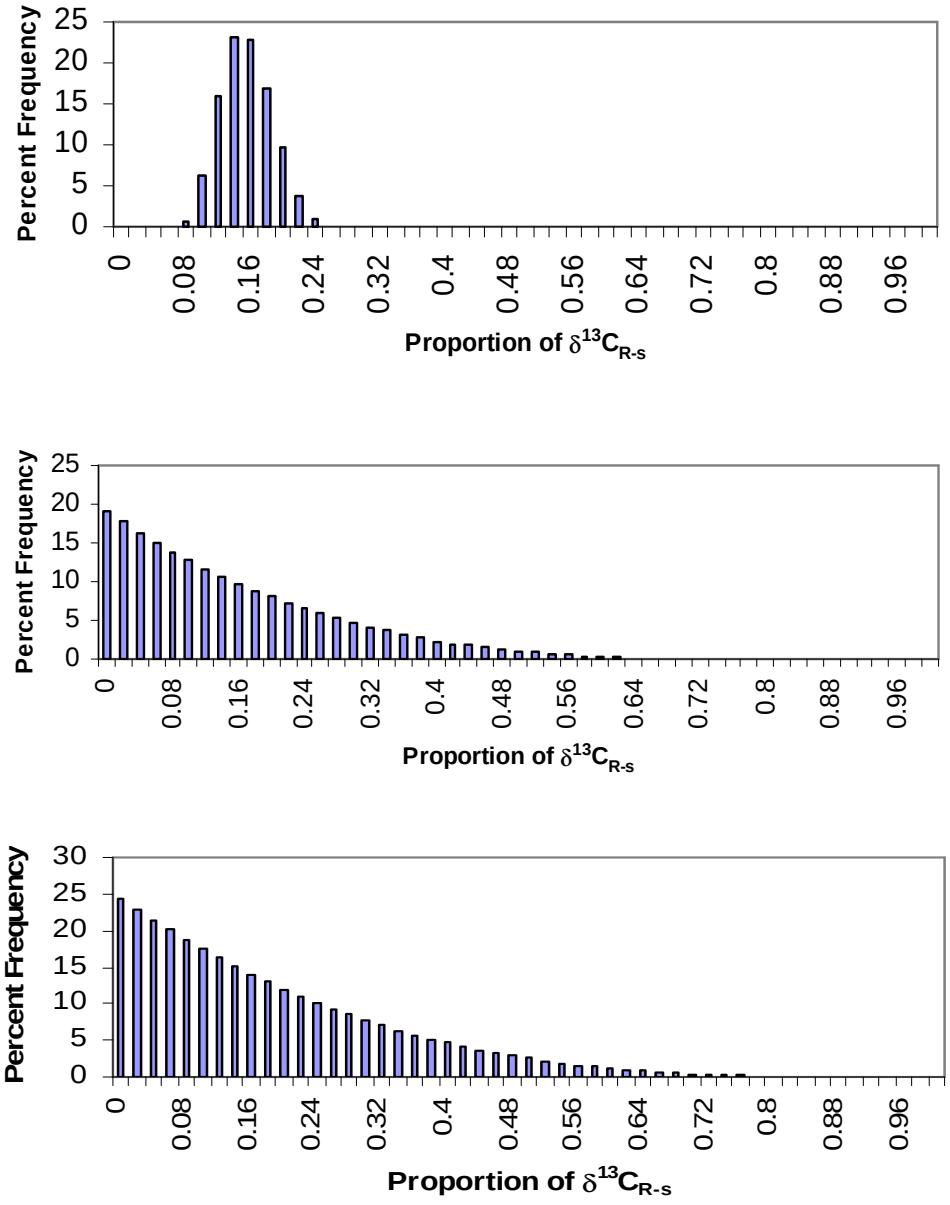

Figure 4.9 Source partitioning results based on $\delta^{13}C_{R-s}$ determined by mini-tower estimate. Contribution proportions are along the x-axis and percent frequency is along the y-axis. The top figure are the solutions for the contributions of the background atmosphere, the middle refers to the aboveground (phloem + foliage) contribution and the bottom figure refers to the combined contributions of SOM samples from 5,15,and 30cm.

Method	Mixing model (45 min)	Mixing model (90 min)	Diffusive model (45 min)	Diffusive model (90 min)	Adv-Diff model (45 min)	Adv-Diff model (90 min)	Δ (Mix Model-Diff Model)	Δ (Mix Model-Adv Diff Model)
Soil Probe 1	-24.7	-24.8	-29.1	-29.1	-27.9	-28.0	4.4	3.2
Soil Probe 2	-25.6	-25.6	-29.1	-28.8	-28.7	-28.5	3.4	3.0
Soil Probe 3	-25.4	-25.4	-29.5	-28.9	-31.7	-30.8	3.8	5.9

Table 4.1 Estimates of the isotopic source of soil respiration by Miller-Tans mixing model, diffusion and advection – diffusion steady state model. Mixing model estimates are uncorrected and differences between the mixing model and gas transport models are listed as apparent fractionation (Δ). All values are in ‰.

Method	$\delta^{13}C_{R\text{-}s}$ (‰)	se
Soil probe	-25.3	0.2
Mini Tower $_{(diffusion\ 1)}$	-23.3	1.2
Mini Tower $_{(advection\ 1)}$	-23.6	1.4
Mini Tower $_{(diffusion\ 2)}$	-24.0	0.7
Mini Tower $_{(advection\ 2)}$	-25.0	0.8
Diffusion model	-29.1	0.1
Adv-Diffusion model	-29.3	0.6

Table 4.2 Averages of isotopic signal of soil respiration ($\delta^{13}C_{R\text{-}s}$) estimated by both belowground (soil probe) and aboveground techniques (mini-tower).

Sample	$\delta^{13}C$ (‰)	sd	%C	%N
Foliage	-29.6	0.8	27.1	0.1
Phloem	-28.0	0.6	40.1	-
SOM 5 cm	-26.5	0.1	5.5	0.2
SOM 15 cm	-25.5	-	2.8	0.1
SOM 30 cm	-25.0	0.1	2.0	0.1

Table 4.3 Tree tissue and soil carbon and nitrogen composition

Chapter 5 Determination of the environmental controls of $\delta^{13}C_{Rs}$ in a Douglas-fir forest of the Pacific Northwest

Zachary Kayler, Elizabeth Sulzman, Holly Barnard, Alan Mix, Barbara Bond

Abstract:

We took advantage of naturally occurring gradients in biotic and abiotic variables across a steep catchment located in a Douglas-fir forest of the Pacific Northwest to identify and quantify the primary drivers of variability in soil respiration and its isotopic signature ($\delta^{13}C_{R\text{-}s}$). We measured soil CO_2 efflux and $\delta^{13}C_{R\text{-}s}$ over the late growing season of 2005 and the entire 2006 growing season along with soil moisture, soil temperature, vapor pressure deficit and transpiration across a transect of six plots that spanned the mouth of the catchment. In this analysis we distributed plots by topographical position. Plots were established in areas near the slope ridge, midslope and valley on both south facing and north facing aspects of the catchment. Our results suggested a close relationship between the physiological activity of trees and respiration of soils, and we inferred that soil CO_2 efflux was dominated by tree belowground inputs over the growing season. Both soil CO_2 efflux and $\delta^{13}C_{R\text{-}s}$ were highly correlated with transpiration rates 0 to 4 days prior. Levels of vapor pressured deficit, however, were only weakly correlated with both measures. Temperature explained 53% of the respiration variability and by including soil moisture we were able to explain 56% of the respiration variation overall. Furthermore, $\delta^{13}C_{R\text{-}s}$ was negatively correlated with soil moisture at our site indicating that soil moisture influences on soil respiration may be related to the oxidation of recently-fixed photosynthates from plants rather than carbon from soil organic matter, since the isotope value of CO_2 respired from soil organic matter does not vary over short time periods. Mixing model estimates of the 2005 $\delta^{13}C_{R\text{-}s}$, measured during the day, tended to be enriched in ^{13}C while the 2006 estimates, measured during the evening, tended to be depleted in ^{13}C with reference to estimates made from an isotopic steady-state model. We attribute the enrichment during the 2005 measurements to possibly a shift in the background atmospheric signal or to incursion of the atmosphere into the soil pore air space. We attribute the depleted measures of $\delta^{13}C_{R\text{-}s}$ made in 2006 to gas transport by advection, resulting in a fractionation value less than 4.4% that occurs with diffusion. Soil moisture from 30cm depth accounted for 33% of the variation in $\delta^{13}C_{R\text{-}s}$.

Introduction

Recently-fixed photosynthates appear to be an important driver of seasonal, diurnal, and spatial patterns of soil respiration (Högberg and Read 2006; Irvine et al. 2005; Steinmann et al. 2004). Much of this insight has been derived from several studies that have observed a strong correlation between environmental variables that influence photosynthesis and CO_2 respired from ecosystems (Bowling et al. 2002; Knohl et al. 2005; Pypker et al. 2008) and soils (Högberg et al. 2001; Ekblad and Högberg 2001; Ekblad et al. 2005; Mortazavi et al. 2004). In these studies, consistent lags in the correlation between respiration and vapor pressure deficit (VPD) and soil moisture levels 1-2 and 4-9 days prior to respiration measurement were attributed to a delay in transport of recently-fixed photosynthates to sites of respiration belowground (i.e. roots and microbes in the rhizosphere) or to a delay in soil gas transport from respiration sources to the soil surface (Stoy et al. 2007). However, many of the environmental variables that correlate with patterns in photosynthesis are also drivers of heterotrophic respiration, the oxidation of carbon in soil organic matter (SOM) by soil microbes, particularly soil moisture and temperature, potentially obscuring the actual relationship between the environmental drivers and the mechanisms behind the patterns in respiration.

Ideally, the impact of these environmental variables could be isolated and observed independently through experiments in the laboratory, but replication of forest characteristics, such as tall, mature trees and a developed soil profile and litter layer, present a formidable challenge. The use of natural occurring gradients is an alternative strategy to understanding controls on ecosystem processes. Conceptually, hypothesized factors of influence vary across a site, creating a gradient, while ecosystem properties such as vegetation and soil parent material are relatively constant over the measurement period. Thus, the response of the ecosystem process of interest can be attributed to the gradient of the hypothesized factor. There is a rich history of gradient analysis used to answer ecological questions concerning many facets of ecosystems such as biogeochemistry (Vitousek and Matson 1991), diversity (Flombaum and Sala 2008), and ecosystem function (Peterson and Waring 1994).

Microclimate is known to vary with different topographic positions (Kang et al. 2000; Kang et al. 2002; Western et al. 1998; Running et al. 1987); yet, investigations using natural gradients associated with topography have yielded equivocal conclusions concerning the environmental controls of soil respiration. For example, Kane et al. (2003) measured respiration across a steep gradient in elevation, percent slope and slope aspect and found soil moisture and temperature to be strong predictors of respiration at the plot scale but not across a full transect of plots. Hanson et al. (1993) also found an inconsistent relationship between soil respiration measured at locations categorized by slope aspect (northeast and southwest facing) and position (valley, ridge top) in an oak forest in Tennessee. However, Kang et al. (2003) found strong patterns relating soil respiration from plots located on different slope aspects and soil moisture. These results suggest other factors than just soil temperature and moisture are needed. Thus, by including biotic and abiotic factors that influence not only mineralization of soil organic carbon but also photosynthesis, then gradient studies of soil respiration may be improved and lead to more conclusive results. However, an additional method is needed to determine the aboveground contribution to the temporal and spatial variation of soil respiration.

There is a suite of strategies available for the separation of carbon sources to soil respiration which has been thoroughly reviewed (Hanson et al. 2000; Bond-Lamberty et al. 2004; Subke et al.2006; Luo and Zhou 2006). Among the available approaches, the use of natural variations in carbon stable isotopes offers the unique possibility of tracing carbon from various sources without disturbing the system of interest. The premise of this approach is based on the fact that each carbon pool in an ecosystem has a distinct isotopic signature (Bowling et al. 2008), and if the contribution of a carbon pool to soil respiration varies over the growing season then so will the isotopic signature of soil respiration ($\delta^{13}C_{R\text{-}s}$). A critical requirement for this strategy is that the magnitude in isotopic signature between the pools must be large enough such that potential contributors can be identified. $\delta^{13}C_{R\text{-}s}$ typically varies by 1 to 4‰ in magnitude seasonally (Ekblad and Högberg 2001; Ekblad et al. 2005; Takahashi et al. 2008; Kodama et al. 2008), requiring very accurate estimates of carbon pools and fluxes. However, with these requirements met, by measuring $\delta^{13}C_{R\text{-}s}$ over different topographic positions we may learn not only

which carbon pools are contributing to soil respiration but also which environmental factors are driving the mechanism behind the contribution.

We took advantage of a natural occurring gradient in microclimate (Pypker et al. 2007) across a steep catchment located in a Douglas-fir forest of the Pacific Northwest to identify and quantify biotic and abiotic factors that influence soil respiration and its isotopic signature ($\delta^{13}C_{R\text{-}s}$). We measured soil respiration and $\delta^{13}C_{R\text{-}s}$ over the late growing season of 2005 and the entire 2006 growing season along with soil moisture, soil temperature, VPD and transpiration across the catchment. We hypothesized that variation in inputs from recently-fixed photosynthates are an important driver of variation in rates of soil respiration during the growing season. If recently-fixed photosynthates are an important driver of variability in soil respiration, then $\delta^{13}C_{R\text{-}s}$ will strongly correlate with environmental controls of photosynthesis. In conifers, stomatal conductance is often strongly influenced by VPD. Changes in VPD and also transpiration may indicate changes in stomatal conductance, which may affect the degree of carbon isotope discrimination by plants during photosynthesis (Ehleringer 1994; Ehleringer and Cerling 1995). Thus, if recent photosynthesis is an important carbon source for respiration, we should be able to detect changes in $\delta^{13}C_{R\text{-}s}$ that are consistent with changes in isotopic discrimination during photosynthesis. However, it is unclear how factors that are traditionally used in soil respiration models, such as soil moisture, may influence aboveground inputs of carbon, via influences on rates of photosynthesis, as opposed to direct influence on metabolic activity of soil microbes. We designed this study to help clarify these issues.

Methods

Site Location The measurements were conducted within a 96 ha watershed ('Watershed 1'), located in the H J Andrews Experimental Forest in the western Cascades of central Oregon, USA (44.2 °N, 122.2 °W) (see Pypker et al. 2007 for a detailed description). The soil has Andic properties and has a loamy to silt loam texture. The organic layer is just 2 cm thick and is composed of primarily recognizable litter fragments with almost no discoloring and no signs of amorphous Oa materials. The A horizon extends to a depth of

9 cm where a diffuse AB transition occurs and extends to 30cm, beyond this the B horizon extends to a depth of 42cm. We used six of the eight plots established across the catchment where we measured soil respiration, $\delta^{13}C_{R\text{-}s}$, transpiration, and the environmental gradient (Figure 5.1). These plots were arrayed across a topographic gradient with one plot each on the south facing (SF) ridge, SF midslope, SF valley, north facing (NF) valley, NF midslope and NF ridge. In data analysis, we used aspect (NF vs SF), and slope position (ridge, midslope, valley) of the plots as independent variables.

Plot Sensors A suite of environmental variables were continuously measured and logged at each plot with a Campbell Scientific CR23x data logger. Plot transect data include soil moisture at four points per plot at 5cm, 30cm and 100cm depths (Decagon Devices; ECHO5s), soil temperature at plot center at the same depths (Campbell Scientific; 107-L), and air temperature and relative humidity at a height of 12-m at plot center (Vaisala; HMP50-L).

Soil respiration

We measured soil CO_2 efflux using a portable infrared gas analyzer (Li-6250, LI-COR Inc, Lincoln, NE) incorporated into a photosynthesis system (Li-6200) and attached to a closed, dynamic soil respiration chamber (Li-6200-09). The chamber was placed on a 10cm diameter by 5 cm tall PVC collar that was installed 2cm into the mineral soil. Soil respiration was measured 8 times over June to November of the 2005 growing season and 11 times over April to late October in 2006. In 2005 respiration was measured during midday and in 2006 respiration was measured during the evening to coincide with ecosystem respiration measurements at the same site (Pypker et al. 2008). The maximum sample size for respiration on each sampling date at a plot was n=4. Respiration values that were ± 2 standard deviations of the plot mean were removed as outliers.

Isotope Sampling

Acquiring and analyzing samples of soil CO_2 involved using soil gas probes (Kayler et al. 2008) to access soil gas at three depths, using a vacuum-withdrawal sampling system,

analyzing the samples through an isotope ratio mass spectrometer, and implementing the isotopic data in a two-end member mixing model.

Gas probe: This method of sampling involves sampling gas to measure isotopic composition at different depths in the soil. The soil probe contains three isolated wells made from PVC (poly-vinyl chloride). These wells are held at a fixed distance (5, 15 and 30cm) by PVC tubing. The soil probe is further described in Kayler et al. (2008).

To sample gas we used a gas tight 3-way ball valve (Whitey, Swagelok, USA) that was fitted with (in order) a hand vacuum pump (Mityvac, Lincoln Indust. Corp., USA), a double-ended needle that received a pre-filled N_2 exetainer (Labco Ltd., UK), and a double-ended needle that connected to the soil probe septum. This allowed for two positions of the valve: in one direction the exetainer was connected in line with the hand pump and when the valve was turned in the opposite direction, the exetainer was in line with the soil probe to sample soil gas. In the field, a N_2 filled exetainer was first connected in line with the hand pump which allowed us to draw a vacuum (-27 kPa) within the exetainer. Then, with the exetainer still under vacuum, we inserted the other needle of the double-ended needle into a septum of the soil probe and turned the valve to allow the flux of soil gas from the probe into the exetainer. We waited 30s to allow for equilibration then detached the exetainer and sealed the puncture of the exetainer septum with silicone sealant. The samples were then transported back to the laboratory and analyzed within 24 hours. A standard gas was sampled in the field to ensure no fractionation occurred during sampling, transport or storage.

The gas sample collected from each well was used in a two end-member isotopic mixing model to identify the isotopic signature of the source gas. We used the Miller-Tans (2003) mixing model which describes a sample of the air in a system as a mixture of two sources of $^{13}CO_2$, the background atmosphere, and the source of respiration. In field studies it is assumed that the soil source of respiration is a single, well mixed gas of CO_2 production from microbial and root respiration. The Miller-Tans mixing model is calculated with the following equation:

$$\delta_{obs} C_{obs} = \delta_s C_{obs} - C_{bg} (\delta_{bg} - \delta_s) \qquad (1)$$

where C is [CO_2] and the subscripts *obs*, *s*, and *bg* refer to the observed (measurement in the field), source and background values. We used a geometric mean regression with the Miller-Tans mixing model from which the slope of the regression is the estimate of $\delta^{13}C_{R\text{-}s}$.We label the mixing-model estimate as $\delta^{13}C_{R\text{-}s}$ (MM) throughout the text to distinguish it from other model estimates. In Equation 1, δ refers to the isotopic value of the component expressed in δ notation:

$$\delta = (R_{sample} / R_{standard} - 1) * 1000‰ \quad (2)$$

where R is the molar ratio of heavy to light isotopes. The carbon isotope ratio ($\delta^{13}C$) is expressed relative to the standard Vienna Pee Dee belemnite.

Because we measured CO_2 from within the soil profile rather than from CO_2 emitted from the soil surface, the Miller-Tans slope identifies the isotopic source of CO_2 based on the samples that have been enriched in $^{13}CO_2$ due to kinetic fractionation associated with diffusion. We can correct for this diffusive enrichment by subtracting 4.4‰ from the mixing model estimate but we must also assume the system is at isotopic steady-state (see Chapter 4 for a detailed explanation of gas transport at steady-state).

Isotopic Analysis For $\delta^{13}C$ analysis of CO_2 samples, we used a Finnigan/MAT DeltaPlus XL isotope ratio mass spectrometer interfaced to a GasBench II automated headspace sampler at the College of Oceanic and Atmospheric Sciences isotope facility, Oregon State University. The GasBench-II is a continuous flow interface that allows injections of several aliquots of a single gas sample into a mass spectrometer for automated isotope determinations of small gas samples. Exetainers of sampled gas were loaded onto a Combi-PAL auto-sampler attached to the GasBench. Helium pushed the sample air out of the exetainer and into the mass spectrometer. A typical analysis consisted of three gas standards (tank CO_2-He mixtures), five sample replicates and an additional 2 gas standards for every sample. The CO_2 concentration of each sample was calculated from the peak volt area produced by the mass spectrometer analysis of each sample.

Respiration Models To investigate the role of temperature and soil moisture on bulk soil respiration we used two models 1) an exponential model (Lloyd and Taylor 1994) to

explore the role of temperature and 2) plot specific statistical models that consider both soil moisture and temperature toward explaining soil respiratory patterns.

The exponential model describes soil respiration (R) as a function of basal respiration (A, μmol $m^{-2}s^{-1}$) at a standard temperature (T, degrees K) and a constant activation energy (E, degrees K) which are estimated parameters resulting from fitting the respiration data.

$$R = Ae^{\frac{-E}{(T-T_\circ)}}$$

Thus, by inputting temperature measured from the field ($T_\circ$, degrees K) into the exponential model, respiration can be predicted.

We used a linear mixed-effects model to determine the role of soil moisture and temperature in soil respiration. Soil respiration was log transformed to fulfill regression assumptions of normality. We also compared seasonal differences between respiration at the plot, catchment aspect and slope position levels. In this analysis the topographic category (Aspect; Ridge, Midslope, Valley) was the fixed variable while respiration collar and plot were nested in the date of collection as random effects. To test whether there were differences between plot, aspect or slope positions during each collection we used analysis of variance.

We used Pearson's product-moment to evaluate the correlation of soil respiration and $\delta^{13}C_{R\text{-}s}$ with measured biotic and abiotic variables (transpiration, vapor pressure deficit, soil moisture). All statistical analyses were performed in S-Plus (Insightful Corporation, Seattle, Wa., USA).

Isotopic Steady-State Model Diffusion of CO_2 at steady state is described by Fick's first law:

$$D_s \frac{\partial^2 C}{\partial z^2} = -\phi \qquad (3)$$

where D_s is the bulk diffusion coefficient of soil ($cm^2\ s^{-1}$), C= the concentration of CO_2 at a given depth in the soil profile (mol cm^{-3}), z = depth in the soil profile (cm) and ϕ = production of CO_2 (mol $cm^{-3}\ s^{-1}$). Cerling (1984) developed a production-diffusion

model of $^{13}CO_2$ based on the observation that the ^{12}C and ^{13}C diffuse along their own concentration gradients. In the review of isotopes of soil C and CO_2, Amundson et al. (1998) tested a similar model through simulations:

$$R^{13}_{(Z)} = \frac{\frac{\phi R^{13}_S}{D^{13}_S}\left(Lz - \frac{z^2}{2}\right) + C_{atm}R^{13}_{atm}}{\frac{\phi}{D_s}\left(Lz - \frac{z^2}{2}\right) + C_{atm}} \quad (4)$$

The model describes the isotopic ratio of ^{13}C to ^{12}C of a gas sample in the profile withdrawn from depth z. The model assumes that bulk CO_2 production and concentration represents ^{12}C given that it is the most relative abundant isotope of terrestrial carbon (98.9%). The isotopic ratio of CO_2 is a function of the production rate, the isotopic ratio of the source (R^{13}_S), and the diffusion coefficient of $^{13}CO_2$ (bulk soil D_s / 1.0044 which accounts for the greater mass of ^{13}C and its subsequent slower diffusivity). The upper boundary for the model (z=0) is the atmospheric isotopic signature and the lower boundary (L) is the lower limit of respiration (z=L) where concentration gradient is constant and further contributions to soil respiration is not encountered. We used the production value estimated from soil respiration measurements and fit the isotopic and concentration profile samples to the above diffusion model. We used a non-linear regression to determine D_s, L and $\delta^{13}C_{R\text{-}s}$. We refer to the isotopic steady-source estimate of soil respiration simply as $\delta^{13}C_{R\text{-}s}$.

We used this model to determine whether $\delta^{13}C_{R\text{-}s}$ was at steady-state when we made our measurements of $^{13}CO_2$ in the soil profile. When the estimate of $\delta^{13}C_{R\text{-}s}$ from the Miller-Tans mixing model and the steady-state model were similar, then we were certain in correcting the MM estimate by 4.4‰. However, if the two estimates are not similar then we did not know how much the $^{13}CO_2$ in the soil has fractionated. Therefore, in the case where the MM estimate and the isotopic steady-state model were not similar, we excluded the estimate in analyses to determine the environmental drivers of $\delta^{13}C_{R\text{-}s}$.

Results:

Atmospheric and pedo- microclimates: There was variability in the measured environmental variables across the transect (Table 5.1). Soil moisture was consistently

greater at all depths in the SF ridge plot while the NF valley plot was typically the driest plot. The vapor pressure deficit was greater along the ridge plots than plots in the valley. Plot average annual soil temperature was similar across the transect; however, the SF ridge plot experienced higher maximum temperatures during both growing seasons. The maximum temperature on the south slope occurred in the NF midslope plot. The NF aspect of the catchment experienced lower minimum temperatures.

Soil flux

We sampled more frequently during the 2006 field campaign than 2005 (Figure 5.2 A,B), and as a result the data from 2006 provided a more complete picture of the seasonal soil CO_2 flux. Soil flux remained below 3 μmol $m^{-2}s^{-1}$ through the first two sample periods at which point respiration reached near maximum values (a range of approximately 7 to 2 μmol m^{-2} s^{-1} for the SF ridge plot and NF valley plot respectively) between day July 14th and 20th. Respiration declined soon after these peak values. These peaks in respiration were followed by either a relatively stable period for a period of about 50 days or else respiration continued to decline. Overall, there was a high degree of variability in the soil flux measurements at the plot level (Figure 5.3). The NF valley plot consistently had the lowest rate of respiration and rates generally increased with slope position (valley to ridge) and slope aspect (NF to SF).

Watershed aspect: The SF slope respiration rates were on average 0.71 and 0.55 μmol $m^{-2}s^{-1}$ greater than the NF slope ($p<0.01$) for the 2005 and 2006 growing seasons respectively (Figures 5.4 A, B). The flux rates exhibited similar seasonal patterns at the plot level: rates of respiration rapidly increase after July 14th. The peak value of soil respiration on the NF aspect was less than the SF and respiration rates declined earlier in the season than the SF aspect. There was a noticeable dip in respiration on July 20th of the NF aspect which was due to the absence in measurement of respiration in the NF ridge plot. The difference in soil respiration between watershed aspects was not significant on any day sampled except for September 21st of the 2005 growing season ($p<0.04$).

Position: The respiration dynamics with reference to slope position (ridge, midslope, and valley) varied between growing seasons (Figure 5.5 A,B). In 2005, the respiration rates between plots located along the ridge were not different from respiration rates of midslope plots. Plots located in the valley however, respired 0.81 and 0.65 μmol $m^{-2}s^{-1}$ less than the midslope ($p<0.01$) and ridge ($p<0.01$) plots respectively. During the 2006 growing season, respiration of plots located in the ridge was 0.67 and 1.00 μmol $m^{-2}s^{-1}$ greater than that of plots located in the midslope ($p<0.01$) and valley ($p<0.01$) respectively. Respiration rates from the midslope and valley plots were not significantly different. In 2005, differences in soil respiration between slope positions were not significant when individual sampling days were analyzed, this was largely similar in the 2006 growing season.

$\delta^{13}C_{R\text{-}s}$

The mixing-model estimate (MM) of $\delta^{13}C_{R\text{-}s}$ measured in 2006 had a distinct oscillatory pattern with two peaks of enrichment occurring on May 30th and September 4th, and two troughs of a depleted signal occurring on April 24th and August 10th. Sampling for the 2005 (Figure 5.6) growing season captured half of this seasonal oscillation. It appeared that 2005 sampling commenced during a period where the $\delta^{13}C_{R\text{-}s}$ (MM) was depleted (June 21st) after which the signal became more enriched with a peak near September 7th. Overall, there was a high degree of variability in the $\delta^{13}C_{R\text{-}s}$ measurements at the plot level (Figure 5.7). A significant difference in $\delta^{13}C_{R\text{-}s}$ (MM) only occurred between the SF midslope plot and the NF midslope and ridge plots (Figure 5.7).

Catchment aspect: When compiled by aspect, the $\delta^{13}C_{R\text{-}s}$ (MM) displays the oscillatory seasonal pattern (Figure 5.8 A, B) seen at the individual plot level but there is a significant ($p<0.01$) enrichment of 0.42‰ on the SF aspect compared with the NF aspect. This difference between watershed aspects was not detectable in the 2005 growing season.

Watershed position: There were weak seasonal patterns of $\delta^{13}C_{R\text{-}s}$ (MM) with slope position exhibited in the 2006 growing season (Figure 5.9) with ridge positions tending to

have more depleted values than the other hill slope positions. However, differences were not significant over the growing season or for any sampling day.

Models

Respiration models: At the plot level, the regression model based on soil moisture and temperature generally explained more of the variation in respiration data than the exponential model (Table 5.2). To asses the model fits over the entire transect we compared all plot level respiration values against the regression model predictions (Figure 5.10). The respiration models based on soil temperature and soil moisture explained, on average, 56% of the variation in the respiration data. The respiration models tended to make better predictions of the early growing season compared to respiration estimates made after the peak in the growing season.

The exponential-temperature model explained 53% of the variation on average and generally underestimated respiration values (Figure 5.11). By inspecting the model predictions, we see that on the south facing aspect of the catchment, the ridge plot had the greatest response to temperature, followed by the midslope plot, and the valley plot essentially did not respond to changes in temperature (Figure 5.12). The predictions of the plots were different because the NF valley and midslope plots had the lowest basal respiration levels while the SF midslope had the smallest activation level (Figure 5.13).We performed an F-test to test whether the plot results were significantly different from a null model where plot levels were not a factor. Only the NF valley, and NF midslope were significantly different than the null ($p(F) < 0.001$).

Isotopic steady-state model: For each depth within the soil profile, the steady-state model predicted a slightly enriched isotopic signal of the soil CO_2 relative to the measured values, but model estimates were consistently within ±2‰ of measured data (Figure 5.14). Both the Miller –Tans mixing model, which is a two-end member mixing model, and the isotopic steady-state model, which is based on soil characteristics and isotopic mixing, are used to estimate the carbon source of soil respiration; at steady-state we would expect the same estimate of $\delta^{13}C_{R\text{-}s}$ from both. However, there were large differences between the carbon source estimated by the isotopic steady-state model and the source estimated by the mixing model (Figure 5.15). Despite a similar range in 2005

and 2006 $\delta^{13}C_{R\text{-}s}$ estimates, the 2005 mixing model estimates of the CO_2 source (from samples collected during the day) tended to be enriched relative to the estimate of the isotopic steady-state model, while the 2006 mixing model estimates (from samples collected at night) tended to be depleted in ^{13}C with reference to the steady-state model.

At isotopic steady-state the MM estimate will be 4.4‰ enriched with respect to the steady-state model, and during some but not all measurements the models did agree (i.e., fall on the 1:1 +4.4‰ line). When model estimates were not equivalent it is plausible that the soil was at isotopic non steady-state in which case the steady-state model of $\delta^{13}C_{R\text{-}s}$ was not valid. Furthermore, we were unable to determine the degree to which CO_2 in the soil profile was fractionated. Because we could not determine the fractionation correction to apply to MM estimates, we used only the data points where the mixing model and steady-state model agreed (± 10%) for subsequent analyses and statistical models in the isotopic signature of respiration. These data represent 36% of the original data set.

Lag analysis: Transpiration, soil moisture and VPD all correlated significantly ($p<0.10$) with soil respiration and $\delta^{13}C_{R\text{-}s}$ but not for all plots or slope positions. For clarity, only the significant correlations are presented graphically.

Transpiration:

The SF ridge plot showed a strong, positive correlation between soil respiration and transpiration, with a Pearson's r ranging between 0.83 and 0.9 ($p<0.01$), during 1-3 and 9-11 days prior to respiration measurement. The isotopic signature for the same plot was negatively correlated with transpiration on the same day, -0.75, and 13 days prior to measurement, - 0.76 ($p<0.10$) (Figure 5.16), but not for any days in between. In the SF valley plot respiration was not correlated with transpiration while $\delta^{13}C_{R\text{-}s}$ was strongly ($p<0.05$) negatively correlated with transpiration levels 3 days prior. The respiration from the NF valley plot was positively correlated with transpiration levels on the day of measurement, ~.55 ($p<.10$) and 10 days prior to measurement, ~0.63 ($p<0.05$). At the same plot, $\delta^{13}C_{R\text{-}s}$ was negatively correlated with transpiration levels 4-5 days prior to soil gas measurement,- 0.91 ($p<0.10$). For both plots located in the valley a strong

positive correlation of $\delta^{13}C_{r\text{-}s}$ occured during longer lag periods (i.e., > 8 lag days). At the NF midslope plot, the correlation between soil respiration and transpiration was strongest 8 days prior to measurement, 0.72 ($p<0.01$), and weakly correlated 2, 4, and 10 days prior to measurement, 0.58 on average ($p<0.10$). At the same plot, $\delta^{13}C_{R\text{-}s}$ was negatively correlated 5 days prior, -0.70 ($p<0.05$).

The patterns in correlation between $\delta^{13}C_{R\text{-}s}$ and transpiration at the catchment level were not significant. However, the strength of correlation between respiration and transpiration at 2-3 and 7-9 days prior to flux measurement on the north aspect is consistent with the plot level patterns as well as the positive correlation between soil flux and transpiration 1-2 and 9-10 prior to measurement on the SF slope. The correlation between $\delta^{13}C_{R\text{-}s}$ and transpiration for each slope aspect followed a similar pattern in magnitude as the soil flux, although the strength of the correlation was slightly less. There were fewer significant peaks in correlation between $\delta^{13}C_{R\text{-}s}$ and transpiration over the growing season compared to the soil flux correlations probably due to the reduction in sample sized after non steady-state data were culled.

The correlation between soil flux and transpiration weakened from ridge to valley slope positions. Because there are a limited number of plots within a slope position category, the patterns generally resemble those seen at the plot level correlation analysis. Thus, the ridge plot patterns are the same as the previously discussed SF ridge plot and the midslope patterns are the same as the NF midslope plot. There was a positive correlation of soil respiration with transpiration levels 1day prior to measurement of respiration in the valley slope position. The correlation with $\delta^{13}C_{R\text{-}s}$ in the valley plots was not significant.

VPD:

At the plot level neither soil respiration nor $\delta^{13}C_{R\text{-}s}$ significantly correlated with VPD. When the data were compiled by slope aspect, soil respiration on the NF slope was positively correlated with VPD levels 1-2 days prior to measurement while $\delta^{13}C_{R\text{-}s}$ correlated negatively with levels 0-1 days prior (Figure 5.17). The correlations for the SF slope and slope position categories were not significant.

SM:

For the SF ridge plot, soil moisture levels at 5cm were significantly, negatively correlated with depth from 1-4 days prior to isotopic sampling. For the SF valley plot, there was a significant, positive correlation with soil moisture at the 100cm depth two days prior to isotopic sampling (Figure 5.18). When plots are grouped by aspect, there was a negative correlation between soil moisture at 5cm and $\delta^{13}C_{R\text{-}s}$ for the SF aspect while plots located on the NF aspect were more correlated to soil moisture at 100cm (Figure 5.19).

Discussion:

The aim of this research was to test the hypothesis that variations in inputs from recently-fixed photosynthates are an important driver of variation in rates of soil respiration during the growing season. We used a gradient approach and isotopic analysis to determine the abiotic and biotic drivers that might influence the input of recently-fixed photosynthate belowground. We found soil temperature and moisture only explained 56% of the respiration data but it is impossible to determine if autotrophic and heterotrophic respiration are responding equally to these environmental variables with the flux data alone. Beyond soil temperature and moisture, we found strong correlations between transpiration with soil respiration and $\delta^{13}C_{R\text{-}s}$ which indicates that canopy processes exert significant control over soil respiration at our site. The consistent negative correlation between $\delta^{13}C_{R\text{-}s}$ and transpiration is additional evidence of this link. High transpiration rates are indicative of high levels of stomatal conductance in addition to high evaporative demand, allowing for a greater concentration of CO_2 in leaf mesophyll and, therefore, an increase in photosynthesis (unless there are corresponding changes in Rubisco activity). The recently-fixed photosynthates are then transported through the tree phloem to sites of respiration belowground. This may explain the positive correlation between soil respiration and transpiration. Furthermore, because these substrates transported through the phloem are recently-fixed photosynthates, they should be depleted in ^{13}C with reference to old carbon located in the soil, which explains the negative correlation of transpiration with $\delta^{13}C_{R\text{-}s}$. In other words, we found a strong

correlation with a large flux of depleted carbon substrates belowground with rates of tree transpiration.

The lag between $\delta^{13}C_{R\text{-}s}$ and transpiration allowed us to make inferences about the time of transport of recently-fixed photosynthates to sites of belowground respiration. The time delay in correlation between $\delta^{13}C_{R\text{-}s}$ and transpiration increased from 0 days at the SF ridge plot to 5 days at NF midslope plot. From these results we inferred that the time lag from photosynthesis to root respiration and respiration of root exudates is on the order of 1-5 days which is consistent with previous studies of soil respiration (Ekblad and Hogberg 2001; Ekblad and Hogberg 2005). We were not able to determine the source of variation in the time lag between plots, although, it could be attributed to different rates of photosynthesis or potentially, different tree heights which lead to longer paths of transport.

Although the spatial variability in VPD at our site was strong, the correlations of $\delta^{13}C_{R\text{-}s}$ and soil flux with VPD were weak to non-existent. There were no significant correlations at the plot level and the NF slope respiration was only weakly correlated, although significant. This is somewhat surprising that the correlation patterns in VPD and transpiration are not more similar given the close relationship between VPD and transpiration (Jones 1992). However, our results are consistent with Pypker et al. 2008, where the isotopic signal of ecosystem respiration did not significantly correlate with VPD but a strong, significant correlation was present with stomatal conductance from five days earlier.

Soil moisture was negatively correlated with $\delta^{13}C_{R\text{-}s}$ at our site. This means that assoil moisture water content increased, $\delta^{13}C_{R\text{-}s}$ became more depleted in ^{13}C and therefore, soil moisture effects on soil respiration were related to the oxidation of recently-fixed photosynthates from plants rather than carbon from SOM. This interpretation is based on the assumption that tree inputs respired belowground (i.e. root respiration or respiration of exudants in the rhizosphere) are consistently more depleted in ^{13}C than carbon from SOM, so we would expect a positive correlation of $\delta^{13}C_{R\text{-}s}$ with soil moisture if SOM was the predominant carbon source. Pypker et al. (2008), found a similar relationship with soil matric potential and the isotopic signal of ecosystem respiration, where respired CO_2 was more depleted with an increase in soil matric

potential. Our findings support the contention of Pypker et al. (2008) that soil moisture had a larger impact on canopy processes that affect the isotopic signature of respiration rather than contributions from heterotrophic respiration of older carbon sources.

We found soil moisture at 5cm depth was more correlated with $\delta^{13}C_{R\text{-}s}$ on the SF slope of the catchment while soil moisture at 100cm depth seemed to play a greater role on the NF slope. The difference in correlation between $\delta^{13}C_{R\text{-}s}$ and soil moisture at a specific depth is partly due to the soil physical properties at our site. There was a distince moisture gradient across the transect where plots along the SF slope were typically more moist than the NF slope. These findings are somewhat counterintuitive because SF slopes are typically associated with low soil moisture availability due to greater solar insolation and water demands by vegetation (Jones 1992). The difference in moisture holding capacity is most likely due to soil physical properties of the catchment slopes. The soil on the SF slope contains more clay and is further developed than the NF slope which is more granular in texture and has evidence of several buried A horizons due to slope failure.

The abiotic and biotic variables we measured largely played a role in regulating aboveground inputs into soil respiration, contributing to recent evidence that emphasize aboveground contributions. For example, similar patterns between transpiration have been found (Irvine et al. 2008) or are implied via correlations with VPD (Ekblad et al. 2001; Bowling et al. 2002; Knohl et al. 2005), and soil moisture has also been observed to have an impact on aboveground inputs as well (Pypker et al. 2008; McDowell et al. 2004). Because we used a gradient approach in our study, our results suggest that recent carbon substrate from photosynthesis is the primary source of soil respiration even when environmental variables vary greatly. However, the results we present from our study are limited to the growing season and a young Douglas-fir forest, and we might expect the relationship between the abiotic and biotic drivers of respiration to change during different seasons and forest type.

It is important to keep in mind that our isotopic data set was significantly reduced due to measurements made at non steady-state. By grouping the data into slope and aspect classifications we were able to see clear patterns of $\delta^{13}C_{R\text{-}s}$ with environmental variables but often a single plot would have a large influence on the patterns of a grouping. For example, the NF valley plot data set was reduced by 70% which means

much of the strength in the correlation at this slope position is represented by the SF valley plot. In addition, transpiration measurements were not available for all the plots during the 2006 growing season and therefore inferences are limited to these positions.

Few other studies have verified whether $\delta^{13}C_{R\text{-}s}$ measurements were collected during isotopic steady-state, and while the reduction of our data set is unfortunate, it was necessary otherwise the analysis including measurements made under non steady-state conditions might have led to incorrect inferences. One striking difference between the 2005 and 2006 $\delta^{13}C_{R\text{-}s}$ measurements was the difference between the mixing model estimates and the steady state model. The 2005 data tended to be more enriched in ^{13}C than the steady-state model predicted while the 2006 data tended to be depleted in ^{13}C with reference to the predicted steady-state value. Fractionation due to gas transport will lead to a smaller fractionation value (Cerling et al.1991; Amundson et al. 1998) and therefore does not explain the heavier $\delta^{13}C_{R\text{-}s}$ values of 2005. What most likely explains the enrichment in these daytime measurements is incursion of atmospheric CO_2 as observed in chapter 3. In this case, atmospheric CO_2 diffuses into soil pore space as soil moisture decreases near the soil surface (Millard et al. 2008).

The depleted $\delta^{13}C_{R\text{-}s}$ of the 2006 season suggests that fractionation may have occurred during transport at our site. To our knowledge, no other study has information regarding the fractionation behavior of soil $^{13}CO_2$ under non steady-state. To better understand this phenomenon we performed a stepwise regression that considered soil temperature and moisture at three depths, VPD, flux and the log transformation of flux as the independent variables and the difference between the isotopic steady-state model estimate of $\delta^{13}C_{R\text{-}s}$ and the MM estimate of $\delta^{13}C_{R\text{-}s}$ as the dependent variable. Through this exploratory analysis we found the soil VWC from 30cm depth and its interaction with soil flux accounted for 33% of the variation in the fractionation data (Table 5.3). Similarly, soil moisture was identified as a major influence in the fractionation of $\delta C^{18}O_2$ in soil flux (Sulzman 2000). This exploratory analysis indicates soil moisture is an important variable when considering non steady-state dynamics of $\delta^{13}C_{R\text{-}s}$.

Soil moisture can affect the diffusion coefficient of soil CO_2 by altering the tortuosity and size of soil pore space (Hillel 1998). Thus, one mechanism of the fractionation process of soil respired CO_2 is a dynamic diffusion regime that alters the

isotopic signal of respiration. In a laboratory study we calculated that a change in the source isotopic of soil respiration can take up to eight hours to come to equilibrium (Kayler et al. 2008). However, longer periods for equilibration may be necessary for low rates of soil respiration, low temperatures, or deeper depths of production. Fractionation associated with CO_2 dissolving into soil water results in an enrichment of the soil gas (Vogel et al. 1970) and could therefore explain any possible enrichment of $\delta^{13}C_{R\text{-}s}$ relative to the source value. It is possible that the fractionation of $^{13}CO_2$ is related to transport and chemical processes that are taking place simultaneously and we are unable to discern which processes dominate with this study. Clearly, a future research challenge is resolving these fractionation processes as non steady-state appears to be similar to most soil attributes: highly variable both temporally and spatially.

Conclusion:

Soil respiration is traditionally predicted by soil moisture and soil temperature (Singh and Gupta 1977; Lloyd and Taylor 1994). We found these traditional models explained 56% of the variation at the transect level soil respiration data. What these models do not explicitly consider are the aboveground inputs from recent photosyntates: the primary driver of soil respiration at our site. This inference is largely drawn from the correlation between soil respiration and transpiration but only by using $\delta^{13}C_{R\text{-}s}$ could we be certain about the carbon source. Our study has demonstrated how natural abundance $\delta^{13}C$ can be used to monitor soil respiration at relatively long scales, although it is critical to be aware of the steady-state assumptions for the measurement and analysis of $\delta^{13}C_{R\text{-}s}$. However, we have illustrated how analysis of $\delta^{13}C_{R\text{-}s}$ can lead to meaningful insight into the role of the autotrophic and heterotrophic components of soil respiration.

References

Amundson, R., L. Stern, T. Baisden and Y. Wang.1998. The isotopic composition of soil and soil-respired CO_2. Geoderma 82(1-3): 83-114.

Bond-Lamberty, B., C. K. Wang and S. T. Gower.2004. A global relationship between the heterotrophic and autotrophic components of soil respiration? Global Change Biology 10(10): 1756-1766.

Bowling, D. R., N. G. McDowell, B. J. Bond, B. E. Law and J. R. Ehleringer.2002. ^{13}C content of ecosystem respiration is linked to precipitation and vapor pressure deficit. Oecologia 131(1): 113-124.

Bowling, D. R., D. E. Pataki and J. T. Randerson.2008. Carbon isotopes in terrestrial ecosystem pools and CO_2 fluxes. New Phytologist 178(1): 24-40.

Cerling, T. E.1984. The stable isotopic composition of modern soil carbonate and its relationship to climate. Earth and Planetary Science Letters 71(2): 229-240.

Ehleringer, J.R. 1994. Variation in gas exchange characteristics among desert plants. In: Schulze E-D, Cadwell MM (eds) Ecophysiology of photosynthesis. Springer, Berlin Heideberg New York, pp 361-392.

Ehleringer, J.R., T.E. Cerling. 1995. Atmospheric CO_2 and the ratio of intercellular to ambient CO_2 concentration in plants. Tree Physiology 25: 513-519.

Ekblad, A., B. Bostrom, A. Holm and D. Comstedt.2005. Forest soil respiration rate and $\delta^{13}C$ is regulated by recent above ground weather conditions. Oecologia 143(1): 136-142.

Ekblad, A. and P. Hogberg.2001. Natural abundance of ^{13}C in CO_2 respired from forest soils reveals speed of link between tree photosynthesis and root respiration. Oecologia 127(3): 305-308.

Flombaum, P. and O. E. Sala.2008. Higher effect of plant species diversity on productivity in natural than artificial ecosystems. Proceedings of the National Academy of Sciences of the United States of America 105(16): 6087-6090.

Jones, G.H. 1992. Plants and Microclimate. New York, Cambridge University Press.

Hanson, P. J., N. T. Edwards, C. T. Garten and J. A. Andrews.2000. Separating root and soil microbial contributions to soil respiration: A review of methods and observations. Biogeochemistry 48(1): 115-146.

Hanson, P. J., S. D. Wullschleger, S. A. Bohlman and D. E. Todd.1993. Seasonal and Topographic Patterns of Forest Floor CO_2 Efflux from an Upland Oak Forest. Tree Physiology 13(1): 1-15.

Hogberg, P., A. Nordgren, N. Buchmann, A. F. S. Taylor, A. Ekblad, M. N. Hogberg, G. Nyberg, M. Ottosson-Lofvenius and D. J. Read.2001. Large-scale forest girdling shows that current photosynthesis drives soil respiration. Nature 411(6839): 789-792.

Hogberg, P. and D. J. Read.2006. Towards a more plant physiological perspective on soil ecology. Trends in Ecology & Evolution 21(10): 548-554.

Irvine, J., B. E. Law and M. R. Kurpius.2005. Coupling of canopy gas exchange with root and rhizosphere respiration in a semi-arid forest. Biogeochemistry 73(1): 271-282.

Irvine, J., B. Law, J. Martin and D. Vickers.2008. Interannual variation in soil CO_2 efflux and the response of root respiration to climate and canopy gas exchange in mature ponderosa pine. Global Change Biology 14(12): 2848-2859.

Kane, E. S., K. S. Pregitzer and A. J. Burton.2003. Soil respiration along environmental gradients in Olympic National Park. Ecosystems 6(4): 326-335.

Kang, S., S. Kim, S. Oh and D. Lee.2000. Predicting spatial and temporal patterns of soil temperature based on topography, surface cover and air temperature. Forest Ecology and Management 136(1-3): 173-184.

Kang, S. Y., S. Doh, D. Lee, V. L. Jin and J. S. Kimball.2003. Topographic and climatic controls on soil respiration in six temperate mixed-hardwood forest slopes, Korea. Global Change Biology 9(10): 1427-1437.

Kang, S. Y., S. Kim and D. Lee.2002. Spatial and temporal patterns of solar radiation based on topography and air temperature. Canadian Journal of Forest Research-Revue Canadienne De Recherche Forestiere 32(3): 487-497.

Kayler, Z. E., E. W. Sulzman, J. D. Marshall, A. Mix, W. D. Rugh and B. J. Bond.2008. A laboratory comparison of two methods used to estimate the isotopic composition of soil $\delta^{13}CO_2$ efflux at steady state. Rapid Communications in Mass Spectrometry 22(16): 2533-2538.

Knohl, A., R. A. Werner, W. A. Brand and N. Buchmann.2005. Short-term variations in $\delta^{13}C$ of ecosystem respiration reveals link between assimilation and respiration in a deciduous forest. Oecologia 142(1): 70-82.

Kodama, N., RL Barnard, Y Salmon, C Weston, JP Ferrio, J Holst, RA Werner, M Saurer, H Rennenberg, N Buchmann, A Gessler.2008. Temporal dynamics of the carbon isotope compositin in a Pinus sylvestris stand: from newly assimilated organic carbon to respired carbon dioxide. Oecologia 156(4): 737-750.

Lloyd, J., JA Taylor. 1994. On the temperature dependence of soil respiration. Functional Ecology 8(3): 315-323.

Luo, Y. and X. Zhou.2006. Soil Respiration and the Environment. San Francisco, Academic Press.

McDowell, N.G., D.R. Bowling, A. Schauer, J. Irvin, B.J. Bond, B.E. Law, and J.R. Ehleringer. 2004. Associations between carbon isotope rations of ecosystem

respiration, water availability and canopy conductance. Global Change Biology 10: 1767.

Millard, P., A. J. Midwood, J. E. Hunt, D. Whitehead and T. W. Boutton.2008. Partitioning soil surface CO_2 efflux into autotrophic and heterotrophic components, using natural gradients in soil $\delta^{13}C$ in an undisturbed savannah soil. Soil Biology & Biochemistry 40(7): 1575-1582.

Miller, J. B. and P. P. Tans.2003. Calculating isotopic fractionation from atmospheric measurements at various scales. Tellus Series B-Chemical and Physical Meteorology 55(2): 207-214.

Mortazavi, B., J. L. Prater and J. P. Chanton.2004. A field-based method for simultaneous measurements of the $\delta^{18}O$ and $\delta^{13}C$ of soil CO_2 efflux. Biogeosciences 1(1): 1-9.

Ohlsson, K. E. A., S. Bhupinderpal, S. Holm, A. Nordgren, L. Lovdahl and P. Hogberg.2005. Uncertainties in static closed chamber measurements of the carbon isotopic ratio of soil-respired CO_2. Soil Biology & Biochemistry 37(12): 2273-2276.

O'leary, M. H., S. Madhavan and P. Paneth.1992. Physical and Chemical Basis of Carbon Isotope Fractionation in Plants. Plant Cell and Environment 15(9): 1099-1104.

Peterson, D. L. and R. H. Waring.1994. Overview of the Oregon Transect Ecosystem Research-Project. Ecological Applications 4(2): 211-225.

Pypker, T. G., M. Hauck, E. W. Sulzman, M. H. Unsworth, A. C. Mix, Z. E. Kayler, D. Conklin, A. Kennedy, H. R. Barnard, C. Phillips and B.J. Bond.2008. Toward using $\delta^{13}C$ of ecosystem respiration to monitor canopy physiology in complex terrain. Oecologia 158(3):399-410.

Pypker, T. G., M. H. Unsworth, B. Lamb, E. Allwine, S. Edburg, E. Sulzman, A. C. Mix and B. J. Bond.2007. Cold air drainage in a forested valley: Investigating the feasibility of monitoring ecosystem metabolism. Agricultural and Forest Meteorology 145(3-4): 149-166.

Running, S. W., R. R. Nemani and R. D. Hungerford.1987. Extrapolation of Synoptic Meteorological Data in Mountainous Terrain and Its Use for Simulating Forest Evapotranspiration and Photosynthesis. Canadian Journal of Forest Research-Revue Canadienne De Recherche Forestiere 17(6): 472-483.

Singh, J. and S. Gupta.1977. Plant decomposition and soil respiration in terrestrial ecosystems. The Botanical Review 43(4): 449-528.

Steinmann, K. T. W., R. Siegwolf, M. Saurer and C. Korner.2004. Carbon fluxes to the soil in a mature temperate forest assessed by ^{13}C isotope tracing. Oecologia 141(3): 489-501.

Stoy, P. C., S. Palmroth, A. C. Oishi, M. B. S. Siqueira, J. Y. Juang, K. A. Novick, E. J. Ward, G. G. Katul and R. Oren.2007. Are ecosystem carbon inputs and outputs coupled at short time scales? A case study from adjacent pine and hardwood forests using impulse-response analysis. Plant Cell and Environment 30(6): 700-710.

Subke, J. A., I. Inglima and M. F. Cotrufo.2006. Trends and methodological impacts in soil CO_2 efflux partitioning: A metaanalytical review. Global Change Biology 12(6): 921-943.

Sulzman, E.W. 2000. Soil water and carbon dynamics: ^{18}O and ^{13}C as system tracers. Dissertation. Colorado State University, Fort Collins, Colorado.

Sulzman, E. W., J. B. Brant, R. D. Bowden and K. Lajtha.2005. Contribution of aboveground litter, belowground litter, and rhizosphere respiration to total soil CO_2 efflux in an old growth coniferous forest. Biogeochemistry 73(1): 231-256.

Takahashi, Y., N. Liang, R. Hirata and T. Machida.2008. Variability in carbon stable isotope ratio of heterotrophic respiration in a deciduous needle-leaf forest. Journal of Geophysical Research-Biogeosciences 113(G1).

Van Bel, A. J. E.2003. The phloem, a miracle of ingenuity. Plant Cell and Environment 26(1): 125-149.

Vitousek, P. M. and P. A. Matson (1991). Gradient Analysis of Ecosystems. Cole, J., G. Lovett and S. Findlay (Ed.). Comparative Analyses of Ecosystems: Patterns, Mechanisms, and Theories; Third Cary Conference, Millbrook, New York, USA, 1989. Xvi+375p. Springer-Verlag New York, Inc.: Secaucus, New Jersey, USA; Berlin, Germany. Illus. Maps: 287-300.

Vogel, J., P. Grootes and W. Mook.1970. Isotope fractionation between gaseous and dissolved carbon dioxide. Zeitschrift fur Physik 230: 225-238.

Western, A. W., G. Bloschl and R. B. Grayson.1998. Geostatistical characterisation of soil moisture patterns in the Tarrawarra a catchment. Journal of Hydrology 205(1-2): 20-37.

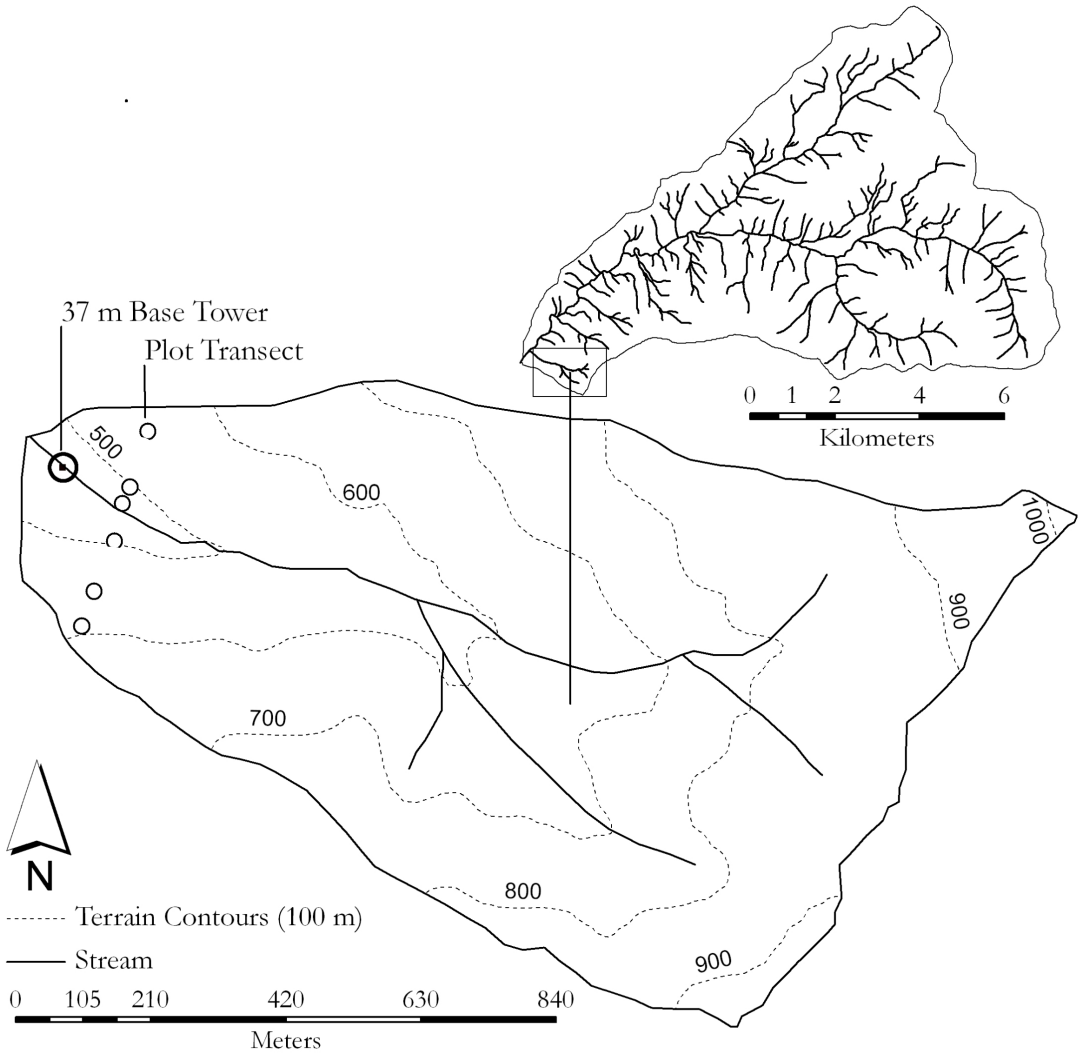

Figure 5.1 Plot transect located in Watershed 1 of the H.J. Andrews Experimental forest.

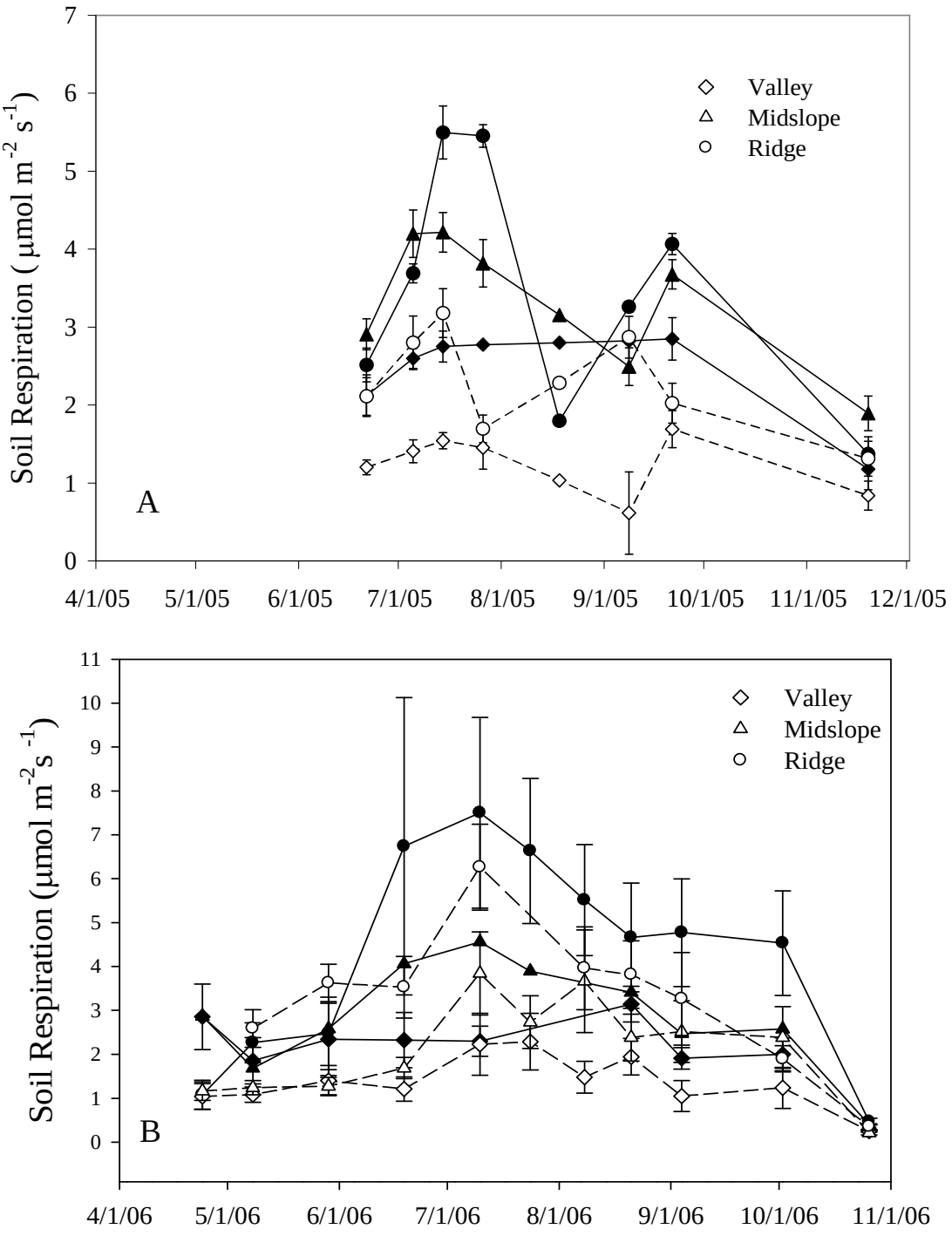

Figure 5.2 Plot averages of soil respiration for the 2005 (A) and 2006 (B) growing seasons. Solid lines refer to south facing plots and dashed lines refer to north facing plots. Error bars represent one standard error of the mean.

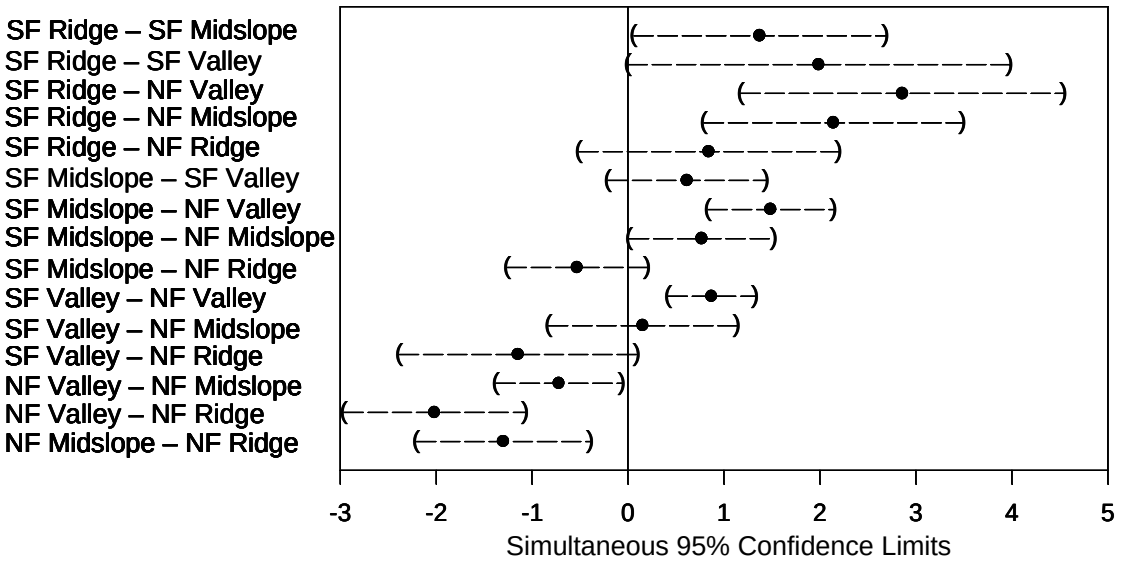

Figure 5.3 Mulit-comparison of plot soil respiration (μmol $m^{-2}s^{-1}$) for the 2006 growing season. Average difference between plots is shown and the 95% confidence interval is enclosed by parentheses.

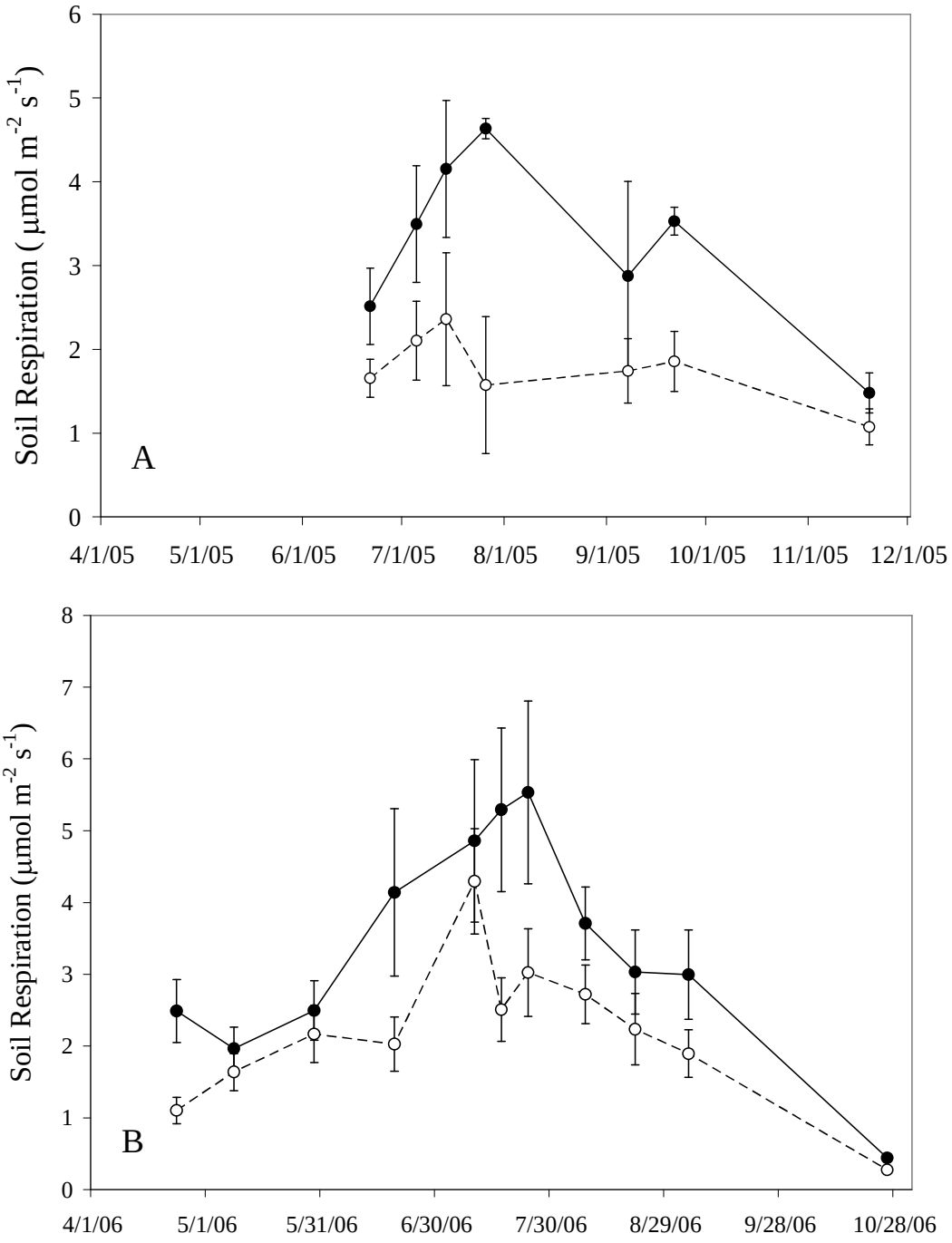

Figure 5.4 Watershed aspect averages of soil respiration for the 2005 (A) and 2006 (B) growing seasons. Solid lines and symbols refer to south facing plots and dashed lines with open symbols refer to north facing plots. Error bars represent one standard error of the mean.

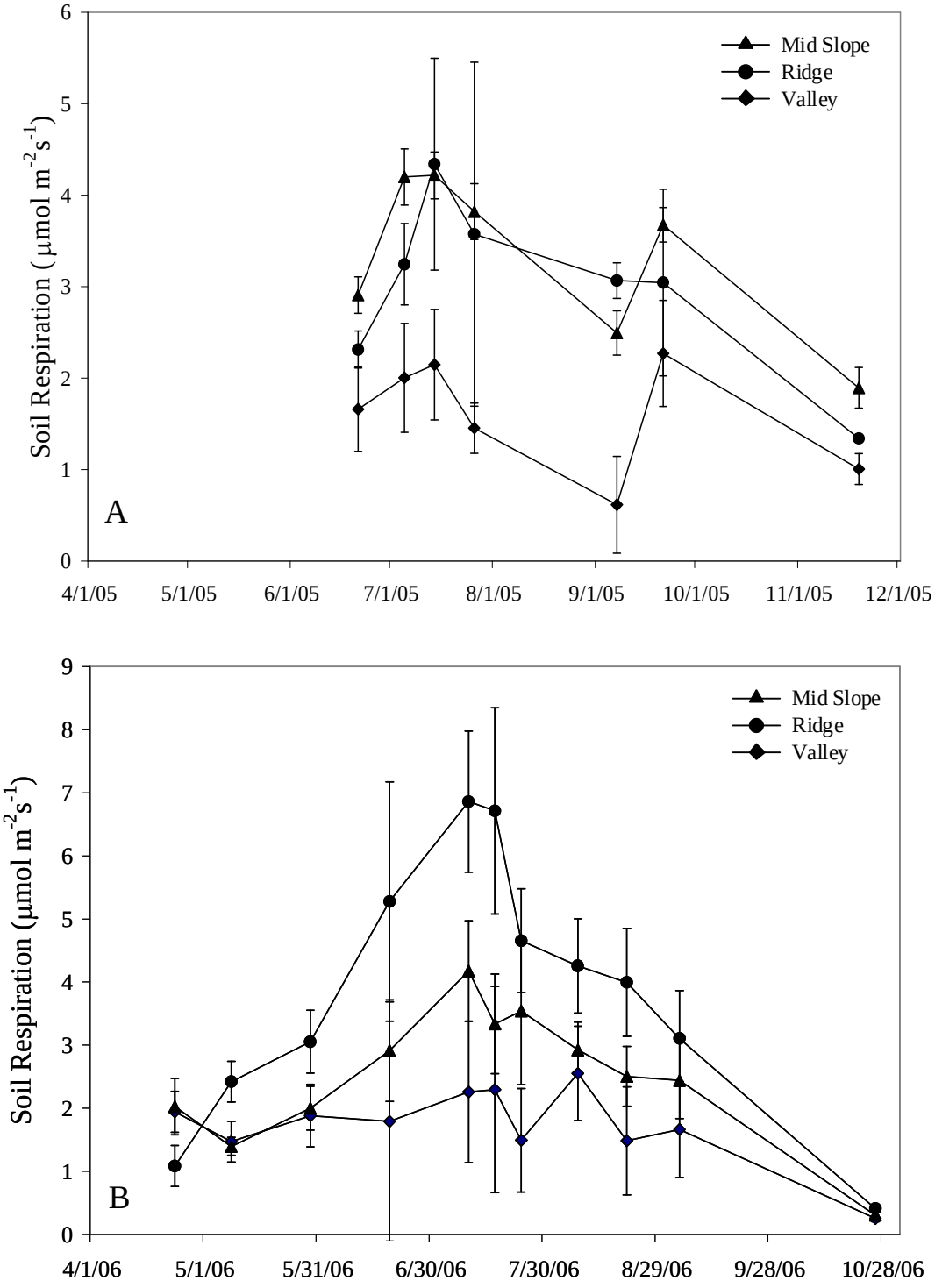

Figure 5.5 Slope position averages of soil respiration for the 2005 (A) and 2006 (B) growing seasons.Error bars represent one standard error of the mean.

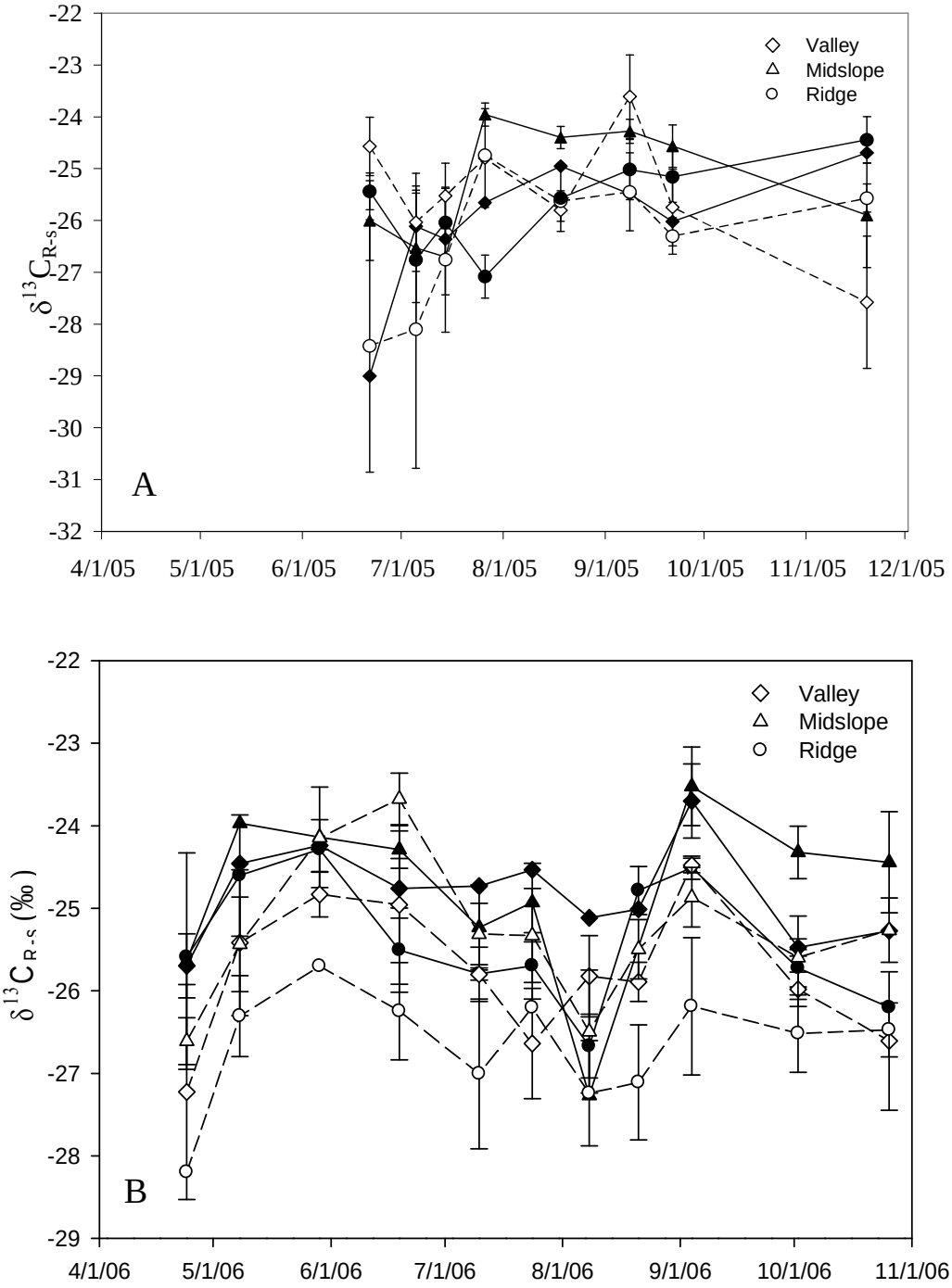

Figure 5.6 Plot averages of $\delta^{13}C_{R\text{-}s}$ (MM) for the 2005 (A) and 2006 (B) growing seasons. Solid lines refer to south facing plots and dashed lines refer to north facing plots. Error bars represent one standard error of the mean.

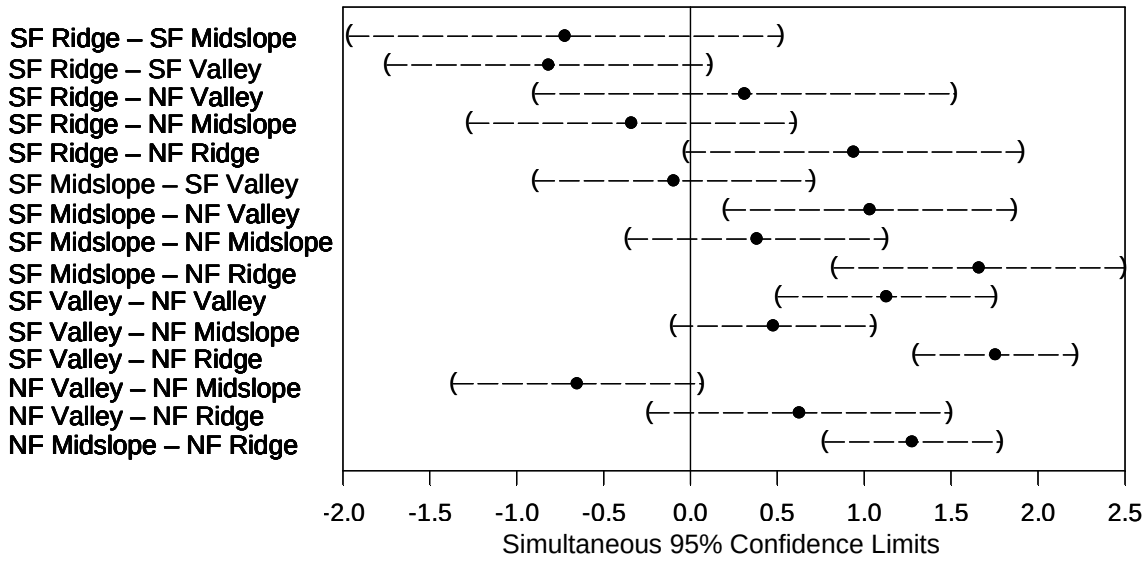

Figure 5.7 Mulit-comparison of plot $\delta^{13}C_{R\text{-}s}$ (MM)(‰) for the 2006 growing season. Average difference between plots is shown and the 95% confidence interval is enclosed by parentheses.

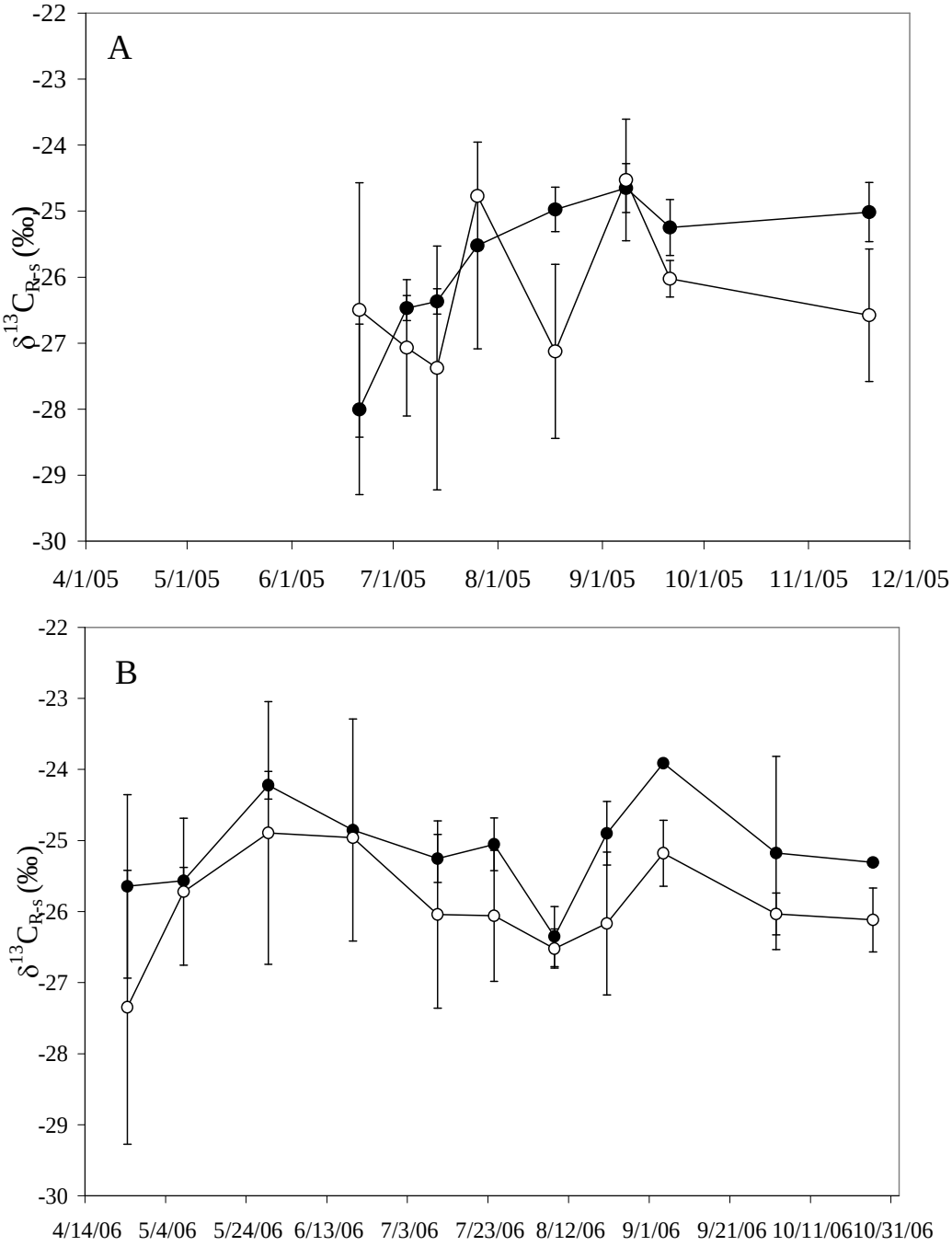

Figure 5.8 Catchment aspect averages of $\delta^{13}C_{R\text{-}s}$ (MM) for the 2005 (A)and 2006 (B) growing season. Solid lines and symbols refer to south facing plots and dashed lines with open symbols refer to north facing plots. Error bars represent one standard error of the mean.

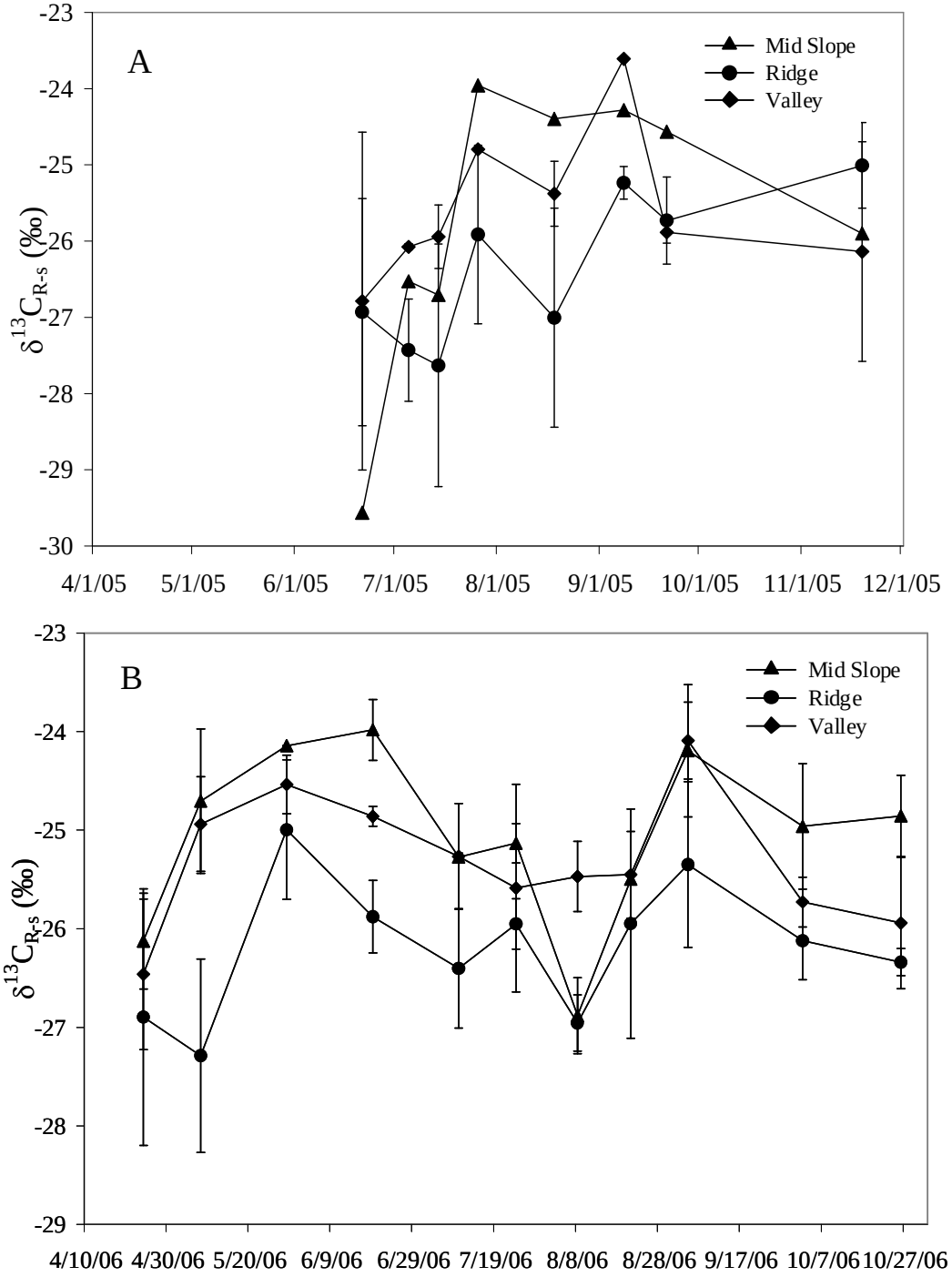

Figure 5.9 Slope position averages of $\delta^{13}C_{R\text{-}s}$ (MM) for the 2005 (A) and 2006 (B) growing seasons.Error bars represent one standard error of the mean.

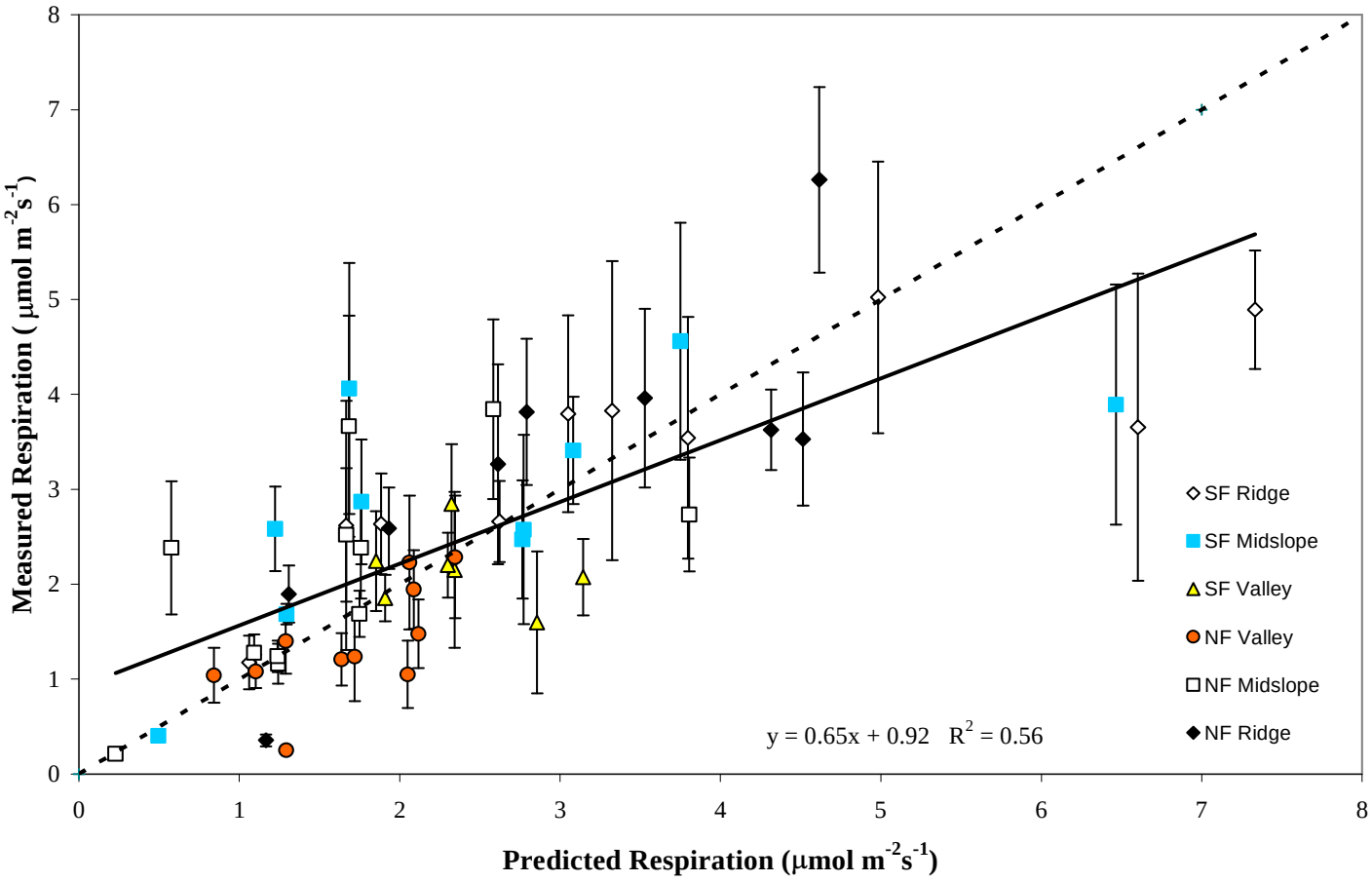

Figure 5.10 Empirical respiration models based on soil moisture and temperature. Regression line (solid) is calculated from respiration from all plots in the transect. The dashed line is the 1:1 line of predicted and measured values. Error bars are standard errors of the measured respiration mean.

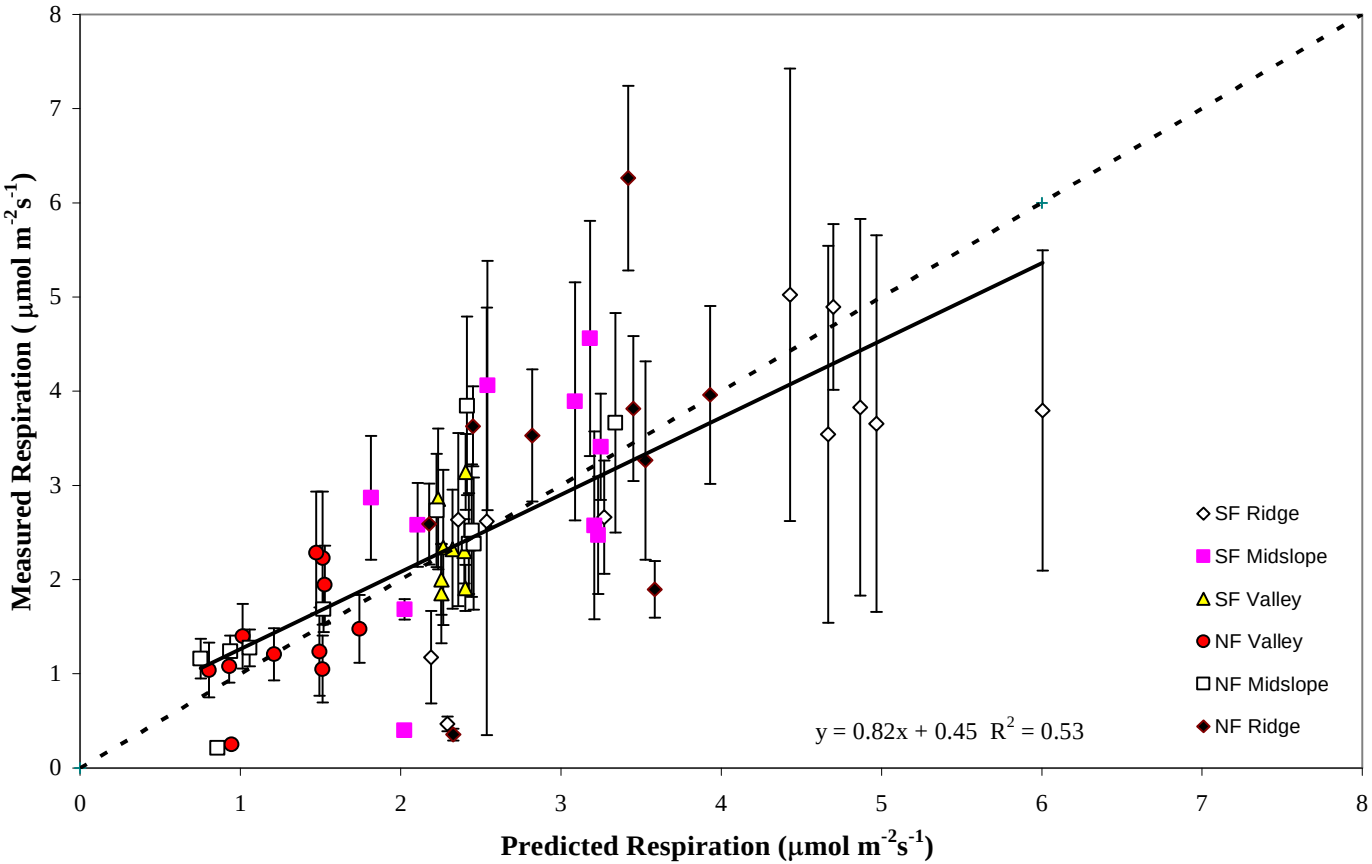

Figure 5.11 Exponential model of respiration based on soil temperature. Regression line (solid) is calculated from respiration from all plots in the transect. The dashed line is the 1:1 line of predicted and measured values. Error bars are standard errors of the measured respiration mean.

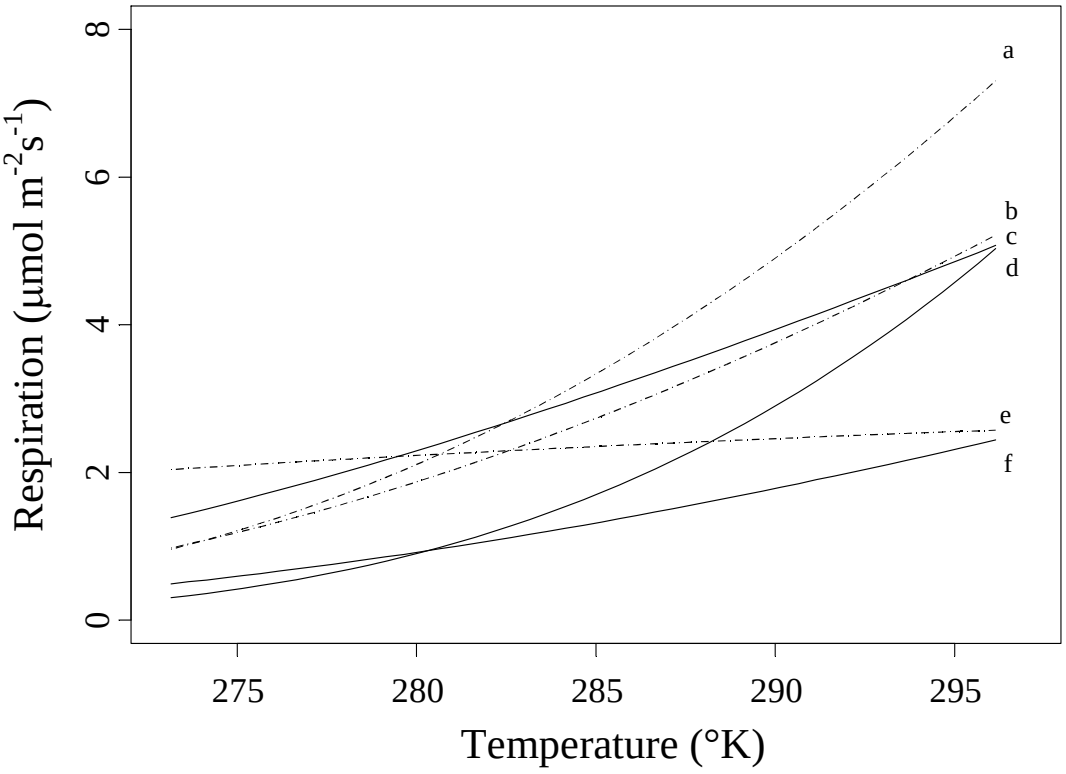

Figure 5.12 Predictions of exponential respiration model. Letters correspond to plot topographic location: a = SF ridge,b = SF midslope, c = NF ridge, d = NF midslope, e= SF valley, f = NF valley. Solid lines are plots located on the NF slope and dotted lines are plots from the SF slope.

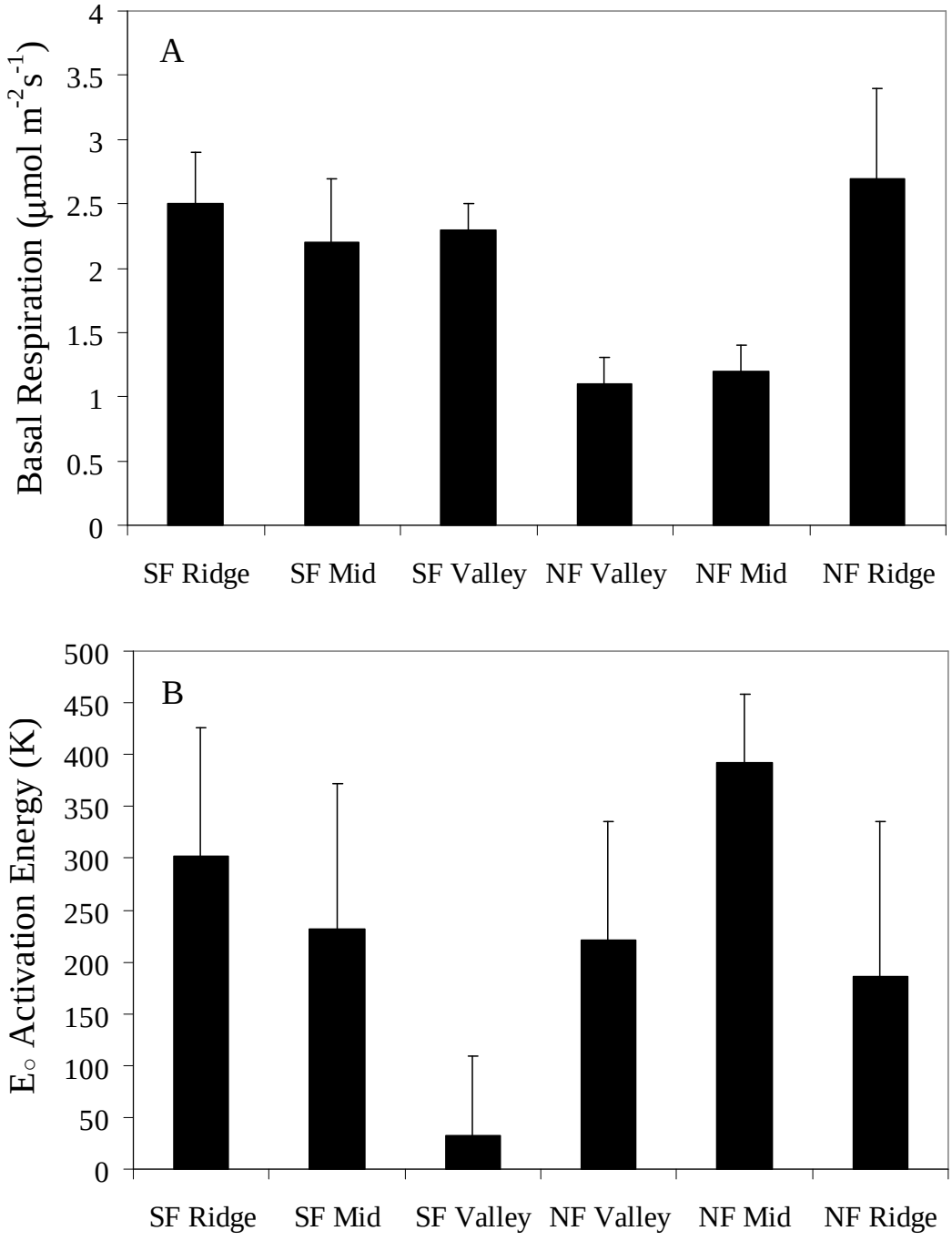

Figure 5.13 Plot level parameter estimates for the exponential respiration model. A) Average basal respiration with standard error B) average Activation energy estimates with standard error.

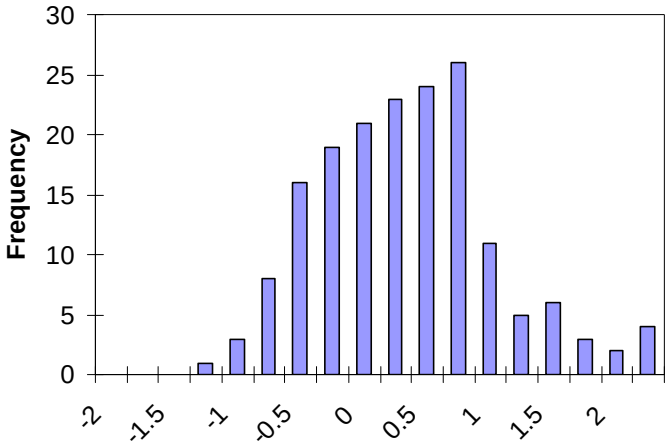

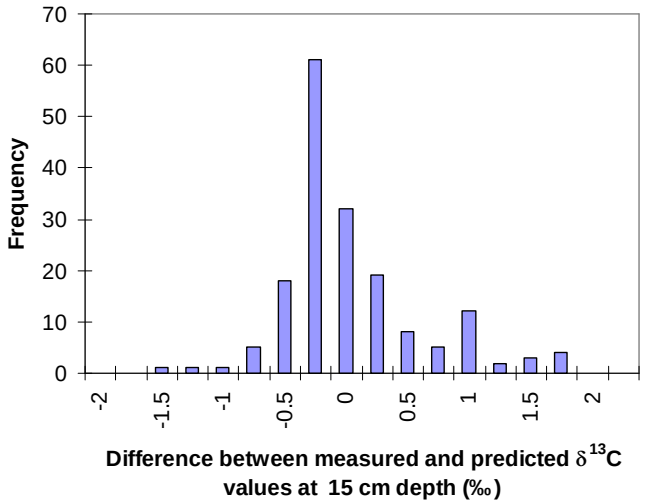

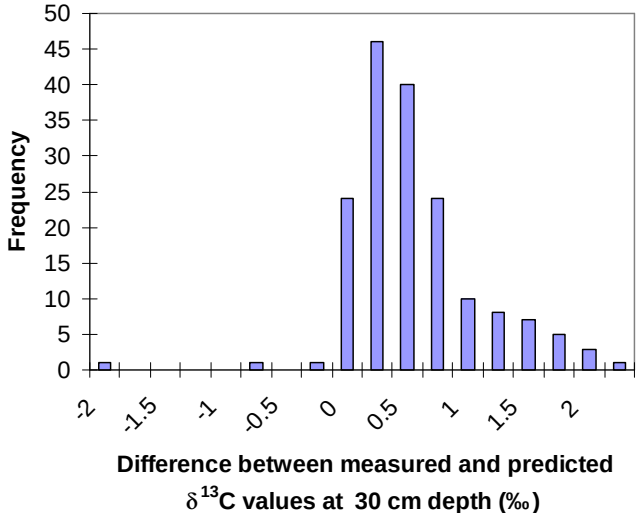

Figure 5.14 Histograms depicting the difference (predicted-measured) between the predictions of the isotopic steady-state model and the measured $^{13}CO_2$ from the field.

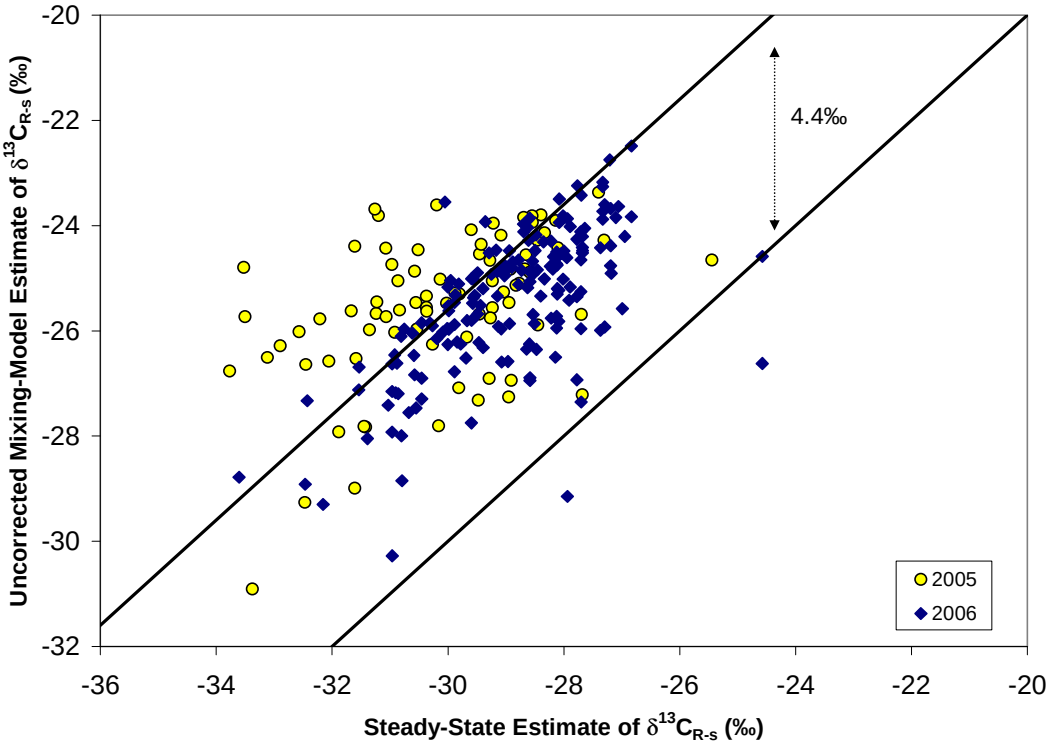

Figure 5.15 Apparent fractionation of $\delta^{13}C_{R\text{-}s}$.The 1:1 line represents $\delta^{13}C_{R\text{-}s}$ predicted by the steady-state model. The second line through the cluster of data is the $\delta^{13}C_{R\text{-}s}$ predicted by the steady-state model plus the 4.4‰ enrichment due to diffusion. Samples of soil gas were taken during the day time for 2005 data and during the evening for the 2006 data.

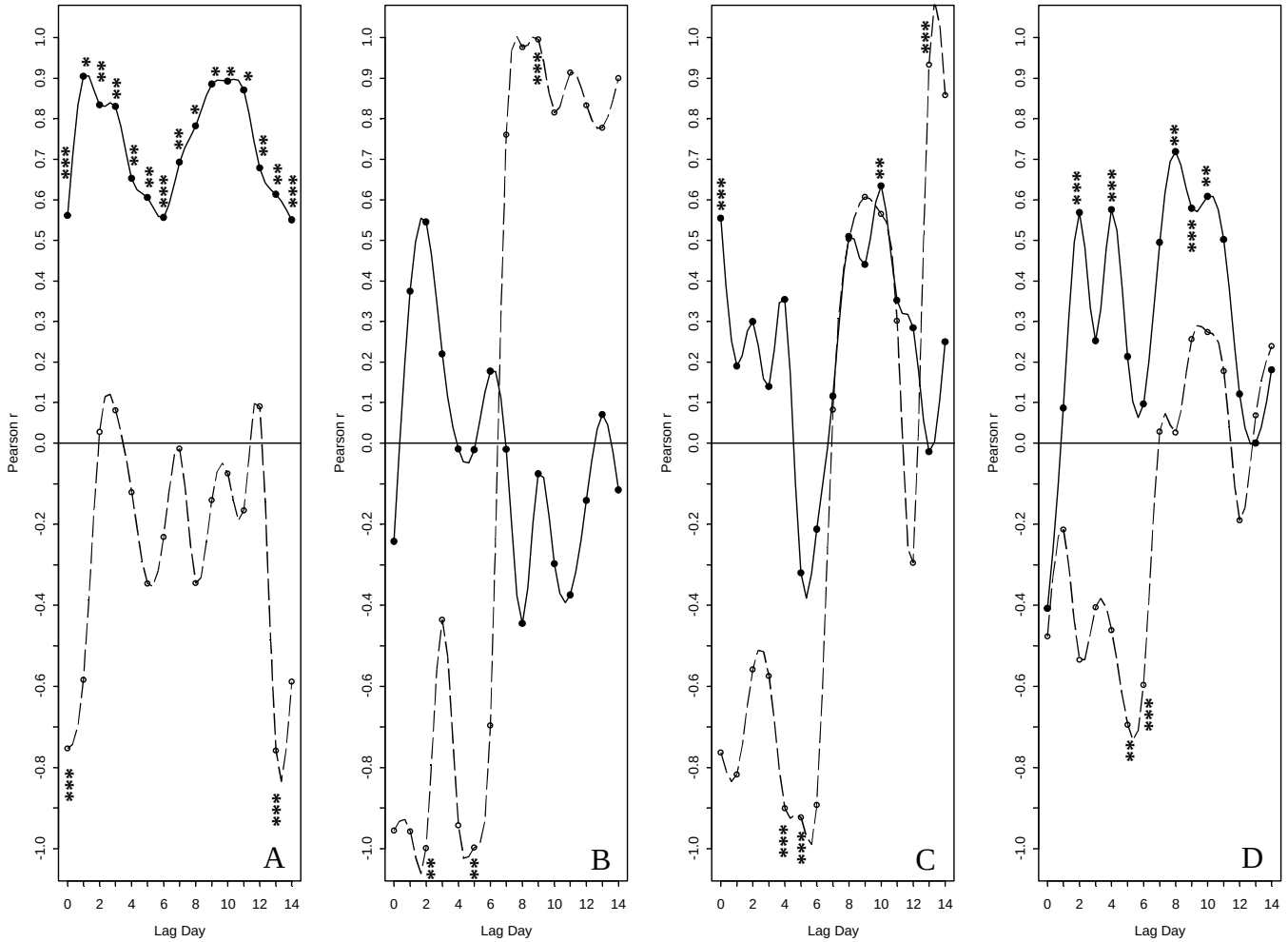

Figure 5.16 Plot level correlogram of 2006 soil respiration and $\delta^{13}C_{R\text{-}s}$ with transpiration. Solid lines show the patterns of correlation for the soil respiration data and dotted lines refer to the patterns of $\delta^{13}C_{R\text{-}s}$. A= SF ridge, B= SF valley, C= NF valley, D= NF midslope. The level of signifcance is shown for three levels < 0.01 (*), <0.05 (**) and < 0.10 (***).

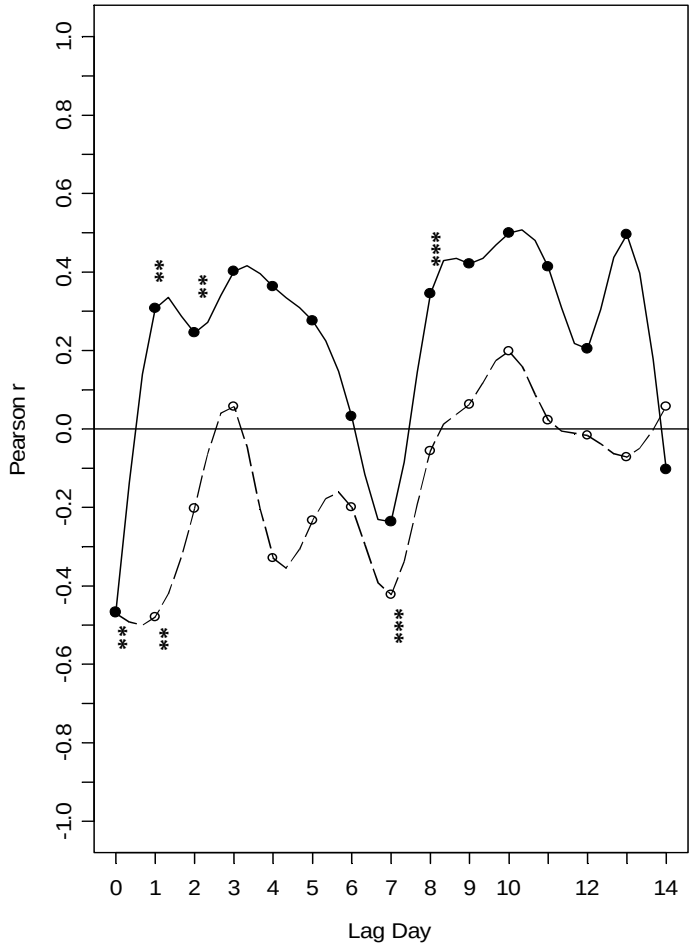

Figure 5.17 Catchment aspect correlogram of 2006 soil respiration and $\delta^{13}C_{R\text{-}s}$ with VPD on the NF slope. Solid lines show the patterns of correlation for the soil respiration data and dotted lines refer to the patterns of $\delta^{13}C_{R\text{-}s}$. The level of signifcance is shown for three levels < 0.01 (*), <0.05 (**) and < 0.10 (***).

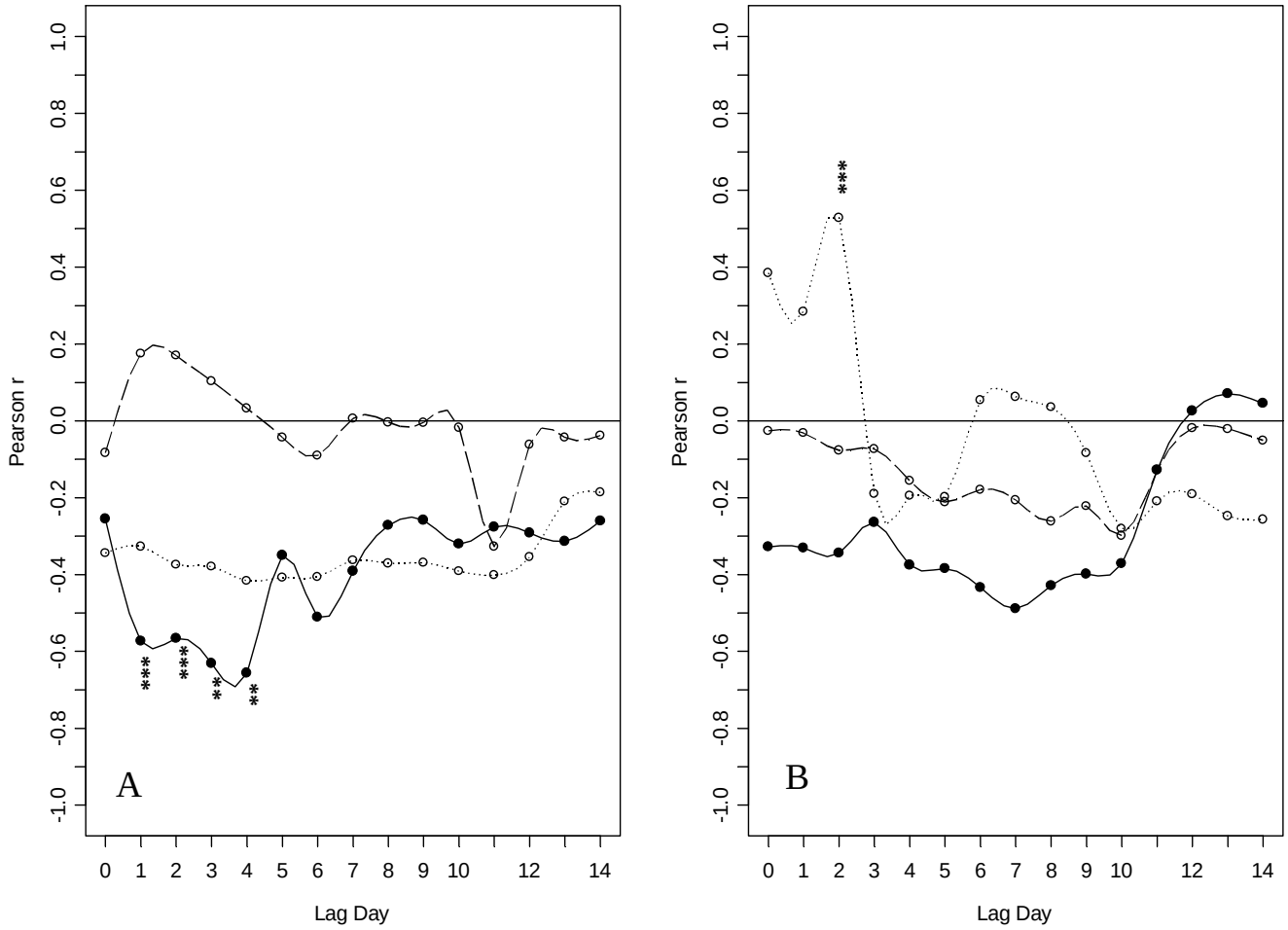

Figure 5.18 Plot level correlogram of 2006 $\delta^{13}C_{R\text{-}s}$ with soil moisture for the ridge (A) and valley (B) plots on the north facing slope. Solid lines show the patterns of correlation for VWC at 5cm, the long dashed line refers to VWC at 30cm and the short dashed line refers to VWC at 100cm. The level of signifcance is shown for three levels < 0.01 (*), <0.05 (**) and < 0.10 (***).

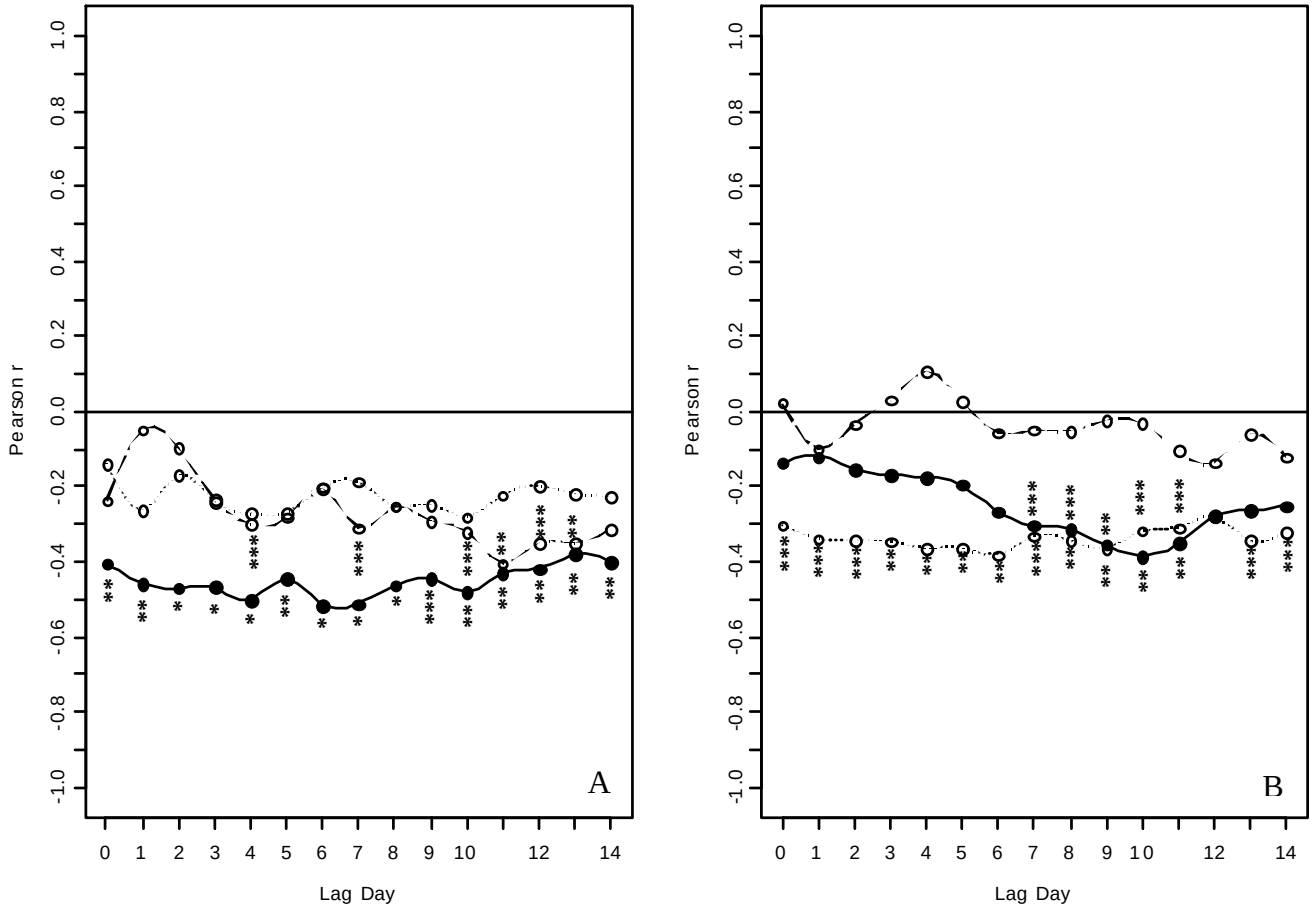

Figure 5.19 Slope aspect correlogram of 2006 $\delta^{13}C_{R\text{-}s}$ with soil moisture at three depths. Solid lines show the patterns of correlation for VWC at 5cm, the long dashed line refers to VWC at 30cm and the short dashed line refers to VWC at 100cm. A = SF slope and B = NF slope plots. The level of signifcance is shown for three levels < 0.01 (*), <0.05 (**) and < 0.10 (***).

Year	Plot	min	sm 5	max	min	sm 30	max	min	sm 100	max	min	st 5	max	min	st 30	max	min	st 100	max	min	VPD	max	min	Et	max
2005	SF Ridge	18.9	**32.2**	42.3	22.2	**35.7**	44.3	28.0	**40.3**	46.6	1.0	**11.0**	20.3	2.5	**10.9**	17.5	4.6	**10.9**	16.5	0.0	**435.1**	4488.9	-	-	-
	SF Mid	15.2	**23.6**	28.8	19.7	**28.1**	35.1	27.0	**33.5**	39.7	1.2	**10.2**	16.9	2.2	**10.2**	15.9	5.9	**9.8**	13.0	0.0	**411.6**	4711.8	-	-	-
	SF Valley	16.4	**27.1**	35.1	18.0	**32.7**	38.7	20.3	**30.6**	39.6	0.9	**11.5**	17.7	1.6	**10.2**	16.9	5.2	**10.2**	14.8	3.8	**334.2**	4286.7	-	-	-
	NF Ridge	10.0	**17.7**	26.1	8.7	**20.6**	29.8	14.6	**23.0**	32.7	1.0	**10.5**	16.7	1.7	**10.5**	15.7	4.6	**10.2**	13.8	-	-	-	-	-	-
	NF Mid	-	-	-	-	-	-	-	-	-	-	**-**	-	-	**-**	-	-	**-**	-	-	-	-	-	-	-
	NF Valley	12.3	**19.9**	31.2	17.3	**23.1**	33.4	22.7	**29.4**	38.1	1.8	**10.7**	17.5	3.5	**10.8**	15.1	4.6	**10.8**	14.2	3.4	**419.0**	4141.6	-	-	-
2006	SF Ridge	13.8	**30.3**	45.0	16.6	**36.7**	48.1	22.7	**40.2**	49.6	0.6	**9.6**	22.6	2.1	**9.6**	18.3	3.0	**9.4**	16.7	0.0	**465.9**	6238.7	0.04	**0.77**	1.86
	SF Mid	13.1	**24.2**	32.5	17.2	**29.0**	41.0	25.6	**36.7**	43.6	0.7	**8.8**	17.8	1.5	**8.8**	15.9	4.2	**8.6**	12.8	0.0	**444.7**	8111.5	-	-	-
	SF Valley	18.3	**27.9**	37.2	20.8	**31.7**	43.3	26.4	**42.1**	52.1	0.4	**8.8**	18.9	0.9	**9.0**	18.6	3.6	**8.4**	13.1	2.0	**371.9**	5663.1	0.08	**0.67**	1.78
	NF Ridge	13.6	**23.9**	37.1	13.2	**23.1**	37.9	10.9	**21.6**	35.7	0.4	**8.4**	18.1	1.0	**8.3**	16.6	3.3	**8.1**	12.8	0.0	**357.1**	5486.6	0.04	**0.53**	1.14
	NF Mid	11.3	**24.2**	38.7	11.3	**23.8**	48.6	11.3	**21.6**	31.9	-6.5	**8.7**	20.5	1.8	**8.1**	25.2	3.6	**8.6**	13.9	0.0	**422.5**	5278.0	0.04	**0.83**	1.98
	NF Valley	18.7	**25.7**	34.8	6.7	**23.9**	43.1	18.7	**31.4**	41.8	-0.3	**8.6**	19.9	2.0	**3.7**	5.9	2.8	**4.2**	5.9	2.4	**608.9**	10528.0	-	-	-

Table 5.1 Plot averages of environmental gradient. Soil moisture (sm) units are volumetric water content (%), soil temperature (st) are degrees Celcius, vapor pressure defecit units are Pa, and tree transpiration (Et) units are mm of water per day.

Plot	Parameter	Estimate	s.e.	p(> | t |)	Regression model r^2	Exponential model r^2
SF ridge					0.65	0.52
	Intercept	3.07	0.87	<0.001		
	SM 30cm	-0.1	0.012	<0.001		
	ST 5cm	0.11	0.012	<0.001		
SF midslope					0.42	0.29
	ST 5cm	0.85	0.17	<0.001		
	ST 30cm	-0.83	0.18	<0.001		
SF valley					0.2	0.03
	SM 5cm	0.03	0.01	<0.02		
	ST 5cm	1.63	0.68	<0.04		
	ST 30cm	-1.61	0.67	<0.04		
NF valley					0.45	0.35
	ST 30cm	0.14	0.02	<0.001		
NF midslope					0.38	0.81
	Intercept	-3.07	0.82	<0.001		
	SM 5cm	-0.11	0.03	<0.001		
	SM 100cm	0.19	0.03	<0.001		
	ST 30cm	0.17	0.03	<0.001		
NF ridge					0.69	0.19
	Intercept	-10.5	2.8	<0.001		
	SM 5cm	0.41	0.09	<0.001		
	ST 5cm	0.32	0.7	<0.001		

Table 5.2 Linear Mixed-Effects model parameters for soil respiration models. The models included soil moisture (SM) and temperature (ST) for three different depths (5cm, 30 cm, 100cm).

Model: Ln(fractionation data)~sm 30cm + sm 30cm:Ln(soil flux)

Parameter	Value	se	p(t)	n	r^2
sm 30cm	0.025	0.004	<0.01	107	0.33
sm 30cm * Ln(soil flux)	-0.01	0.003	<0.01		

Table 5.3 Exploratory analysis of soil profile $^{13}CO_2$ under non steady-state conditions. The final model is shown for a step wise regression using abiotic and biotic variables to explain the variation present in the data.

Chapter 6 Conclusion

Zachary Kayler

The largest terrestrial pool of carbon is soil (Amundson 2001) and soil respiration is the second largest flux of carbon globally, approximately an order of magnitude greater than the combined flux of fossil fuel and deforestation (Schimel et al. 1995). We have entered a period of great uncertainty with regards to the global climate and it is crucial that we develop a thorough understanding of the physical and biological controls of the evolution and egress of soil CO_2. Analyses of the isotopic composition and rate of CO_2 evolution from soil has increasingly been used in studies of C dynamics in the soil-plant-atmosphere system (Högberg et al. 2005; Högberg et al. 2006). However, while the processes of C isotope fractionation within plants are reasonably well known (Högberg et al. 2005), considerable uncertainty exists regarding the processes determining the isotopic composition of CO_2 efflux from soils.

In this dissertation I contributed towards refining the methods we use to measure the isotopic signal of soil respiration ($\delta^{13}C_{R\text{-}s}$) and the models we use to interpret these measurements. I have also identified and quantified the many pitfalls associated with conducting field studies using $\delta^{13}C_{R\text{-}s}$. Specifically, I found:

- The time to isotopic steady-state with respect to diffusion can be on the order of 48 hours.
- The soil probe replicates the isotopic and concentration values of the soil profile and will correctly estimate $\delta^{13}C_{R\text{-}s}$ when soil respiration is at steady-state.
- A lack of evidence for the static chamber at equilibrium to identify $\delta^{13}C_{R\text{-}s}$, although the chamber may be able to correctly estimate $\delta^{13}C_{R\text{-}s}$ when measured data are applied in a two end-member mixing model and soil respiration is at steady-state.
- It is important to distinguish between large (> 1000 μmol mol^{-1}) and small (< 100 μmol mol^{-1}) concentration regimes when applying a mixing model (Keeling plot or Miller-Tans) and regression approaches (ordinary least squares or geometric mean regression) to the respiration isotopic data.
- The combination of geometric mean regression and the Miller-Tans mixing model provide the most accurate and precise estimate of $\delta^{13}C_R$ when the range of CO_2 is equal to or greater than 1000 μmol mol^{-1}.

- The patterns of model bias and uncertainty in high concentration regimes were primarily driven by CO_2 error.
- For large CO_2 concentration error levels, the ordinary least squares estimate could have a positive bias.

- increasing the sample size in a mixing-model approach to estimate $\delta^{13}C_{R\text{-}s}$ will increase the estimate precision but can also lead to a decrease in accuracy.
- A -1‰ difference between the aboveground estimate under diffusive and advective conditions and may represent an upper bounds of the effects of advection on the apparent fractionation of ^{13}C.
- We found that aboveground measurements may be particularly susceptible to atmospheric incursion which may produce $\delta^{13}C_{R\text{-}s}$ estimates that are enriched in ^{13}C.
- The phloem isotopic signature was approximately enriched by 1‰ with respect to foliar extracts of Douglas-fir trees.
- In a Douglas-fir forest, potentially 90% of the carbon respired from soil can be from a depleted isotopic source that is similar to the signature of foliar extracts for the early growing season in a stand of Douglas-fir trees.
- During the growing season, soil respiration and its isotopic signature is primarily driven by aboveground inputs.
- The strongest gradient that soil respiration and $\delta^{13}C_{R\text{-}s}$ responded to was transpiration.
- Soil moisture was negatively correlated with $\delta^{13}C_{R\text{-}s}$ at our site indicating that soil moisture influences on soil respiration are related to the oxidation of recently-fixed photosynthates from plants rather than carbon from SOM.
- Exploratory analysis revealed the soil moisture volumetric water content from 30cm depth and its interaction with the soil flux accounted for 33% of the variation in the isotopic fractionation data.

Future research

The most important lesson I have learned through this dissertation research is that $\delta^{13}C_{R\text{-}s}$ is affected by seemingly every biotic and abiotic factor available in a forest. The ultimate goal of this research pursuit is to have robust estimates of the flux of carbon and its isotopic composition so that inferences can be made into the mechanisms behind forest carbon metabolism. The future of this research area may not lie solely in the continued monitoring of $\delta^{13}C_{R\text{-}s}$, but instead using the information presented here and in other work towards constructing a process model of carbon transfers and isotopic fractionation that occur along the atmosphere-plant-soil continuum. From such a model more precise hypothesis could be generated concerning the various mechanisms behind soil respired carbon.

References

Amundson, R.2001. The carbon budget in soils. Annual Review of Earth and Planetary Sciences 29: 535-562.

Högberg , P., A. Ekblad, A. Nordgren, A. H. Plamboeck, A. Ohlsson, Bhupinderpal-Singh and M. Hoegber (2005). Factors determining the 13C abundance of soil-respired CO2 in Boreal Forests. Stable Isotopes and Biosphere-Atmosphere Interactions. L. B. Flanagan, J. R. Ehleringer and D. E. Pataki. San Francisco, USA, Elsevier: 47-68.

Högberg , P. and D. J. Read.2006. Towards a more plant physiological perspective on soil ecology. Trends in Ecology & Evolution 21(10): 548-554.

Schimel, D. S.1995. Terrestrial Ecosystems and the Carbon-Cycle. Global Change Biology 1(1): 77-91.